Aeroelastic Simulation of Wind Turbine Dynamics

by

Anders Ahlström

April 2005
Doctoral Thesis from
Royal Institute of Technology
Department of Mechanics
SE-100 44 Stockholm, Sweden

Akademisk avhandling som med tillstånd av Kungliga Tekniska högskolan i Stockholm framlägges till offentlig granskning för avläggande av teknologie doktorsexamen fredagen den 8:e april 2005 kl 10.00 i sal M3, Kungliga Tekniska högskolan, Valhallavägen 79, Stockholm.

Abstract

The work in this thesis deals with the development of an aeroelastic simulation tool for horizontal axis wind turbine applications.

Horizontal axis wind turbines can experience significant time varying aerodynamic loads, potentially causing adverse effects on structures, mechanical components, and power production. The needs for computational and experimental procedures for investigating aeroelastic stability and dynamic response have increased as wind turbines become lighter and more flexible.

A finite element model for simulation of the dynamic response of horizontal axis wind turbines has been developed. The developed model uses the commercial finite element system MSC.Marc, focused on nonlinear design and analysis, to predict the structural response. The aerodynamic model, used to transform the wind flow field to loads on the blades, is a Blade-Element/Momentum model. The aerodynamic code is developed by The Swedish Defence Research Agency (FOI, previously named FFA) and is a state-of-the-art code incorporating a number of extensions to the Blade-Element/Momentum formulation. The software SOSIS-W, developed by Teknikgruppen AB was used to generate wind time series for modelling different wind conditions.

The method is general, and different configurations of the structural model and various type of wind conditions can be simulated. The model is primarily intended for use as a research tool when influences of specific dynamic effects are investigated.

Verification results are presented and discussed for an extensively tested Danwin 180 kW stall-controlled wind turbine. Code predictions of mechanical loads, fatigue and spectral properties, obtained at different conditions, have been compared with measurements. A comparison is also made between measured and calculated loads for the Tjæreborg 2 MW wind turbine during emergency braking of the rotor. The simulated results correspond well to measured data.

Keywords: wind turbine; aeroelastic modelling; rotor aerodynamics; structural dynamics; MSC.Marc; AERFORCE; SOSIS-W

Förord

I skrivande stund är det näst intill fem år sedan jag började som doktorand på KTH och det slår mig hur fort dessa år har passerat. Förklaringen är att jag för det mesta har haft ett både roligt och stimulerande jobb. Undantagen är förstås när allt har gått, för att uttrycka det milt, mindre bra. Som tur är har jag då haft min handledare att fråga om råd. Anders, utan dina fantastiska kunskaper och ditt stöd skulle den här tiden känts betydligt mycket längre och tråkigare.

Jag vill också passa på att tacka Ingemar Carlén och Hans Ganander på Teknikgruppen AB, samt Jan-Åke Dahlberg på FOI, som alla har varit till stor hjälp i projektet. Jag vill även tacka Anders Björck för hjälp med den aerodynamiska modellen och för din medverkan i referensgruppen. Tack också till övriga medlemmar i referensgruppen, Lennart Söder, Sven-Erik Thor och Anders Wikström.

Ett stort tack vill jag rikta till Kurt S. Hansen och Stig Øye på DTU för alla frågor ni villigt besvarat. Ett stort tack riktar jag också till Gunner Larsen för ett varmt välkomnande till Risø.

Lunchen har utan avvikelse inmundigats klockan 11.30 på någon finare restaurang. När man inmundigar en finare lunch är det viktigt med trevligt sällskap. Det har jag haft och det vill jag tacka mina lunchkompisar för. Alla skratt har definitivt bidragit till den höga trivselfaktorn här på mekanik.

Tack till alla vänner på mekanik och forna byggkonstruktion för att ni gjort tiden som doktorand till en mycket positiv upplevelse.

Tack till Energimyndigheten för ekonomiskt stöd.

Slutligen vill jag tacka min familj och min älskade Jeanette.

Stockholm, Februari 2005

Anders Ahlström

Contents

List of symbols

a'	tangential induction factor, 23
α	angle of attack, 23
c	blade cord length, 22
C_D	drag coefficient, 22
C_L	lift coefficient, 22
C_N	projected drag coefficient, 23
$c(r)$	chord at position r, 24
C_T	projected lift coefficient, 23
D	drag force, 23
F_N	force normal to rotor plane, 23
F_T	force tangential to rotor plane, 23
L	lift force, 22
N	number of blades, 24
ω	rotation speed, 23
ϕ	angle between disc plane and relative velocity, 23
r	radius of the blade, 23
σ	solidify factor, 24
θ	local pitch of the blade, 23
U_∞	undisturbed air speed, 23
V_{rel}	relative air speed, 22

List of Figures

List of Tables

Chapter 1

Introduction

1.1 Background

For a successful large-scale application of wind energy, the price of wind turbine energy must decrease in order to be competitive with the present alternatives. The behaviour of a wind turbine is made up of a complex interaction of components and sub-systems. The main elements are the rotor, tower, hub, nacelle, foundation, power train and control system. Understanding the interactive behaviour between the components provides the key to reliable design calculations, optimised machine configurations and lower costs for wind-generated electricity. Consequently, there is a trend towards lighter and more flexible wind turbines, which makes design and dimensioning even more demanding and important.

Wind turbines operate in a hostile environment where strong flow fluctuations, due to the nature of the wind, can excite high loads. The varying loads, together with an elastic structure, creates a perfect breeding ground for induced vibration and resonance problems. The needs for computational and experimental procedures for investigating aeroelastic stability and dynamic response have increased with the rated power and size of the turbines. The increased size of the rotor requires that the dimension of the other components must be scaled up, e.g., the tower height. With increasing size, the structures behave more flexibly and thus the loads change. As wind turbines become lighter and more flexible, comprehensive systems dynamics codes are needed to predict and understand complex interactions.

1.2 Scope and aims

The goal of this project is to produce an aeroelastic model with such accuracy and flexibility that different kinds of dynamic phenomena can be investigated. The majority of the present aeroelastic models are based on a modal formulation or a finite element (FE) representation. The modal models are computationally efficient because of the efficient way of reducing the number of degrees of freedom (DOFs).

However, the modal models are primarily suited for design purposes and will, because of the reduced DOF and linear deflection assumption, often not be suitable for research areas, including e.g. large blade deflections, where nonlinearities might be present. In this project, the finite element method has been chosen to accurately predict the wind turbine loading and response in normal as well as in extreme load cases. The main features of the developed tool, as opposite to the majority of the existing codes, is that kinematically large displacements and rotations are included, and that loads are applied on the deformed geometry.

1.3 Outline of thesis

- Chapter 2 presents the wind turbine from a historical point of view and gives a short description of the layout and the general function. The different design concepts are discussed and presented.
- Chapter 3 reviews the current state-of-the-art wind turbine design codes. Aspects regarding wind turbine design calculations, e.g. wind field representation, rotor aerodynamics, loads and structural stresses are discussed and explained.
- Chapter 4 describes aspects of modelling a wind turbine within the FEM. The three main parts of the simulation program are treated:
  SOSIS-W for generation of the turbulent wind field [9].
  AERFORCE package for the calculation of aerodynamic loads [7].
  MSC.Marc commercial finite element program for modelling of the structural dynamics [50].
- Chapter 5 shows some numerical examples.
- Chapter 6 concludes the study and gives some suggestions for further research.
- Appendix A gives airfoil data of the studied turbines.
- Appendix B gives examples of input files used in the simulations.
- Paper 1. Aeroelastic FE modelling of wind turbine dynamics, *Submitted to Computers & Structures.*
- Paper 2. Emergency stop simulation using a FEM model developed for large blade deflections, *Accepted for publication in Wind Energy.*
- Paper 3. Influence of wind turbine flexibility on loads and power production, *Submitted to Wind Energy.*

The writing of the submitted papers 1–3, as well as the numerical results presented, was carried out by A. Ahlström.

Chapter 2

Wind turbine technology and design concepts

2.1 Wind power from a historical point of view

Wind energy has been used for a long time. The first field of application was to propel boats along the river Nile around 5000 BC [69]. By comparison, wind turbines are a fairly recent invention. The first simple windmills were used in Persia as early as the seventh century for irrigation purposes and for milling grain [18]. In Europe it has been claimed that the Crusaders introduced the windmills around the eleventh century. Their constructions were based on wood. In order to bring the sails into the wind, they were manually rotated around a central post. In 1745, the fantail was invented and soon became one of of the most important improvements in the history of the windmill. The fantail automatically orientated the windmill towards the wind. Wind power technology advanced and in 1772, the spring sail was developed. Wood shutters could be opened either manually or automatically to maintain a constant sail speed in winds of varying speed [35].

The modern concept of windmills began around the industrial revolution. Millions of windmills were built in the United States during the 19th century. The reason for this massive increase in use of wind energy stems from the development of the American West. The new houses and farms needed ways to pump water. The proceeding of the industrial revolution later led to a gradual decline in the use of windmills.

However, while the industrial revolution proceeded, the industrialisation sparked the development of larger windmills to generate electricity. The first electricity generating wind turbine was developed by Poul la Cour [13]. In the late 1930's Americans started planning a megawatt-scale wind turbine generator using the latest technology. The result of this work was the 1.25 MW Smith-Putnam wind turbine, Figure 2.1. Back in 1941 it was the largest wind turbine ever built and it kept its leading position for 40 years [64].

The popularity of using the energy in the wind has always fluctuated with the

Figure 2.1: The 1.250 MW Smith-Putnam wind turbine. Reproduced from [37].

price of fossil fuels. Research and development in nuclear power and good access to oil during the 1960's led to a decline of the development of new large-scale wind turbines. But when the price of oil raised abruptly in the 1970's, the interest for wind turbines increased again [23].

Today, wind energy is the fastest growing energy technology in the world. The world wind energy capacity installations have surged from under 2000 MW in 1990 to the present level of approximately 39500 MW (November 2004) [77]. By comparison, the nuclear power plants in Sweden have a gross capacity of 10500 MW [65].

2.2 General description and layout of a wind turbine

Almost all wind turbines that produce electricity for the national grid consists of rotor blades that rotate around a horizontal hub. The hub is connected to a gearbox and a generator (direct-drive generators are present as well and makes the gearbox unnecessary), which are located inside the nacelle, Figure 2.2. The nacelle houses some of the electrical components and is mounted on top of the tower. The electric

current is then distributed by a transformer to the grid. Many different design concepts are in use. The most common ones are two- or three-bladed, stall or pitch regulated, horizontal-axis machines working at variable or near fixed rotational speed.

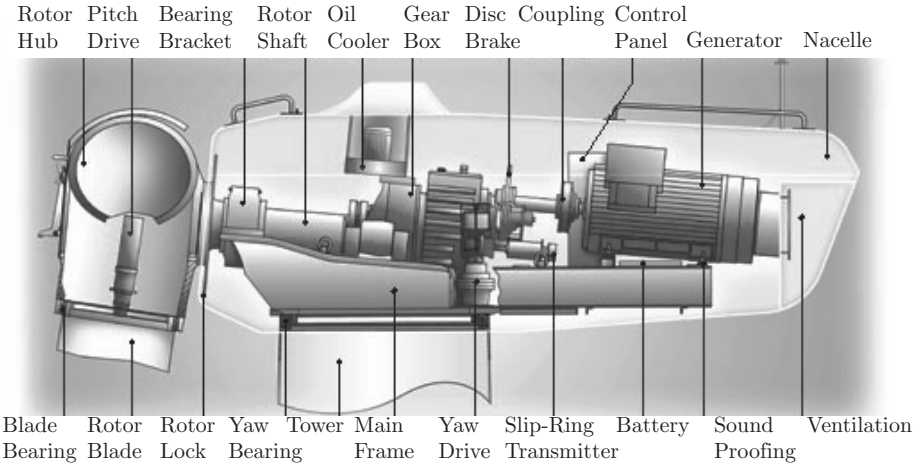

Figure 2.2: Wind turbine layout. Reproduced from [53].

2.3 Blades

All forms of wind turbines are designed to extract power from a moving air stream. The blades have an airfoil cross-section and extract wind by a lift force caused by a pressure difference between blade sides. For maximum efficiency, the blades often incorporate twist and taper.

LM Glasfiber in Denmark is the largest independent blade manufacturer with a product range that consists of standard blades in lengths from 13.4 to 61.5 metres for turbines from 250 kW to 5 MW, Figure 2.3. The information in this section is based on references [3, 22, 24].

2.3.1 Material

Wood has a natural composite structure of low density, good strength and fatigue resistance. The drawbacks are the sensitivity to moisture and the processing costs. There are, however, techniques that overcome these problems.
Most larger wind turbine blades are made out of Glass fibre Reinforced Plastics (GRP), e.g. glass fibre reinforced polyester or epoxy. According to [33], is a weight

Figure 2.3: LM Glasfiber 61.5 meters blade developed for 5 MW turbines. Reproduced from [46].

advantage of up to 30 % achieved when using epoxy compared to the cheaper polyester resin.
Carbon Fibre Reinforced Plastic (CFRP) blades are used in some applications. It has been assumed that this material system was strictly for aerospace applications and too expensive for wind turbines. However, by using effective production techniques, some manufacturers produce cost effective wind turbine blades. The advantage with carbon fibre is the high specific strength.

2.3.2 Number of blades

Since the beginning of the modern wind power era, the preferred designs for wind turbines have been with either two or three blades. Many early prototypes have two blades, e.g. Näsudden (Sweden), but the three-bladed concept has been the most frequently used during recent years.

Basic aerodynamic principles determine that there is an optimal installed blade area for a given rotational speed. A turbine for wind farm applications generally has a tip speed of 60–70 m/s. With these tip speeds a three-bladed rotor is 2–3% more efficient than a two-bladed rotor. It is even possible to use a single bladed rotor if a counterbalance is mounted. The efficiency loss is about 6% compared with the two-bladed rotor construction. Although fewer blades gives lower blade costs, there are penalties. The single-bladed rotor requires a counterbalance and is therefore not lighter than a two-bladed design. The two-bladed rotor must accept very high cyclic loading if a rigid hub system is employed. However, the loading can be reduced by using a teetered hub, [8]. The teeter system allows the rotor blades to rock as a pair to make it possible for the rotor to tilt backwards and forwards a few degrees away from the main plane during rotation. The three-bladed rotor is dynamically simpler and a little more aerodynamically efficient. Three-bladed designs have also

been preferred since they are considered to look more aesthetic in the landscape. Against that, the two-bladed rotors offer potential reductions in both fabrication and maintenance costs [12].

2.3.3 Airfoil design

In the beginning, most wind turbine blades where adaptations of airfoils developed for aircraft and were not optimised for wind turbine uses. In recent years developments of improved airfoil sections for wind turbines have been ongoing. The prevailing tendency among blade manufacturers is to use NACA 63 sections, [74], that may have modifications in order to improve performance for special applications and wind conditions. To gain efficiency, the blade is both tapered and twisted. The taper, twist and airfoil characteristic should all be combined in order to give the best possible energy capture for the rotor speed and site conditions.

A number of technologies known from aircraft industry are being adapted for use in wind turbine applications. A problem with wind turbine blades is that even at relatively low wind speed, the innermost part of some blades begin to stall. Normally stall-controlled wind turbine blades are supposed to control power at 14–15 m/s when the outer part of the blade begins to stall. If the innermost part of the blade will stall, say at around 8–9 m/s, the efficiency will decline. In practice, however, it is not possible to design a thick profile that does not suffer from premature stall, but vortex generators may improve the dynamic behaviour. The company LM Glasfiber claims that improvements of up to 4–6% of the annual production can be obtained using vortex generators [45].

2.3.4 Lightning protection

Lightning damage to wind turbines has been a serious problem for power companies since towers have become higher. The off-shore installations that currently are being raised will be even more exposed to lightning threats. Experiences with lighting damage to wind turbines in Denmark in the years 1985–1997 shows that the average damage occurrence was 4.1 faults per 100 turbine years. About 50% of the reported damages are related to the control system, 20% to the power system and 18% are connected to the mechanical components [63]. Lightning protection of wind turbines can be accomplished in many ways, but the common idea is to lead the lightning from the tip of the blade, down to the blade hub from where it is led through the nacelle and the tower down into the ground.

2.3.5 Structural modelling

From a modelling viewpoint, properties as weight, mass and stiffness distributions are of great importance for the dynamic behaviour of the wind turbine. The spar is the most important structural part for structural analysis and acts like a main beam.

The blade can therefore be treated as a beam structure and classical beam element theory can be used. A correct description of the coupling between the blades and the hub, especially in pitch regulated turbines, where the stiffness of the pitching system will influence the overall dynamics and control system, is also of major importance.

2.4 Tower

The most common types of towers are the lattice and tubular types constructed from steel or concrete. For small wind turbines, the tower may be supported by guy wires. The tower can be designed in two ways, soft or stiff. A stiff tower has a natural frequency which lies above the blade passing frequency. Soft towers are lighter and cheaper but have to withstand more movement and will suffer higher stress levels.

2.4.1 Tubular steel towers

Most modern wind turbines have conical towers made of steel. The tubular shape allows access from inside the tower to the nacelle, which is preferred in bad weather conditions. The towers are manufactured in sections of 20–30 metres with flanges at both ends. Sections are then transported to the foundation for the final assembly.

2.4.2 Lattice towers

Lattice towers are assembled by welded steel profiles. Lattice towers are cheap but the main disadvantages are the poor visual appeal and that access to the nacelle is exposed. Lattice towers are rare, but may still be found in e.g. the uninhabited desert of California [27, 74].

2.4.3 Structural modelling

The tower is coupled to the foundation and the bedplate. Depending on the type of foundation, the coupling can be more or less elastic. In a soft connection the foundation will affect the dynamics and must be treated and modelled as a part of the wind turbine. A yaw mechanism is used in the connection between tower and bedplate. The connection will affects the dynamics of the complete wind turbine and most be considered. From a modelling viewpoint, the tower's mass and stiffness distribution must be known. A correct matching of the tower's eigenfrequencies to the other components is crucial for a successful wind turbine design.

2.5 Hub

The hub connects the turbine blades to the main shaft. Blades are bolted to the hub flanges by threaded bushes that are glued into the blade root. The flange bolt holes can be elongated, in order to enable the blade tip angle to be adjusted. As mentioned in Section 2.3.2, the hub type can be either rigid or teetered.
Complicated hub shapes make it convenient to use cast iron. The hub must also be highly resistant to metal fatigue, which is difficult to achieve in a welded construction.

2.5.1 Structural modelling

The hub connects the rotor to the rotor shaft. The hub of a three-bladed rotor is relatively rigid and does not contribute much to the overall dynamical behaviour. However, as the hub transmits and must withstand all the loads on the blades, the design is crucial for a reliable wind turbine. If a teetering hub is used, which is common for two-bladed machines, the dynamics of the wind turbine will be highly dependent on e.g. the damping and stiffness properties of the teeter system.

2.6 Nacelle and bedplate

The nacelle contains the key components of the wind turbine, including the gearbox and the electrical generator. The bedplate is generally made of steel. In modern wind turbines, service personnel may enter the nacelle from the tower of the turbine. Figure 2.4 shows a schematic example of four different drive train configurations: A. Long shaft with separate bearings; gearbox supported by the shaft with torque restraints, B. Rear bearing integrated in the gearbox; gearbox mounted on the bedplate, C. Rotor bearings completely integrated in the gearbox, D. Rotor bearings on a stationary hollow axle; power transmission by a torque shaft.

2.6.1 Structural modelling

As the bedplate is rigid compared to the other components, it does not contribute significantly to the dynamical behaviour of the wind turbine. However, the nacelle also houses the shaft and yaw bearings. Their stiffnesses highly contribute to the dynamics of the wind turbine and must be carefully modelled in simulations.

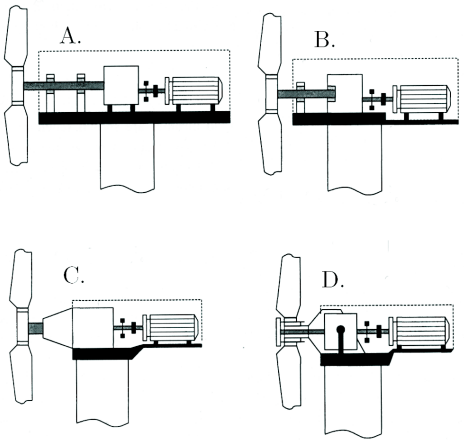

Figure 2.4: Schematic examples of drive train configurations. Reproduced from [32].

2.7 Braking system

The power in the wind is proportional to the cube of the wind speed. Considerable forces must therefore be controlled during high winds in order to attain safe operation. There are usually at least two independent braking systems, each capable of bringing the wind turbine to a safe condition in cases of high winds, loss of connection to the network or other emergencies [74].

2.7.1 Aerodynamic brakes

Aerodynamic brakes operate by pitching the blades or turning the blade tip (depending on the power control system) in order to prevent the aerodynamic forces from assisting rotation of the blades. The aerodynamic brake is the preferred brake for stopping as less stress is being placed on the working components than if mechanical brakes are used. The systems are usually spring or hydraulic operated and constructed to work in the case of electrical power failure. The centrifugal force is generally used to pull the blade tip forward in case of tip braking. When the tip shaft is released, the mechanism will rotate the blade tip 90° into a braking position and the rotor will stop.

2.7.2 Mechanical brakes

A mechanical brake is fitted to the main transmission shaft to bring the rotor to a complete stop. It is desirable to fit the brake between the rotor and the gearbox

in case of a gearbox failure. However, the torque on the low speed shaft can be very large, so manufacturers often fit the brake on the high speed shaft between the gearbox and the generator. The mechanical brake is generally a disc brake made of steel. Like the aerodynamic brake this is also a fail-safe system. For instance, hydraulic oil pressure can be used to prevent the brakes from locking. Should oil pressure be lacking, a powerful spring will cause the wind turbine to stop by activating the brakes. The brake disc is made of a special metal alloy that can endure temperatures of up to 700°C, [8, 67].

2.7.3 Structural modelling

When the turbine is braked, either by a disc brake or by pitching the blades, the turbine will be highly stressed. The braking will give transient loads that will affect the dynamics of the complete turbine. From a modelling point of view, the applied brake torque, in case of disc braking, or the pitch rate in the case of pitching, needs to be specified. Depending on how fast the rotor is braked, the brake situation will be more or less dynamic.

2.8 Yaw mechanism

It is necessary to align the rotor axis with the wind in order to extract as much energy from the wind as possible.
Most horizontal axis wind turbines use forced yawing. An electrical or hydraulic system is used to align the machine with the wind. The yaw drive reacts on signals from, e.g. a wind vane on top of the nacelle. Almost all manufacturers of upwind machines brake the yaw mechanism whenever it is not used. In slender wind turbines, like the Swedish Nordic 1000, the yaw mechanism is of importance for the dynamic behaviour of the system. The yaw mechanism must fulfil the requirements of a soft and damped connection between the nacelle and the tower. A hydraulic system is used to give the right characteristics whether it is yawing or not. This specific system is not furnished with any mechanical brakes.

In some wind situations, the turbine will rotate in the same direction for a long time. The cables that transport current from the generator down the tower will then be twisted. By using a device that counts the number of twists the cable can be twisted back [14, 71, 74].

2.8.1 Structural modelling

The dynamics of the yaw mechanism depends on if the turbine is yawing or not, as the yaw mechanism is generally braked whenever it is unused. The stiffness and damping properties of the yaw mechanism, may to some extent affect the fatigue loads, especially of the blades.

2.9 Generator

The wind turbine generator converts mechanical energy to electrical energy. The efficiency of an electrical generator usually falls off rapidly below its rated output. Since the power in the wind fluctuates widely, it is important to consider the relation between rated wind speed and rated power. In order to make the wind turbine as efficient as possible manufactures have developed techniques to rise efficiency at low revolution velocities. Whether it is worthwhile to use techniques able to efficiently handle low wind speeds depends on the local wind distribution and the extra cost associated with more expensive equipment.

The most common generator in wind turbines is the induction generator, sometimes called the asynchronous generator. Another type of generator is the synchronous one. The synchronous generator dominates in directly driven turbines, but is not very common in other wind power applications. The advantages of the induction generator are mechanical simplicity, robustness and closed cooling. A weakness is that the stator needs to be magnetised from the grid before it works. It is possible to run an asynchronous generator in a stand alone system if it is provided with additional components. The synchronous generator is more complicated than the induction one. It has more parts and is normally cooled with ambient air internally. Compared to the induction generator, a synchronous generator can run without connection to the grid [15, 68].

2.9.1 Constant speed generators

2.9.1.1 Two generators

To increase efficiency in low wind speed, solutions with two generators of different sizes are used. The smaller generator operates near its rated power at low wind speed and the bigger one is taking over at higher winds.

2.9.1.2 Pole changing generators

Pole changing generators are more common than two generator systems. A pole changing generator is made, e.g. with twice as many magnets (generally four or six). Depending on the local wind distribution, the generator is designed for different velocities. The benefits of lowering the rotational speed at low wind speeds are e.g. higher aerodynamically efficiency and less noise from the rotor blades, [13].

2.9.2 Variable speed generators

There are several advantages in operating wind turbines at variable speed: The increase in aerodynamic efficiency, which makes it possible to extract more energy

than in fixed speed operation. The possibility to decrease turbine speed in low wind speeds to reduce noise while avoiding too much torque and cost in the drive train at a relatively high top speed. The capability to prevent overloading of the gearbox or generator in pitch controlled turbines.

2.9.2.1 Variable slip generators

Usually the slip in an asynchronous generator will vary about 1% between idle and full speed. By changing the resistance in the rotor windings, it is possible to increase generator slip cope with violent gusts of winds.

The slip is very useful in pitch controlled turbines. The pitch control is a mechanical device controlling the torque in order to prevent overloading of the gearbox and generator by pitching the wings. In fluctuating wind speeds, the reaction time for pitching the wings is critical. Increasing the slip while nearing the rated power of the turbine makes it possible for the wings to pitch. When the wings have pitched, the slip is decreased again. In the opposite situation, when wind suddenly drops, the process is applied in reverse.

There are also methods for adjusting the slip continuously in order to get the required slip. The Optislip® is an example of such system. The system is produced by Vestas but is used by some other manufactures as well [15, 72].

2.9.2.2 Indirect grid connection

With indirect grid connection it is possible to let the wind turbine rotate within a wide range. On the market there are manufactures offering turbines with a slip of up to $\pm 35\%$.

If the generator is operated by variable speed, the frequency will fluctuate widely. The alternating current needs, therefore, to be transformed to match the frequency of the public electrical grid. There are three major parts in such systems, generator, direct current (DC)-rectifier and an alternating current (AC)-inverter. The first step is to convert the fluctuating current into DC. The DC is then inverted to AC with exactly the same frequency as the public grid. The inverter produces different kinds of harmonics that have to be filtered before reaching the public grid [15, 42, 68].

2.9.2.3 Direct drive system

The rotational speed of a standard wind turbine generator is about 1500 revolutions per minute (r.p.m.) while a typical turbine speed is 20 to 60 r.p.m. Therefore a gearbox is needed between generator and rotor. By using a low speed generator, the turbine could be directly coupled to the generator. Direct driven generators are commercially in use by e.g. Enercon and Lagerwey, Figure 2.5. The expected benefits of direct driven systems are e.g. Lower cost than a gearbox system. Reduced tower-

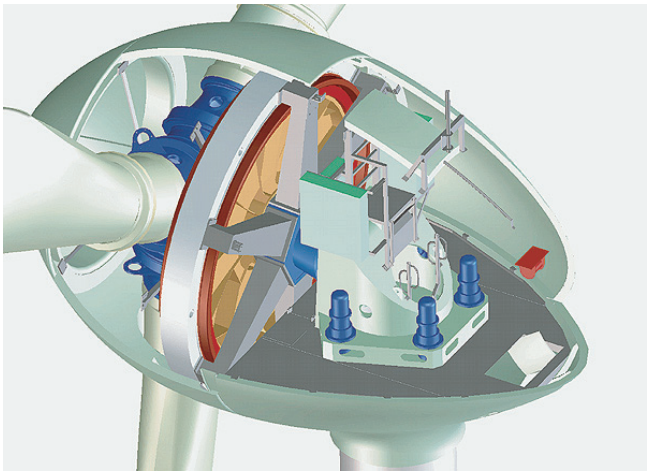

Figure 2.5: Enercon E-40 direct drive system. Reproduced from [21].

head mass and nacelle length. Efficiency savings of several percents.
Both Enercon and Lagerwey use synchronous generators. As mentioned before, the generator speed needs to be around 20–60 r.p.m. to make the gearbox unnecessary. That requires that the number of poles have to be sufficiently large to produce a suitable output frequency. In comparison to an ordinary generator, the direct-driven generator is bigger [24, 29].

2.9.3 Structural modelling

From a structural point of view, the generator type used will highly affect the dynamics and loads of the blades in primarily the edgewise direction. Variation of the rotational speed is an important feature to reduce transient loads, for constant speed generators as well as for variable speed generators. The generator dynamics will affect the dynamical behaviour of the complete wind turbine.

2.10 Power control

Wind turbines are designed to produce electricity as cheaply as possible. Since wind speeds rarely exceed 15 m/s, wind turbines are generally designed to yield maximum output (rated power) at a speed around 10–15 m/s (rated wind speed). As the wind speed increases past the rated speed of the turbine, the control mechanism of the rotor limits the power drawn from the wind in order to keep the drive train torque constant. To avoid damage to the generator and excessive mechanical stresses, the wind turbine is shut off when reaching a predetermined speed, normally about 25 m/s. Figure 2.6 shows the variation of a turbine's power output as a function of the wind speed; the graph is generally known as the power curve for a specific turbine.

2.10.1 Pitch controlled wind turbines

On pitch regulated turbines, the blades are mounted on the rotor hub with turntable bearings. They can be turned around their longitudinal axis during operation. In high winds, the pitch setting is continuously adjusted away from stall point to reduce lift force and thereby actively adjust the generated power. As mentioned in Section 2.9.2.1, the reaction time for pitching the wings is critical in order to follow the variations in wind speed to prevent excessive peak loads. Therefore, pitch regulation in practice requires a generator with full or partial speed, allowing a slight acceleration in rotor speed at wind gusts. The pitch mechanism is usually operated using hydraulics.

2.10.2 Stall controlled wind turbines

Passive control relies on the turbine's inherent machine characteristics, where the aerodynamic properties of the rotor limit the torque produced at high wind speeds. The geometry of the rotor blade has been designed to create turbulence on the side of the rotor blade that faces the wind, if the wind speed becomes too high. A blade is said to stall when the laminar flow over the airfoil breaks down and it loses lift. The blade on a stall-regulated turbine is slightly twisted to ensure that the stall conditions occur progressively from the blade root. The higher the wind speed, the greater the area of the blade is in stall.

The basic advantages of stall regulated wind turbines are the lack of moving parts and an active control system. However, stall regulation presents a highly complex aerodynamic design problem and related design challenges in the structural dynamics of the whole wind turbine, like stall introduced vibrations, etc.

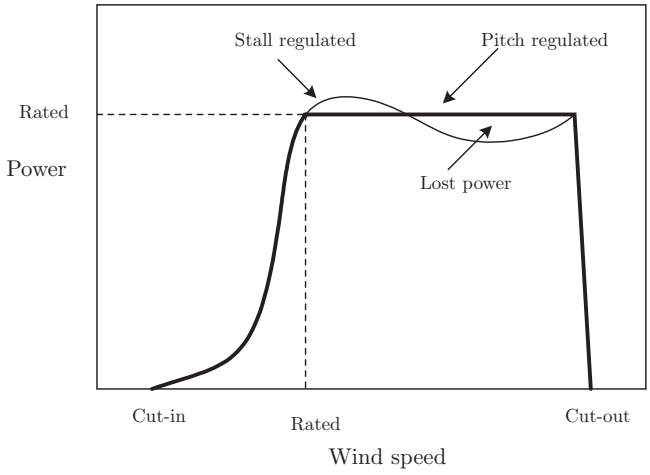

Figure 2.6: Power curves for stall and pitch regulated machines.

2.10.3 Active stall controlled wind turbines

Active stall is a combination of the two above mentioned methods for power limitation. In low and medium wind speeds the pitch method is used to yield maximum power output at any given wind speed. However, the actual power limitation in high wind speeds is obtained by using the stall phenomena. When the rated power is reached, the blades are adjusted to a more negative pitch setting in the opposite direction from the normal pitch regulation method. By adjusting the pitch setting in the negative direction, stall occurs at exactly the power level decided. The benefits is that the power level can be maintained at a constant level with a simple constant speed generator when exceeding the rated wind speed.

2.10.4 Other control mechanisms

Some older machines use ailerons to control the power of the rotor. Aileron control is common in aircraft for take-off and landing. However, the use of ailerons in modern wind turbines is not very common.

2.10.5 Structural modelling

From a structural modelling point of view, the two dominating power controls, stall and pitch regulation, give raise to different modelling considerations. In the case of stall regulation the thrust will increase with the wind above rated power, while in the pitching case the thrust will decrease as soon as the blades start pitching. Structurally, the stiffness of the pitch servo and the pitch bearing plays a role for the dynamics. The control system that adjust the pitch angle is of great importance for the dynamics of the turbine. Control systems for e.g. cyclic pitching can be used to reduce loads.

2.11 Gearbox

The gearbox is required to speed up the slow rotational speed of the low speed shaft before connection to the generator. The speed of the blade is limited by efficiency and also by limitations in the mechanical properties of the turbine and supporting structure. The gearbox ratio depends on the number of poles and the type of generator. As mentioned in Section 2.9.2.3, there are direct driven generators. A direct driven generator would require a generator with 600 poles to generate electricity at 50 Hz. A fixed speed generator generally has a gearbox ratio of 50:1 to give accurate frequency.

2.11.1 Structural modelling

Structurally the gearbox must withstand various dynamic loads depending on the configuration. Steady, as well as transient, loads are present and they will all contribute to the fatigue damage and wear of the generator. From a structural modelling point of view, the stiffness and damping properties are generally included in the settings for the complete drive train. However, the stiffness of the drive train is of great importance and must be properly set in order to accurately predict, e.g. the edgewise loads.

Chapter 3

Wind turbine design calculations

3.1 Introduction

Wind energy technology has developed rapidly over the last 10 years. Larger machines as well as new design trends are introduced, which demands more sophisticated design tools, capable of providing more accurate predictions of loads. The need and interest of placing wind turbines in complex terrain areas have increased. In such sites, high wind speed, high turbulence levels and strong gusts are frequently present. The weather conditions need careful consideration as they are suspected to seriously affect the reliability of the wind turbines. In order to back-up further exploitation of wind energy it is important to provide the industry and the certifying institutions with computational tools capable of performing complete simulations of the behaviour of wind turbines over a wide range of different operational conditions [70].

3.2 Present wind turbine design codes

A number of design codes have been used over the last ten years to model the wind turbine's dynamic behaviour, or to carry out design calculations [49, 58, 59].

In the wind energy community, the following wind turbine design codes are or have been commonly used:

- ADAMS/WT (Automatic Dynamic Analysis of Mechanical Systems – Wind Turbine). ADAMS/WT is designed as an application-specific add-on to ADAMS/SOLVER and ADAMS/View. The ADAMS package is developed by Mechanical Dynamics, Inc., and the add-on module WT is developed under contract to the National Renewable Energy Laboratory (NREL) [57].
- Alcyone is developed at the Center for Renewable Energy Sources together with the National Technical University of Athens in Greece. Alcyone uses the FE method. The code is briefly described in [62].

- BLADED for Windows. BLADED for Windows is an integrated simulation package for wind turbine design and analysis. The software is developed by Garrad Hassan and Partners, Ltd. The Garrad Hassan approach to the calculation of wind turbine performance and loading has been developed over the last fifteen years and has been validated against monitored data for a wide range of turbines of many different sizes and configurations [26].

- DUWECS (Delft University Wind Energy Converter Simulation Program). DUWECS has been developed at the Delft University of Technology with financial support from the European Community. The program has been improved in order to make DUWECS available for simulating offshore wind turbines. Lately the code has been extended to incorporate wave loads, and a more extensive soil model [39].

- FAST (Fatigue, Aerodynamics, Structures, and Turbulence). The FAST code is being developed through a subcontract between National Renewable Energy Laboratory (NREL) and Oregon State University. NREL has modified FAST to use the AeroDyn subroutine package developed at the University of Utah to generate aerodynamic forces along the blade. This version is called FAST-AD [76].

- FLEX5. The code is developed at the Fluid Mechanics Department at the Technical University of Denmark. The program simulates, e.g., turbines with one to three blades, fixed or variable speed generators, pitch or stall power regulation. The turbine is modelled with relatively few degrees of freedom combined with a fully nonlinear calculation of response and loads [55].

- FLEXLAST (Flexible Load Analysing Simulation Tool). The development of the program started at Stork Product Engineering in 1982. Since 1992, FLEXLAST has been used by Dutch industries for wind turbine and rotor design. The program has also been used for certification calculations by a number of foreign companies [73].

- GAST (General Aerodynamic and Structural Prediction Tool for Wind Turbines). GAST is developed at the fluid section, of the National Technical University of Athens. The program includes a simulator of turbulent wind fields, time-domain aeroelastic analysis of the full wind turbine configuration and post-processing of loads for fatigue analysis [70].

- HAWC (Horizontal Axis Wind Turbine Code). HAWC is developed at Risø in Denmark. The model is based on the FE method using the substructure approach. The code predicts the response of horizontal axis two- or three-bladed machines in time domain [41].

- PHATAS-IV (Program for Horizontal Axis Wind Turbine Analysis Simulation, Version IV). The PHATAS programs are developed at ECN Wind Energy of the Netherlands Energy Research Foundation. The program is developed for the design and analysis of on-shore and offshore horizontal axis wind turbines. The program includes a model for wave loading [44].

- TWISTER. The program is developed at Stentec B.V. The development of the aeroelastic computer code of Stentec was started in 1983 and was called FKA. For commercial reasons, the name has been changed to TWISTER in 1997. Since 1991 the code supports stochastic windfield simulation and has been used for the development and certification of a number of wind turbines, mainly from Dutch manufacturers, like Lagerwey, DeWind and Wind Strom Frisia [66].

- VIDYN. VIDYN is a simulation program for static and dynamic structural analysis for horizontal axis wind turbines. The development of VIDYN began in 1983 at Teknikgruppen AB, Sollentuna, Sweden, as a part of an evaluation project concerning two large Swedish prototypes: Maglarp and Näsudden [25].

- YawDyn. YawDyn is developed at the Mechanical Engineering Department, University of Utah, with support of the National Renewable Energy Laboratory (NREL), National Wind Technology Center. YawDyn simulates e.g. the yaw motions or loads of a horizontal axis wind turbine, with a rigid or teetering hub. In 1992, the aerodynamics analysis subroutines from YawDyn were modified for use with the ADAMS program, which is mentioned above [30].

The structural dynamic methods found in these codes can be roughly classified into three types of approach: multiple rigid bodies (MBS), finite element methods, and the assumed-modes approach. Despite certain differences in implementation, it can be said that MBS is used in ADAMS/WT, DUWECS and FLEXLAST, FEM is used in Alcyone, GAST, HAWC and TWISTER, and the assumed-modes approach is used in BLADED, FAST-AD, FLEX5, GAROS and VIDYN, [17, 62].

There are noticeable differences between the codes, e.g. not all codes include torsional blade deflections and most of them assume that deflections are small and that the aerodynamic loads can be applied to the un-deformed structure [61]. In reference [61] it is also concluded that these assumptions are becoming less relevant with the present development towards flexible turbines. According to [61], the current key issues of aeroelastic modelling are stability, large blade deflections and prediction of aerodynamic modal damping using 3D computational fluid dynamics (CFD).

The main motivation of the code developed in the present project is to include effects due to large blade deflections. Typical effects are e.g. reduced rotor diameter of the rotor, coupling between edgewise and torsional forces and motions, increased flapwise stiffness caused by centrifugal relief due to geometric nonlinearities, etc. Further are all loads applied on the deformed geometry.

3.3 Wind field representation

It is very important for the wind industry to accurately describe the wind. Turbine designers need the information to optimise the design of their turbines and turbine investors need the information to estimate their income from electricity generation.

Various parameters need to be known concerning the wind, including the mean wind speed, directional data, variations about the mean in the short term (gusts), daily, seasonal and annual variations, and variations with height. These parameters are highly site specific and can only be determined with sufficient accuracy by measurements at a particular site over a sufficiently long period. From the point of view of wind energy, the most striking characteristic of the wind resource is its variability. The wind is changing both geographically and temporally. Furthermore, this variability persists over a wide range of scales, both in space and time, and the importance of this is amplified by the cubic relationship to the available power [47]. There are many computer programs available for numerical simulations of the fluctuating wind fields. A review of the underlying theory will not be presented in this thesis. However, a relatively detailed description is given in e.g. [8]. The wind generator used in the present work is presented in 4.5.3.

3.4 Rotor aerodynamics

Various methods can be used to calculate the aerodynamic forces acting on the blades of a wind turbine. The most advanced ones are numerical methods solving the Navier-Stokes equations for the global compressible flow as well as the flow near the blades. The method that is generally used for aeroelastic time calculation is based on the blade element momentum theory. The blade element method is used in the present work and a brief introduction to the theory is presented in the following section.

3.4.1 Blade element theory

For the use of aeroelastic codes in design calculations, the aerodynamic method has to be very time efficient. The Blade Element Momentum (BEM) theory has been shown to give good accuracy with respect to time cost.

In this method, the turbine blades are divided into a number of independent elements along the length of the blade. At each section, a force balance is applied involving 2D section lift and drag with the thrust and torque produced by the section. At the same time, a balance of axial and angular momentum is applied. This produces a set of non-linear equations which can be solved numerically for each blade section. The description follows [31, 36].

The classical actuator disc theory considers the forces in flow direction. The BEM theory also takes notice of the tangential force due to the torque in the shaft. The lift force L per unit length is perpendicular to the relative speed V_{rel} of the wind:

$$L = \frac{\rho c}{2} V_{\text{rel}}^2 C_L \tag{3.1}$$

where c is the blade cord length. The drag force D per unit length, which is parallel

to V_{rel} is given by

$$D = \frac{\rho c}{2} V_{\text{rel}}^2 C_D \tag{3.2}$$

Since we are interested only in the forces normal to and tangential to the rotor-plane, the lift and drag are projected on these directions, Figure 3.1.

$$F_N = L\cos\phi + D\sin\phi \tag{3.3}$$

and

$$F_T = L\sin\phi - D\cos\phi \tag{3.4}$$

The theory requires information about the lift and drag airfoil coefficients C_L and C_D. Those coefficients are generally given as functions of the angle of incidence, Figure 3.2.

$$\alpha = \phi - \theta \tag{3.5}$$

Further, it is seen that

$$\tan\phi = \frac{(1-a)U_\infty}{(1+a')\omega r} \tag{3.6}$$

In practice, the coefficients are obtained from a 2D wind-tunnel test. If α exceeds about 15°, the blade will stall. This means that the boundary layer on the upper surface becomes turbulent, which will result in a radical increase of drag and a decrease of lift. The lift and drag coefficients need to be projected onto the NT-direction.

$$C_N = C_L\cos\phi + C_D\sin\phi \tag{3.7}$$

and

$$C_T = C_L\sin\phi - C_D\cos\phi \tag{3.8}$$

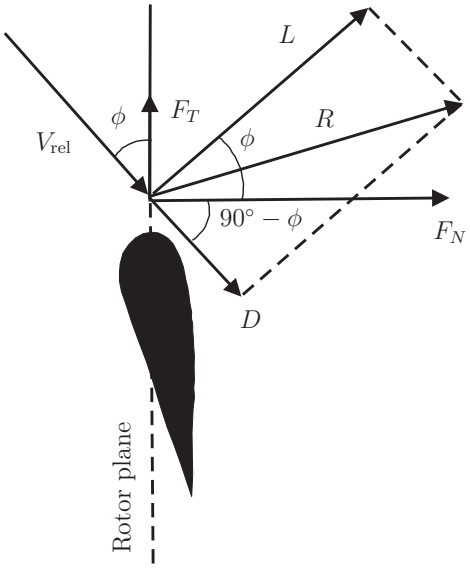

Figure 3.1: The local forces on the blade. Redrawn from [31].

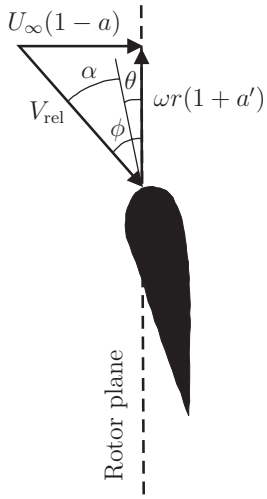

Figure 3.2: Velocities at the rotorplane. Redrawn from [31].

Further, the solidify σ is defined as the fraction of the annular area in the control volume, which is covered by the blades

$$\sigma(r) = \frac{c(r)N}{2\pi r} \tag{3.9}$$

where N denotes the number of blades.

The normal force and the torque on the control volume of thickness $\mathrm{d}r$, is since F_N and F_T are forces per length

$$\mathrm{d}T = NF_N\mathrm{d}r = \frac{1}{2}\rho N\frac{U_\infty^2(1-a)^2}{\sin^2\phi}cC_N\mathrm{d}r \tag{3.10}$$

and

$$\mathrm{d}Q = rNF_T\mathrm{d}r = \frac{1}{2}\rho N\frac{U_\infty(1-a)\omega r(1+a')}{\sin\phi\cos\phi}cC_t r\mathrm{d}r \tag{3.11}$$

Finally, the two induction factors are defined as

$$a = \frac{1}{\dfrac{4\sin^2\phi}{\sigma C_N} + 1} \tag{3.12}$$

and

$$a' = \frac{1}{\dfrac{4\sin\phi\cos\phi}{\sigma C_T} - 1} \tag{3.13}$$

All necessary equations have now been derived for the BEM model. Since the different control volumes are assumed to be independent, each strip may be treated separately and therefore the results for one radius can be computed before solving for another one. For each control volume, the algorithm can be divided into eight steps:

1. Initialize a and a', typically $a = a' = 0$.
2. Compute the flow angle, ϕ, using (3.6).
3. Compute the local angle of attack using (3.5).
4. Read $C_L(\alpha)$ and $C_D(\alpha)$ from the airfoil data table.
5. Compute C_N and C_T from (3.7) and (3.8).
6. Calculate a and a' from (3.12) and (3.13).
7. If a and a' has changed more than a certain tolerance: go to step 2, else continue.
8. Compute the local forces on each element of the blades.

In a FE implementation the loads of each blade element are transformed to the corresponding node in structural model. It is of course possible to use more elements in the BEM method, compared to the FEM model, and then integrate the loads to the available FEM node.

This is, in principle, the BEM method, but in order to get better results, the BEM model needs to be extended. For instance, in AERFORCE [7], a package used in the present work for calculation of the aerodynamic forces, the BEM method has been extended to incorporate:

- Dynamic inflow: unsteady modelling of the inflow for cases with unsteady blade loading or unsteady wind.
- Extensions to BEM theory for inclined flow to the rotor disc (yaw model).
- Unsteady blade aerodynamics: the inclusion of 2D attached flow, unsteady aerodynamics and a semi-empirical model for 2D dynamic stall.

The theory has been found to be very useful for comparative studies in wind turbine developing. In spite of a number of limitations, it is still the best tool available for getting good, first order predictions of thrust, torque and efficiency for turbine blades over a large range of operating conditions. The used model AERFORCE with its dynamic stall model DynStall have been verified in [54].

3.5 Loads and structural stresses

Wind turbines are exposed to very specific loads and stresses. Due to the nature of the wind, the loads are highly changeable. Varying loads mean that the material of the structure is subjected to fatigue which must be accounted for in the dimensioning of the wind turbine. Further, because of the low density of air, the blades need a

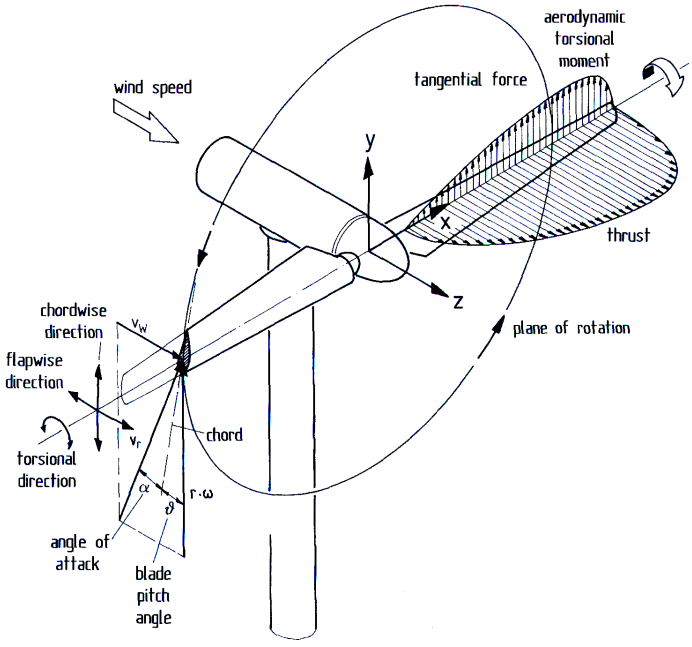

Figure 3.3: Terms used for representing displacements, loads and stresses on the rotor. Reproduced from [33].

large area in order to capture the wind efficiently. However, with increasing size, the structure will behave more elastically. The combination of the flexible structure and the varying loads will create a complex interplay, which may cause instability problems. Computationally it is very convenient to evaluate loads, stresses and strains in the developed tool. Most of the directions and loads referred to are illustrated in Figure 3.3. The chordwise direction is often called edgewise direction.

3.5.1 Uniform and steady flow

The most simple load case for the primary function of the turbine is assuming uniform and steady flow. That assumption is an idealisation which does not exists in the free atmosphere. The concept is nevertheless useful for calculating the mean load level, occurring over a longer period of time. The wind loads on the rotor blades, when assuming uniform and steady flow, will depend mainly on the effective wind speed increasing from blade root to blade tip. The bending moments on the rotor blades in the chordwise direction, Figure 3.4, result from the tangential loading. The thrust force distribution, Figure 3.5, is generating the moments in flapwise direction. The thrust and tangential force distributions change with wind speed or from start-

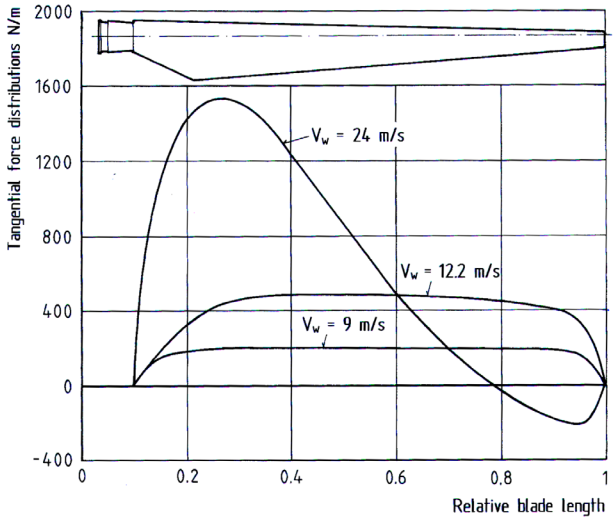

Figure 3.4: Aerodynamic tangential load distribution over the blade length of the experimental WKA-60 wind turbine. Reproduced from [33].

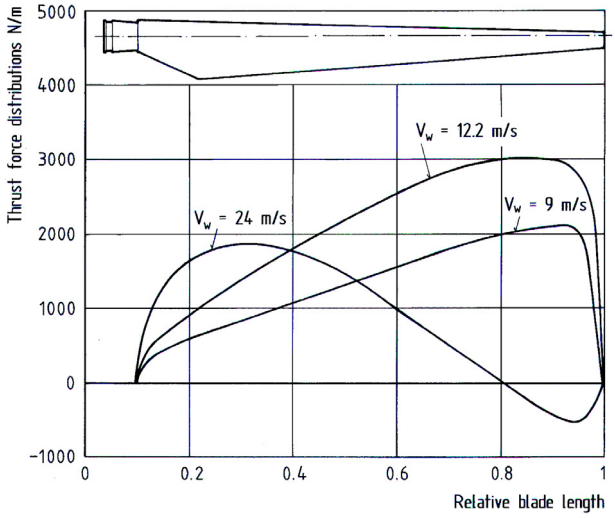

Figure 3.5: Aerodynamic thrust load distribution over the blade length of the experimental WKA-60 wind turbine. Reproduced from [33].

up speed to the shut-down speed. The rotor blade twist is the main reason for this. The blade twist is optimised for nominal wind speed only, so that the aerodynamic forces correspond to an optimum only for the nominal speed.

3.5.2 Nonuniform and unsteady flow

The increase of wind speed with altitude is known as wind shear. The asymmetry of the incoming wind flow will make the rotor blades in the upper rotational sector more exposed to higher loads than in the sector near the ground. A similar asymmetry is the crosswinds which are caused by fast changes in wind direction. The vertical wind shear and crosswinds on the rotor lead to cyclic increasing and decreasing load distribution over the rotor blades. Turbulence is the source of both the extreme gust loading and a large part of the blade fatigue loading. From the simulation viewpoint, turbulence can be seen as random wind speed fluctuations imposed on the mean wind speed. These fluctuations occur in all three directions: longitudinal (in the direction of the wind), lateral (perpendicular to the average wind) and vertical. The wind conditions are modelled in a wind generator software like e.g. SOSIS-W [9] that is further described in 4.5.3.

3.5.3 Tower interference

The air flow is blocked by the presence of the tower, which results in regions of reduced wind speed, both upwind and downwind the rotor. In order to keep the nacelle as short as possible, the clearance of the rotor rotational plane to the tower is small. However, the small distance creates an aerodynamic flow around the tower which will influence the rotor. The reduced flow towards the rotor blades, when the tower's wake is passed, leads to a sudden decrease of the rotor blade lifting forces. The sharp dip in blade loading caused by tower shadow is more prone to excite blade oscillations than the smooth variations in load due to wind shear, shaft tilt and yaw [8]. The tower shadow effects are accounted for in the simulations by a tower shadow model, [6], that calculates the reduction of wind speed depending on e.g. the clearance between the blade and the tower.

3.5.4 Gravitational, centrifugal and gyroscopic forces

It is fairly straightforward to calculate the loads caused by the weight of the components and by centrifugal and gyroscopic forces when the masses are known. However, as the mass introduced loads only can be calculated as a consequence of the complete load spectrum, several iterations are required in the structural dimensioning before the final properties can be decided. It is noted that several of these effects will only be complicated in an analysis if a detailed discretisation is used.

Naturally, the weight from all the different components must be taken into account for a correct physical model of the wind turbine. The rotor blade weight is of special significance for the blades themselves, but also for the connected components. Due to the rotor revolution, the blade weight will generate sinusoidally varying tensile and compressive forces along the length of the blade, but, above all, a varying moment around the chordwise (edgewise) axis of the blades, Figure 3.3. As for any other structure, when scaling up the dimension, the gravity induced loads will be a

problem. The effects of the increased gravity loads will become even more evident in the case of a rotating rotor where alternating loads occur.

Due to their relatively low speed of revolution, centrifugal forces are not very significant for stiff wind rotors. Thrust loading causes flexible blades to deflect downwind, with the result that centrifugal forces will generate out-of-plane moments in opposition to those due to the thrust. This reduction of the moment due to thrust loading is known as centrifugal relief [33]. The effects of centrifugal loads are more evident in the case of flexible blades. In a modelling point of view the centrifugal loads are calculated based on the deformed displacements so that the effects of centrifugal relief are taken into account.

When the turbine yaws, the blades experience gyroscopic loads perpendicular to the plane of rotation. A fast yaw motion leads to large gyroscopic moments that act on the rotor axis. In practice, the controller is programmed to yaw the rotor so slow that gyroscopic moments do not play a role.

Computationally the loads mentioned above are in FEM automatically accounted for through the mass matrix.

Chapter 4

Finite element modelling of wind turbines

Most aeroelastic codes used in practical design work assume small blade deflections and application of loads on the un deflected structure. However, with the design of lighter and more flexible wind turbines, these assumptions may not longer be valid. This thesis has had the objective to improve current modelling possibilities by including effects of geometrical nonlinearities primarily introduced by large blade deflections.
This chapter describes the development of the aeroelastic tool, that is based on the commercial software MSC.Marc [50], and how the different components can be modelled within the FE method in general and with MSC.Marc in particular.

The choice of FEA program is always a compromise since all programs have their strengths and drawbacks. A fundamental requirement for this specific application was the possibility to write user supplied load subroutines. For instance ABAQUS, ANSYS and SOLVIA have this support. Aeroelastic calculations based on the FE software SOLVIA, [43], are described in the author's licentiate thesis [1]. The conclusion was that SOLVIA lacked some features required for advanced wind turbine simulations. The main problem was that only pipe elements could be used in large rotation analyses. Consequently, the stiffness properties could only be given in one direction. Further conclusions were that constraint equations, concentrated springs and dampers etc. were needed to be associated with local coordinate systems updated by the user in each iteration.
Since the licentiate thesis was presented in 2002, SOLVIA has been replaced by MSC.Marc [50]. A more detailed description of MSC.Marc is given in Section 4.5.1.

4.1 General feature requirements

FE modelling of wind turbines requires special considerations due to both large displacements and rotations. The use of constraint equations that defines one or several DOFs as function of one or several other DOFs is one of the key features for

wind turbine modelling within the FEM theory. In MSC.Marc, user-defined constraint equations are given through user subroutines. This constraint can be linear or nonlinear, i.e., it can be dependent on time or previous deformations. Constraint equations are typically used to specify the connection between rotor shaft and bedplate. Another example is modelling of a possible pitch system. Constraints could then be set to, e.g. tie all DOFs except the rotational DOF in the pitching point (pitch bearing). All constraint equations must be specified on the deformed geometry to allow for large displacement analysis. The constrained nodes must therefore be specified in local coordinate systems. The general method in MSC.Marc is to implement user-defined local coordinate systems through subroutines. This allows transformation of degrees of freedom at an individual node from global directions to a local direction through an orthogonal transformation. The transformations could then be updated by user in each increment. User-defined systems are also used to specify springs and dashpots in local systems.

4.2 Element considerations

Simulating wind turbine response in time, using FEM, is computationally intensive. Time simulations are therefore generally made using beam elements to reduce DOFs. There are several blade element types available. The most common types are based on the Euler-Bernoulli or the Timoshenko beam theories, [56]. The Timoshenko element, class C^0, takes into account shear deformation and rotary inertia but uses low order shape functions, which basically mean discontinuous first derivatives. The Euler-Bernoulli element belongs to the class C^1 which means continuous first derivatives between blade elements. The Euler-Bernoulli theory does not include rotary inertia in the formulation of the kinetic energy, as it is implicitly contained in the translation terms. The only rotary inertia neglected is the rotational inertia of the cross-section which always remains low for a slender beam. However, concentrated nodal inertias are supported by MSC.Marc. Both element types are included in the element library together with beam elements including warping DOFs.
There are very few restrictions in MSC.Marc regarding the choice of element type. The main reason for not using shell elements is the computational cost. The Domain Decomposition (DDM) method is implemented. The method makes it possible to split up the problem into domains and solve the system in parallel.
The Euler-Bernoulli beam was chosen because of the slender nature of the structure, which make shear effects small. Comparisons have been made between the two element types in time simulations and the results are nearly identical. All elements used are 3D beams with six-DOFs per node. The DOFs are three global displacements and three global rotations.

4.3 Component modelling

4.3.1 Tower

The tower is one of the main components of a wind turbine and its physical properties will highly influence the overall dynamics. By using a commercial FE program, it is possible to relatively easily model different types of tower concepts, like tubular or lattice towers, different geometries and materials, but also the used discretisation. In most cases, it is sufficient to describe the tower with a rather sparse beam element model in order to catch the overall structural behaviour. If the purpose of the model is to study the tower in detail, e.g. optimising dimension or study buckling phenomena, a shell element formulation might be a better choice, but this would only lead to minor modifications of an existing model. The number and type of element is always a balance between computational cost and accuracy.

Most wind turbine towers are shaped conically. The procedure used to describe the conical shape in the current work was to produce a number of pipe elements and associate each element with constant thickness and diameter properties. The element used is a thin-walled Euler-Bernoulli beam with 16 numerical integration points in the circumference. Tapered beam elements would have been preferred but are unfortunately not implemented in MSC.Marc.

4.3.2 Blades

The function of the rotor is to convert part of the power contained in the wind stream into mechanical energy. While it is theoretically possible to design a turbine with any number of blades, current implementation is limited to work with two or three bladed rotors.
The blades are modelled with beam elements. MSC.Marc offers the possibility to specify user defined cross-sections of any shape, allowing non-coincident mass and shear centres. Standard rectangular cross-sections are defined by area, moment of inertia about local x and y axis, Figure 4.1. The torsional stiffness can be calculated based on the specified bending moment of inertias, or be directly specified. The results presented in this thesis were calculated with rectangular cross-sections, where for simplicity shear centre, mass centre and pitch axis were assumed to coincide. The aerodynamic forces are calculated on the blade's 25% chord axis. The offset of the aerodynamic centre introduces a torque that is accounted for in the simulations.

The mass of the blade can be calculated automatically from the mass density or be specified as concentrated nodal masses. Further, the element mass matrices can be specified to be either consistent or lumped.

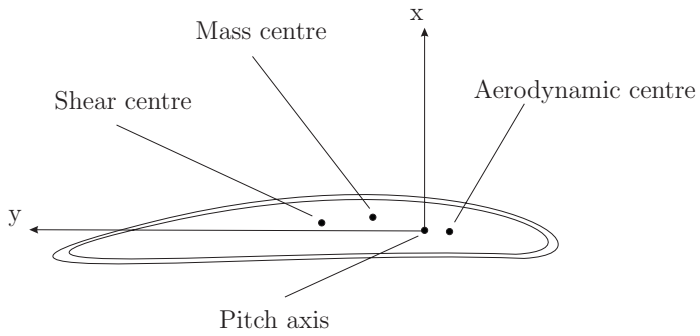

Figure 4.1: Airfoil.

4.3.3 Drive train and bedplate modelling

In most cases it is possible to model the drive train with finite elements. By using constraint equations it is possible to accomplish the speed ratios between the different shafts. Only the low speed shaft is modelled in the current implementations. Hence all moments of inertia were derived based on the low speed shaft.

Figure 4.2 illustrates the bedplate and the rotor axle as a FEM model. In the figure, the node pairs *A-B*, *C-D*, *E-F* are located at the same coordinates, but for illustrative reasons the axle is shown above the bedplate. The double nodes are used to specify constraint equations expressing slave (dependent) degrees of freedom as linear or nonlinear combinations of master (independent) degrees of freedom. In the figure, the nodes *A, C, E* are modelled as master nodes and the nodes *B, D, F* as slaves. For each master/slave node combination, constraints are set for translation in *X, Y, Z*, respectively. By using springs in addition to the constraint equations, the bearing stiffnesses can be set in all translational and rotational DOFs. That approach has been used in the Alsvik example in Paper 1, to give the turbine correct stiffness in yaw and tilt directions. The mass of the bedplate is typically applied as a point mass at the centre of gravity. At the same point are the moments of inertia applied for each rotational DOF.

The type of generator used in the present work has been the constant speed type. The basic idea is that the rotational speed of an asynchronous generator varies slightly with the load. In practice, the slip is low, about 2–3%. The generator's ability to slightly vary its speed is a very useful mechanical property. The variation means that there will be, due to lower peak torque, less fatigue in the gearbox. Figure 4.3 shows the generator torque as function of the shaft speed. When the current is connected, the machine starts turning like a motor at a speed which is just slightly below the synchronous speed of the rotating magnetic field from the stator. However, the wind causes the turbine to run faster than the rotating magnetic field from the stator and a strong current in the stator is induced. The higher the wind velocity, the more power will be transferred as an electromagnetic force to the stator, and the more electricity is transferred into the grid.

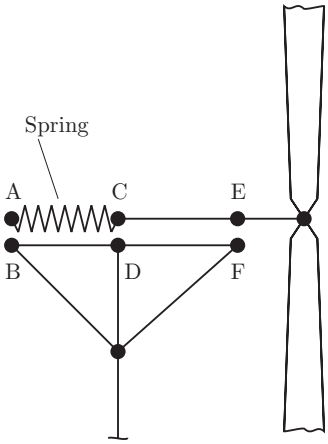

Figure 4.2: Bedplate model.

A simple constant speed asynchronous generator with data based on the Alsvik turbine is, in the present work, implemented as:

$$M_{\text{gen}} = 457600 \left[\omega_{\text{rot}} - \frac{42.35\pi}{30} \right] \tag{4.1}$$

where ω_{rot} is the generator rotational velocity, measured in each time iteration. The expression introduces a penalty moment, striking towards the correct rotational speed. The linear function derived in (4.1) above is a simplification of the torque-

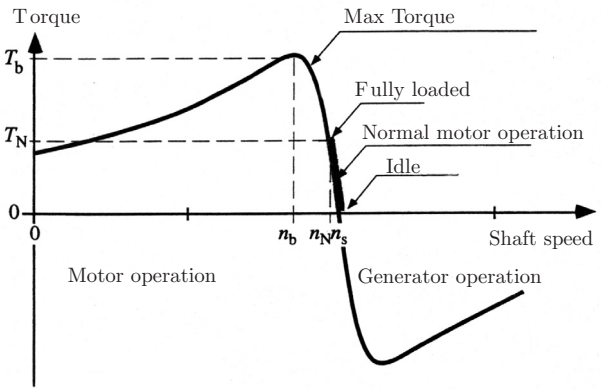

Figure 4.3: Torque as a function of the shaft speed for an asynchronous machine. Reproduced from [75].

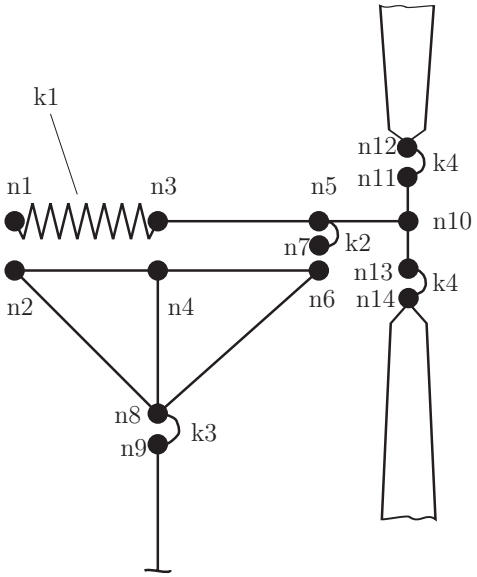

Figure 4.4: Pitching constraints schematic.

speed graph in Figure 4.3 around the idle speed.
A modification is made to equation (4.1) in order to prevent overloading at startup. The modified equation is in use the first 20 seconds of simulation and will give a softer startup sequence. A time variable t is introduced as:

$$M_{\text{gen}} = 457600 \left[\omega_{\text{rot}} - \frac{42.35\pi}{30} \left(\frac{t}{20} \right) \right], (t \leq 20) \tag{4.2}$$

In performed experiments, this method has been found successful.

4.3.4 Pitching system

Pitching of the blades to control the produced power or for braking the turbine are achieved by using constraint equations in a rotating coordinate system. All degrees of freedom are locked, except the rotational degree of freedom around the blade axis. Figure 4.4 illustrates the connections between rotor hub and blades, where the constrained node pairs are n11–n12 and n13–n14. The two nodes in each node pair are located at the same coordinate. Rotational dampers are used between the nodes in a pair, to give a softer settling to the desired pitch angle. The stiffness of the pitch actuator can be set by using linear or nonlinear springs updated by user depending on, e.g. pitch angle or pitch rate. The actual pitching of the blades is carried out by control moments that are set depending on each blade's desired pitch angle. A simple implementation of a pitch control system is described in Figure 4.5. This type has been used to model the Tjæreborg pitching system in Paper 2. In the

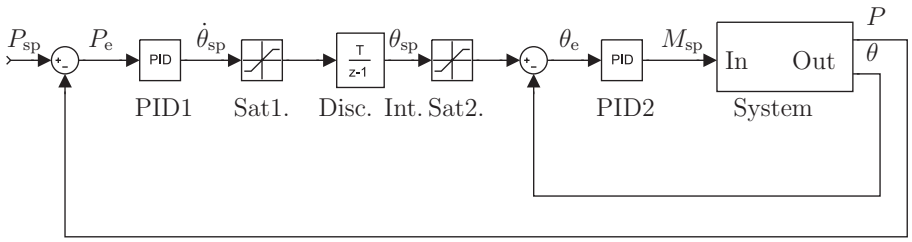

Figure 4.5: Simple blade pitch control system.

figure, PID1 controls the pitch rate depending on the power. Sat1 limits the pitch rate. The integrator integrates the pitch rate to the corresponding pitch angle. Sat2 limits the pitch angle. PID2 adjusts the pitching moment to the desired pitching angle. The system box represents the wind turbine dynamics. P is the electrical power; set point, error and actual. $\dot{\theta}_{sp}$ is the pitch rate set point. θ is the pitch angle; set point, error and actual. M_{sp} is the pitch moment set point.
The implemented pitching system means real pitching of the beam cross sections. The drawback is that an additional control system for setting the pitching moment is needed. The two control systems must be properly designed to avoid instabilities.

An alternative method, currently not implemented, is to introduce pitching of the blades by the use of actuator links. The actuator link is a simple linear straight truss with a constant cross section. The strain-displacement relations are written for large strain, large displacement analysis. The length of the actuator link element can be prescribed during a dynamic analysis by user subroutines. The subroutine allows control of the length of the actuator in an incremental analysis. Figure 4.6 illustrates the pitch mechanism of the Tjæreborg turbine. A representative FE implementation could be to model the safety cylinder as a actuator link element. The actuator links can then be connected to the blade and yoke by pin joints formulated in the rotating system. The actuator link element is implemented in MSC.Marc and would give a simpler control system. Both implementations described above introduce additional dynamics compared to when kinematics are directly prescribed. In the first implementation, a direct coupling between control of the pitching moment and the external torsional forces and torsional vibrations is achieved.

4.3.5 Yaw system

The yaw mechanism is achieved by using constraint equations between tower top and bedplate. The translational DOFs between node n8–n9 in Figure 4.4 are locked. The stiffnesses in yawing, rolling and tilting are then set by rotational springs. These are associated with a local coordinate system to allow large rotation yawing.

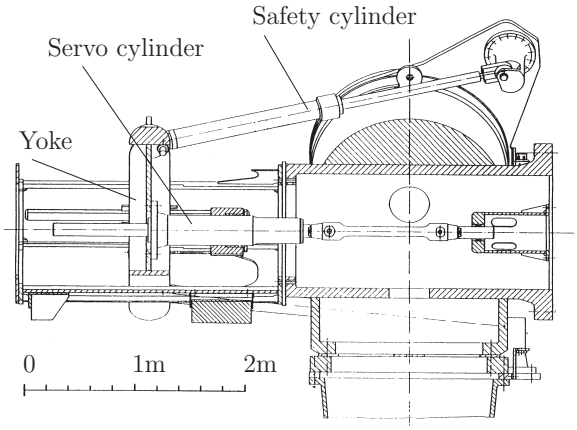

Figure 4.6: Blade pitch system. Reprinted from [34].

4.3.6 Foundation

Current implementation has assumed rigid connection to ground. However, linear or nonlinear elastic foundations could easily be implemented, if this would be considered of importance for dynamic behaviour.

4.4 Solution methods

4.4.1 Damping

In a transient dynamic analysis, damping represents the dissipation of energy in the structural system. For direct integration damping, it is possible to specify the damping matrix as a linear combination of the mass and stiffness matrices of the system.

$$\mathbf{C} = \sum_{i=1}^{n} \{\alpha_i \mathbf{M}_i + (\beta_i + \frac{\gamma_i \Delta t}{\pi}) \mathbf{K}_i\} \tag{4.3}$$

where $\mathbf{C}$ is the global damping stiffness, $\mathbf{M}_i$ and $\mathbf{K}_i$ the mass and stiffness contributions of the ith element. α_i, β_i and γ_i are the damping coefficients of the ith element. The damping coefficients can be set individually for each element (for example the bedplate could be given one set of parameters and the tower another set). If the same damping coefficients are used throughout the structure, the type of damping is equivalent to Rayleigh damping, [28]. A disadvantage with the method is that it damps the rigid motions as well. Hence, the method is not suitable for blade damping. The alternative method is to introduce damping through springs and mass points. The method makes it possible to set unique damping properties for each nodal DOF and associate them to local coordinate systems updated in each

increment. The damping forces are then calculated based on the local velocities, in the rotating blade root system, of each blade element.

The method used in the present work to introduce damping to the blades, is to assign a corotational blade root system to each blade node. The damping is thereby referred to the blade root system and the damping properties can be set independently in flap, edge and torsional direction. The damping properties are determined by loading and unloading the rotor. The logarithmic decrements are then calculated from the time responses of the free oscillating displacements in respective direction. It is also possible to use non-linear dampers and dampers with different behaviours in positive and negative directions, although this is currently not implemented.

A modal analysis of a LM19 m blade is described in [40]. The damping characteristics derived as logarithmic decrements are in the range 2–5 %. The damping are, for a given type of mode (flap dominated, edge dominated or torsion dominated), increasing with increasing natural frequency.

4.4.2 Numerical methods and tolerances

Numerical simulations in the time domain highly depend on the time integration algorithm concerning accuracy, numerical stability and calculation effort. Many time integration schemes are available, all of which have some advantages and disadvantages in special cases.

Explicit schemes are only conditionally stable and very short steps are often necessary. In explicit methods dynamic equilibrium is considered at time t and possible previous steps to evaluate the solution at time $t + \Delta t$ in a closed step. If Δt exceeds a certain fraction of the smallest vibration period of the structure, computed displacement and velocity errors grow without bound. For this reason, these algorithms are commonly used for simulations of very short periods (e.g. impact or crash simulations). In civil engineering structures these schemes are rarely needed as most systems respond in low frequencies [60].

Implicit methods, such as Newmark methods, attempt to satisfy the differential equation at time $t + \Delta t$ after the solutions at time $t - i\Delta t \;\; (i = 0, 1, 2, ..., n)$ are found. These methods require the solution of a set of equations at each time step. However, larger time steps may be used. Implicit methods are conditionally or unconditionally stable, depending on the defining parameters.

While unconditional stability can be guaranteed in linear analysis for many implicit methods, nonlinear simulations are stable only when there is no additional dissipation of energy due to numerical characteristics (especially due to geometrical nonlinearities). An arbitrary increase of energy arises from very high frequency oscillating within the current time step. By suppressing these oscillations sufficiently, the calculation can be stabilised.

In MSC.Marc it is possible to choose between three integration methods, namely: Newmark-beta, Houbolt and the Single Step Houbolt (SSH) method, [2,10,28]. All of

the above mentioned methods have been tested. The first eigenfrequencies of a wind turbine are generally located well below 10 Hz. Therefore, high frequencies could be damped out without any particular influence on the dynamic behaviour. The SSH method, which introduces numerical damping, has been used in the present work. The SSH method, developed by Chung and Hulbert [10], is unconditionally stable, second-order accurate and asymptotically annihilating. The method is designed to include numerical dissipation characteristics, particularly for higher frequencies. Particular choices of the SSH method parameters, γ and γ_1, influence the global error growth and velocity overshoot. In general, γ_1 is related to γ as $\gamma = \frac{1}{2}(\frac{1}{2} - \gamma_1)$. Depending on the problem it is possible to choose either $\gamma_1 = 3/2$ to minimize velocity error or $\gamma_1 = 1/2$ to avoid velocity overshoot.

The chosen time step is of extreme importance for a successful simulation. A general recommendation is that the time step should not exceed one tenth of the period of the highest frequency of interest, [51]. The time step used in most of the simulations was 6 ms, which corresponds to 167 Hz. The chosen time step has been proven successful in current work.

There exist several options for how to formulate the finite element equations for nonlinear deformations. MSC.Marc includes three types of approaches: Lagrangian Formulation, Eularian Formulation and the Arbitrary Lagrangian-Eulerian Formulation. In the total Lagrangian formulations all static and kinematic variables are referred to the initial un deformed configuration, while in the updated Lagrangian formulation all static and kinematic variables are referred to the current configuration, [4]. Both the total Lagrangian and updated Lagrangian formulations include all kinematic nonlinear effects due to large displacement, large rotations and large strains. The updated Lagrangian approach is most suitable of the three types in large rotation analysis and is therefore used in the simulations. The reasons are the many rotations in a simulation and that the results are given in the floating reference frame, which make interpretation of the results easy.

There are four iterative procedures available in MSC.Marc: Newton-Raphson, Modified Newton-Raphson, Newton-Raphson with strain correction modification, and a secant procedure. The full Newton-Raphson was used in the simulations for equilibrium iterations in each time increment, together with a sparse direct solver or a multifrontal direct sparse solver. The multifrontal direct sparse solver solves the nonsymmetric system of equations which is important for studying Coriolis effects in transient dynamic analysis. However, the nonsymmetric problem uses twice as much memory for storing the stiffness matrix and the solution time is substantially increased. An approximate solution is obtained using the symmetric solver. Simulations have been performed with both solvers, but the results are almost unchanged in normal operational conditions.

Three possible convergence criteria are available in MSC.Marc: residual checking, displacement checking and strain energy checking. Combined convergence checking could also be used. Displacement checking was used as the criterion for convergence. The tolerance for the ratio of iterative change to increment in displacements, $\| \delta u \|_\infty \; / \; \| \Delta u \|_\infty < tol_1$, was typically set to 10^{-4}. Here, Δu is the displacement in-

crement vector and δu the correction to the incremental displacement vector. With this method, convergence is satisfied if the maximum displacement of the last iteration is small compared to the actual displacement change of the increment. A disadvantage of this approach is that it produces at least one iteration, regardless of the accuracy of the initial prediction for the time step.

4.5 Program structure

The developed wind turbine simulation tool consists of three main parts: The MSC.Marc finite element program for modelling the structural dynamics, AERFORCE for the calculation of the aerodynamic loads and SOSIS-W for the generation of the turbulent wind field. The idea of using a commercial FE program is to take advantage of the stability and versatility of a well documented program. Another advantage is that the software may be used as a tool throughout the complete design process. For instance to dimension specific parts off the structure, or to include effects from waves, etc. The generality also makes it possible to use shell elements, in future implementations, instead of the generally used beam element when modelling the blades.

When a structure is deformed, the directions and the loads are changed. For most deformed structures, such changes are so small that the effect on the equilibrium equation can be ignored. But for some structures such as a soft wind turbine, which may deflect considerably, the effects on the results can be quite significant. As described in Section 3.2, the main motivation for the developed code is to include effects due to large blade deflections. Typical effects are, e.g. reduced rotor diameter of the rotor, coupling between edgewise and torsional forces and motions, increased flapwise stiffness caused by centrifugal relief due to geometric nonlinearities, etc. In order to successfully model these effects, all loads must be applied to the deformed geometry.

4.5.1 Structural modelling

MSC.Marc allows modelling of linear and nonlinear problems involving, e.g. contacts, nonlinear material effects and structural dynamics, [50]. A main advantage with MSC.Marc is the subroutine feature that allows user to substitute existing subroutines with subroutines adopted to the specific problem. Subroutines for implementation of loads, tying constraints and local coordinate systems are especially useful in wind turbine applications. The user-supplied load is defined as a nodal load type. User-supplied routines for nonuniform distributed loads are present but are currently not implemented. The user-supplied loads are evaluated in each time step and in each iteration. These loads are added to the global load vector normally established in the response calculation for the time steps. The user-supplied loads can be calculated based on a number of different nodal parameters. Typical parameters used are e.g. information about nodal displacements and velocities. The load

contribution calculated for a node may depend on nodal quantities for other nodes.

The MSC.Marc subroutines, [52], used in the present model are *forcdt* for the input of time dependent nodal quantities as nodal forces, prescribed displacements etc. *utrans* for implementation of local coordinate systems. The user subroutine allows for local coordinate systems to be implemented at user-specified nodes. The user defined systems may be updated in each iteration by updating the rotation matrix from the local to global coordinate system. *uforms* defines constraint conditions (tying). The tyings are used for applying arbitrary homogeneous constraints between nodal displacements in global or local coordinate systems. *impd* allows for output of nodal quantities. The subroutine is used to write nodal displacements, velocities, accelerations etc. to file. *elevar* allows output of element quantities and is used for writing element (integration point) quantities to file. *nodvar, nodnum, vecftc* are used for accessing the database to get information about total and incremental nodal displacements.

Other subroutines that have been used and tested, but have not been used in the numerical examples presented in this work, are e.g. *forcem* for the input of nonuniformly distributed loads. The subroutine makes it possible to apply e.g. aerodynamic loads as line forces and moments. The loads are then consistently distributed to nodes. *usprng* for the input of nonlinear springs, dashpots and foundation stiffness. Can be used e.g. to model the stiffness and damping properties of the pitch bearing.

All Fortran subroutines as well as MSC.Marc are written in double precision. The user subroutines are linked with the MSC.Marc library and a new executable is created using *Compaq Visual Fortran Standard Edition 6.6.B* [11].

4.5.2 Aerodynamic modelling

For the calculation of the aerodynamic forces acting on the blades of the wind turbine, a subroutine package named AERFORCE [7] has been used. The aerodynamic model used in this package is based on the BEM method which has been found to be very time efficient, see Section 3.4.1. The AERFORCE subroutine is called with a number of formal parameters but communication via common blocks is also used.

Forces and velocities in AERFORCE are described in three coordinate systems. The coordinate systems are obtained from the structural dynamic program and are utilised by the AERFORCE subroutine:

- The global system: the system in which the free wind is given. The system is designated the g-system.
- The rotor system: a system that is attached to the rotor. The system is rotating with the rotor and has its Y- and Z-axes in the disc-plane. In this system the normal induction is in the X-axis direction and the tangential induced velocity is an in-plane velocity. The system is designated the r-system, Figure 4.7.

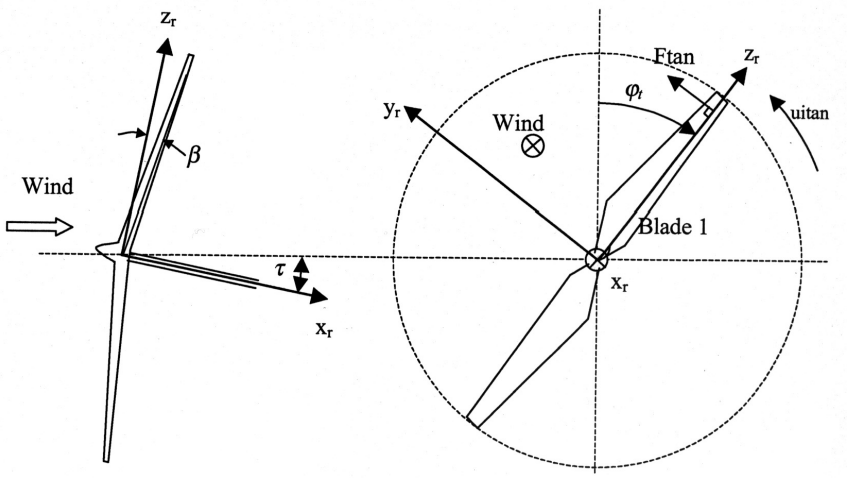

Figure 4.7: View of the rotor in the Y_r-direction and view in the X_r-direction. Reproduced from [7].

- The blade-element system: a coordinate system attached to each blade element. The blade-element system has its Y-axis aligned with the local blade chord axis. The Z-axis is aligned with the blade 25% chord axis. The system is designated the e-system. Figure 4.8 shows the relation between the r- and e-systems.

In AERFORCE, three transformation matrices are needed. Figure 4.9 illustrates an overview of the different systems and transformation matrices used in AERFORCE. The transformation matrices are named:

- Transformation from the global system to the rotor system, $\mathbf{S}_{\mathrm{gr}}$.
- Transformation from the global system to the element system, $\mathbf{S}_{\mathrm{ge}}$.
- Transformation from the rotor system to the element system, $\mathbf{S}_{\mathrm{re}}$.

The derivation of the transformation matrices is further explained in Section 4.5.4.1.

Each blade is divided into a number of blade elements. The positions of the blades and the blade elements are determined by a number of parameters. Figure 4.10 illustrates some of the parameters needed. Other blade specific parameters are needed, e.g. the chord and area of each blade element. These data are derived in the deformed state, updated in each iteration, and are defined as: r the radius to each blade element. r_{tip} the tip radius. r_{tipmom} the radius r_{tip} projected perpendicular to the X_r-axis. r_{mom} the projection of each radius r perpendicular to the X_r-axis. $\mathrm{d}r_{\mathrm{mom}}$ the blade element length $\mathrm{d}r$ projected perpendicular to the X_r-axis.

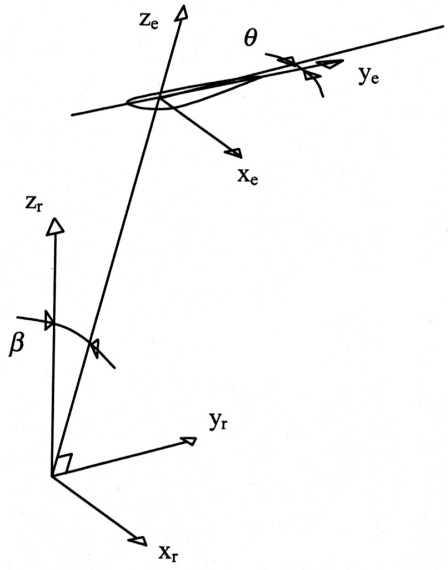

Figure 4.8: Element coordinate system. Reproduced from [7].

Other parameters used in order to predict wind loads are, for instance, the wind velocity and the upcoming velocity on each blade element. The wind velocity used in the calculations is described by three components, one in each global direction. The wind data are derived either manually in case of constant wind speed or by a wind data generator like SOSIS-W, see Section 4.5.3. The velocity of each blade element is obtained by the nodal velocities given by MSC.Marc.

The BEM theory requires information about the lift and drag airfoil coefficients C_L and C_D. If torsional pitching torque of the blades is considered, it is necessary to specify C_M. The coefficients are specified as functions of the angle of attack and are essential for accurate calculations. Each particular airfoil has its own data table describing the coefficients. The range of angles of attack in each airfoil data table must cover the angles of attack encountered during the calculations. There are also parameters that need to be set by the user, for example parameters for calculation of time varying inflow. Further information is given in [7].

The outputs from AERFORCE are the normal and tangential forces in the blade element system. If C_M is present in the airfoil data table, the blade element pitching torque is also given as output.

4.5.3 Wind modelling

SOSIS-W is an artificial wind data generator developed by Ingemar Carlén, Teknikgruppen AB [9]. The program is developed for providing time domain series of a

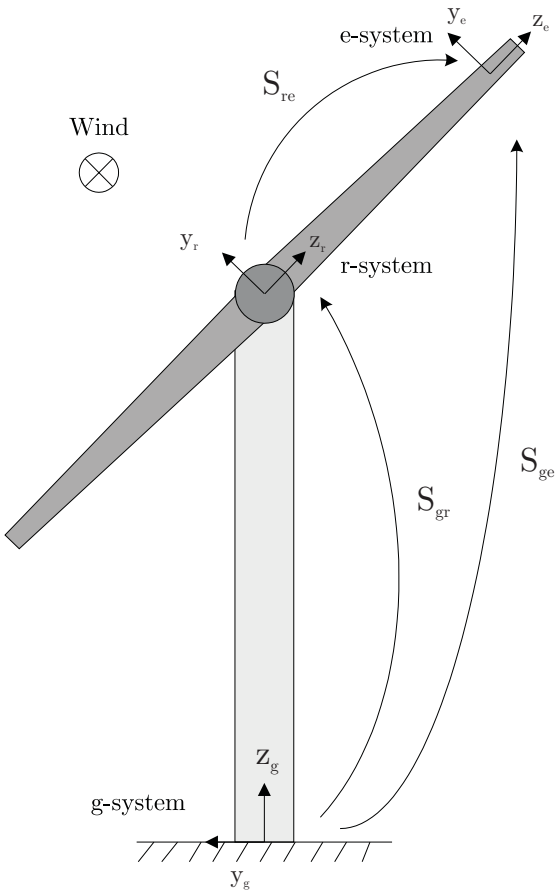

Figure 4.9: Overview of the different systems and transformation matrices used in AERFORCE.

turbulent wind field. SOSIS-W simulates three dimensional wind vectors, corresponding to gridpoints in a plane uniform Cartesian grid, where the grid plane is perpendicular to the mean wind direction.

In SOSIS-W the wind model spectral densities of u-, v-, and w-component are defined either by the International Electrotechnical Commission (IEC) version of the Kaimal spectra, the IEC-version of the von Karman spectra, or the Engineering Science Data Unit (ESDU) version of the von Karman spectra. For additional information about SOSIS-W and its abilities, see [9].

SOSIS-W creates three output files, one for each global direction. The output data are arranged in rows and columns where each row represents a time series and each element in a time series represents the velocity at a specific coordinate.

Figure 4.11 shows an example of a grid net of size 4×4 and a rotor with its blades di-

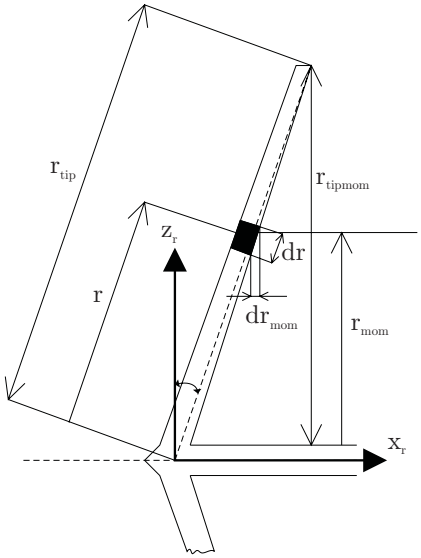

Figure 4.10: Geometric definitions of the rotor.

vided into 4 elements. However, in real simulations the resolution must be increased, typically a grid net size of 12×12 are used in the simulations. Depending on the angle ϕ, the time and the distance from the hub to the centre of each blade element, the velocity is evaluated. The program is separated from the aeroelastic code and is used as a stand alone program for providing the files with the pseudo-random wind field condition before the structural simulation. Depending on the data specified in the input file to SOSIS-W, it is possible to model different types of wind models and situations. The normal procedure in SOSIS-W is to give a seed for generation of the

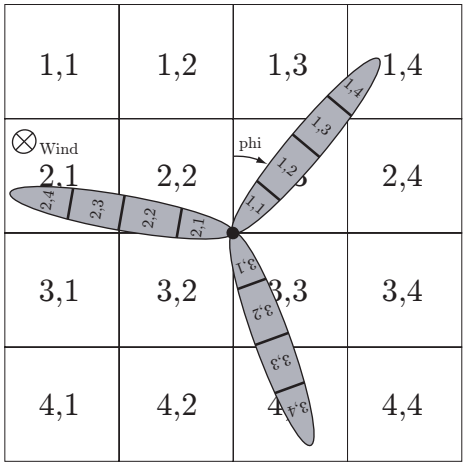

Figure 4.11: Wind field mesh and rotor.

random wind fields. However, it is also possible to use wind measurements at one elevation as input. The measured wind is then spatially distributed in space with the properties given in the input file. Examples of inputs are e.g. inclination, wind profile, mean wind speed at hub height and the corresponding standard deviation, coherence exponentials, etc.

Wind series are generated with a sampling time of typically 0.08–0.1 s. To match the time step used in the simulations, the wind data are extrapolated in time. The extrapolation in time is performed by using a Matlab procedure, [48].

The program is further described in [1, 9] and a complete input file is presented in Appendix B.

4.5.4 Calculation scheme

The section aims to give a brief insight into the calculation steps performed through Fortran subroutines and the data read as input, in a simulation. As described in Section 4.5.2, AERFORCE needs a number of input data in order to give the aerodynamic forces. The wind turbine model itself is determined in the MSC.Marc input file by giving node coordinates, element types and connections, stiffness and mass properties, constraint equations, etc. The main effort in developing the aeroelastic tool has been to implement routines for adaption of the structural model to the aerodynamic code. As the loads are varying over time and space, the equations of motion are solved numerically in a step-by-step manner using an implicit integration scheme. During the step-by-step response calculation, the aerodynamic loads are evaluated at each iteration and time step.

The following sequence is called by MSC.Marc in each iteration:

1. Save x,y,z displacement components for nodes of interest, e.g. blade nodes and orientation nodes.
2. Save x,y,z velocity components for each blade node and the rotational speed of the rotor.
3. Derive the transformation matrices, $\mathbf{S}_{\text{gr}}$ and $\mathbf{S}_{\text{ge}}$, based on the x,y,z components saved at step 1. Calculate the transformation matrices between the rotor and the global system, $\mathbf{S}_{\text{re}}$.
4. Read input data and calculate aerodynamic forces.
   (a) read data from input file, e.g. blade information such as chord length, thickness, area, twist, pitch, profile number, etc. Step 4(a) is only performed at the first time step since the values are not time dependent.
   (b) process the data read at step 4(a) For instance, interpolate data between input airfoil tables and modify $\mathbf{S}_{\text{re}}$ to include the contributions from twist.
   (c) Calculate the wind speed acting on each blade element depending on the rotor position.

(d) Input necessary parameters to AERFORCE and calculate the forces acting on each blade element.

5. Transform blade element forces to the global load vector.

6. Calculate generator moment and write result to the global load vector.

The data are then transferred back to MSC.Marc, where the equilibrium iterations of the time step are performed. A block diagram of the wind turbine simulation tool is given in Figure 4.12. When performing the simulation, the pseudo-random wind field is already evaluated.

The scheme described above should be seen as a very general description of the steps performed in a simulation. To allow for large deformations, all tying constraints and springs, etc. must follow the deformed geometry. That is achieved by specifying local coordinate systems. In addition to the coordinate systems mentioned in Section 4.5.2, systems are used for the non-rotating rotor shaft, the yaw system, the pitch system, etc.

4.5.4.1 Derivation of transformation matrices

All transformation matrices are, in the present implementation, based on the position of an additional element configuration. For instance, to find the transformation matrix between the global system and a system attached to the deformed blade, two help nodes and two elements are necessary. The first element is connected to the blade node and a help-node perpendicular to the blade node in the Y-Z plane. The second element is connected to the blade node and a help-node perpendicular to the blade node in the X-direction, Figure 4.13. The two help nodes are then forced to follow the blade's node motion when elastic deformation and rigid motion is present. With the information available about the coordinates of the two help nodes and the rotor node, two base vectors can be calculated. After normalising the vectors, the third direction vector is calculated as the vector product between the two base vectors. The elements used for keeping track of the position of the blades are modelled with zero mass to avoid influences on the results due to forces introduced by inertia effects. An alternative way to calculate the transformation matrices is to use a rigid link configuration. However, there seems to be problem using rigid links in large rotation analysis in the current version of MSC.Marc. The main benefit of using rigid links compared to beam elements for this purpose is to reduce the number of DOFs.

4.5.4.2 Information needed through input files

To make a simulation, the program needs parameters from two input files. One file describes the structural model and one file gives the input to the aerodynamic subroutine.

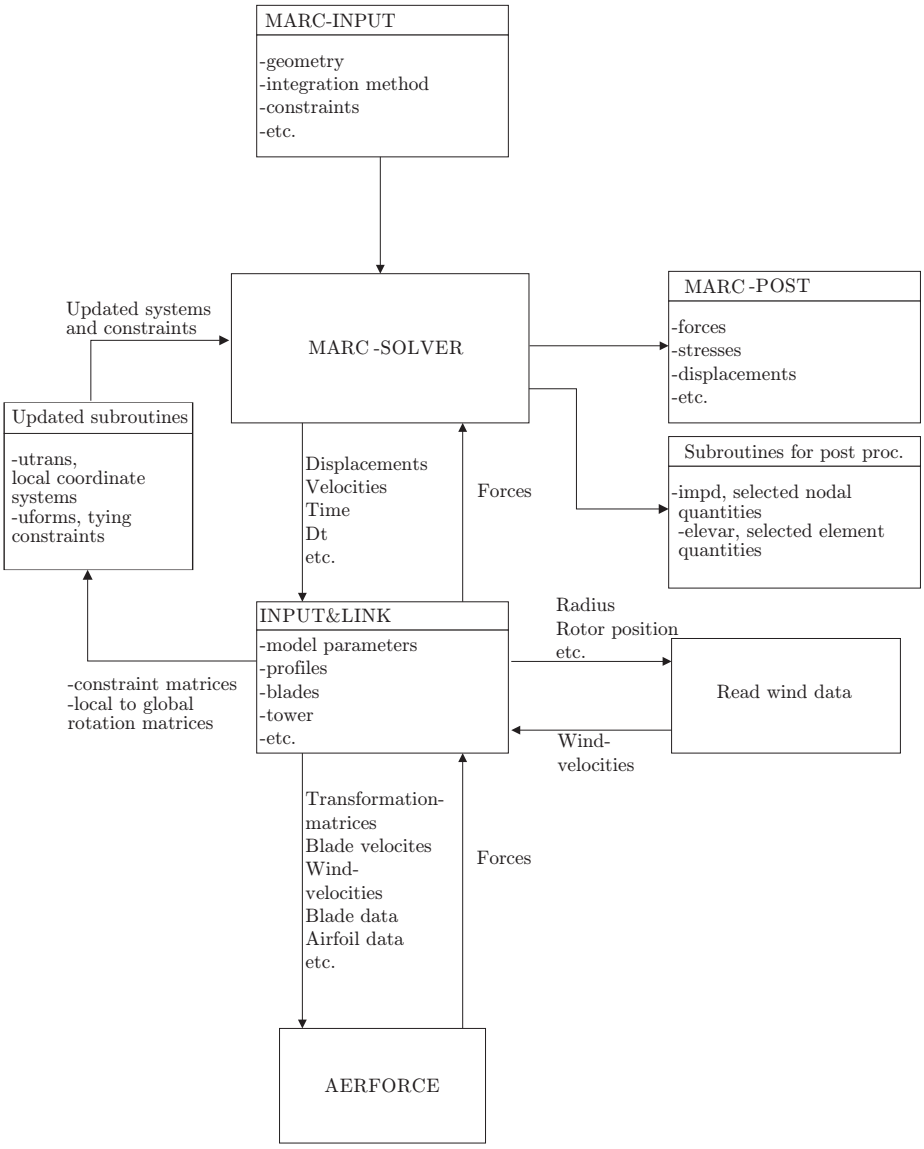

Figure 4.12: Basic block diagram of the wind turbine simulating tool.

Information about the geometrical model, but also numerical methods, tolerances and output demands are specified in the MSC.Marc input file.

The aerodynamic subroutine requires geometrical properties of each blade element such as chord lengths, areas, twist and relative thickness, etc. To each element is also given a profile number, which corresponds to an airfoil data table. The airfoil tables are read in from files. The radius to each blade element and the effective

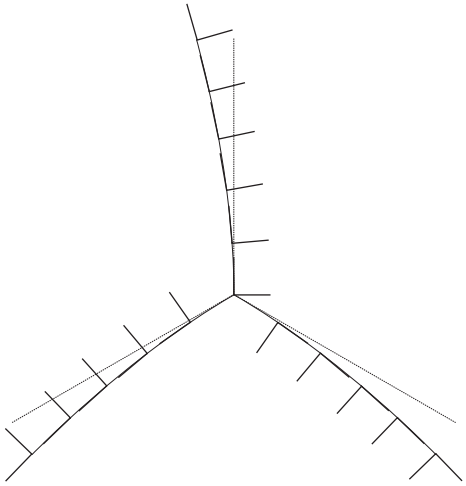

Figure 4.13: Element configuration on a rotor divided in five elements/blade.

blade element length are calculated based on the deformed geometry. Hence no information about those parameters needs to be specified. Tower radii on some heights must be given as input to the tower shadow model. Linear interpolation is performed between height/radius pairs. The tower shadow model is included as a sub-package to AERFORCE and is further described in [6].
Several other parameters are given to set calculation methods and constants. A sample input file is given in Appendix A. Further information about AERFORCE and the dynamic stall model DYNSTALL is given in [5, 7], respectively. The inputs were previously described in the author's licentiate thesis, [1].

It is possible to handle most of the possible wind turbine configurations via input files. However, some changes, like generator model change, requires re-compilation of the code. The compilation and linking of the executable are done rather straightforward, which makes it easy to include, e.g. a new pitch regulation system.

Chapter 5

Numerical examples

5.1 Alsvik turbine

The wind turbine studied is one of four turbines located on the west shoreline in Alsvik on the island Gotland in the Baltic sea.

The wind farm is specifically designed for the purpose of experimental measurements and consists of four strategically placed wind turbines, Figures 5.1 and 5.2. Three of the turbines stand on a line that runs along the shoreline in a NNW-SSE direction. The fourth turbine is located to the east of this row, thus deliberately subjected to wind turbine wakes during westerly winds. The land behind them, to the northeast, is low and flat consisting mainly of grazed grasslands and a low growing pine forest. Since the Alsvik wind farm was intended for experimental measurements, it was equipped with two meteorological masts, each being 52 m high. The masts measure the wind speed and the direction on seven elevations above ground.

Figure 5.1: Alsvik wind turbine park. Reproduced from [16].

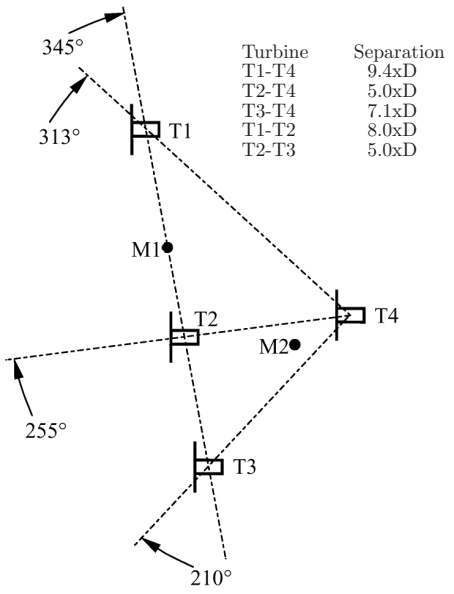

Figure 5.2: Layout of the wind farm at Alsvik, with turbines T1-T4 and masts M1, M2. Reproduced from [16].

The wind turbines are three-bladed and stall regulated with a rated power of 180 kW each. The rotor, which rotates at 42 r.p.m., has a diameter of approximately 23 m and is supported by a 30 m high tower. Some basic properties are tabulated in Table 5.1. A more detailed description is given in Paper 1.

Table 5.1: Basic description of the Alsvik turbine.

Rotor		**Blades**		**Masses (kg)**	
Number of blades	3	Material	GRP	Blade	700
Rotor diameter	23.2 m	Blade length	10.52 m	Rotor and hub	2990
Hub height	30.0 m	Root chord	1.45 m	Nacelle without rotor	5880
Rotor speed	42.8 rpm	Tip chord	0.59 m	Tower	10400
Tilt	5°	Blade profiles	NACA 63-2xx series	Total weight	19300

Results calculated during normal operational wind conditions, based on the Alsvik turbine, are presented in Paper 1.

5.1.1 Example of blade failure simulation

A very dramatic load case, that fortunately happens very rarely on modern wind turbines, is a failure leading to blade loss. However, accidents do happen and [38] reports a recent accident on an old turbine in Denmark, where part of the blades were thrown 200 m away, due to a failure causing rotor overspeed.

To demonstrate the versatility of the developed code, an example is presented on the Alsvik turbine where one blade comes loose. In opposite to the accident described above, the blade loss failure occurs at normal operational speed. Two cases are exemplified; case 1 for studying the transient behaviour and loads of the remaining turbine after blade loss and case 2 for studying the motion of the free falling blade. In case 1, the aerodynamic loads act as normal on all three blades. The assumption is valid until and short after the blade is released. The limitation is, in the current implementation of the BEM method, averaging of, e.g. the induction factor. Hence, loads and displacements are believed to be reasonably correct during the failure and shortly there after. In case 2, the only loads that are acting on the free blade are loads due to gravity, i.e. no aerodynamic loads are applied. The aerodynamic loads on the two remaining blades, after the failure, are in the current work assumed to be the same as just before the failure. However, until the failure, the aerodynamic loads act normally. The simulations are performed at turbulent wind conditions with a mean wind speed of 25 m/s. The usually used time step of 6 ms is reduced to 2 ms in order to better capture the transients at blade loss. The structural damping corresponds to a logarithmic decrement of 5 % in both edge and flap direction.

The simulation is carried out by using the possibility to change tying constraints in time. At a specific time, the constraints that are keeping the blade in normal position are turned off, hence the blade is no longer connected to the wind turbine.

Case 1 is of interest to get an estimation of the resulting loads on the remaining structure. The main interest is if the wind turbine will break, i.e. will the extraordinary loading situation cause stresses up to the strength limit. Case 2 is a very simplified case, with e.g. motion without air resistance, and should be seen as an example of simulations that can be performed with the developed code.

5.1.1.1 Results of blade failure simulation

Blade 1 is released at time $t = 60$ s. Figure 5.3(a) gives the root flap moment of blade 2. The maximum flap moment reached during normal operation, in this particular example, is 103 kNm and the minimum 47 kNm. After 50 ms, the first negative peak of 46 kNm is reached from an initial load of about 90 kNm. The maximum flap moment, 127 kNm, occurs at time $t = 60.232$ s and the minimum, 32 kNm is reached 7 ms later. Figure 5.3b gives the root edge moment of blade 2. The maximum root edge moment before blade 1 is released is 45 kNm and the minimum moment is -25 kNm. The maximum edge load after the blade loss is 58 kNm at time $t = 60.19$ s and the minimum, -55 kNm, is reached at $t = 60.80$ s.

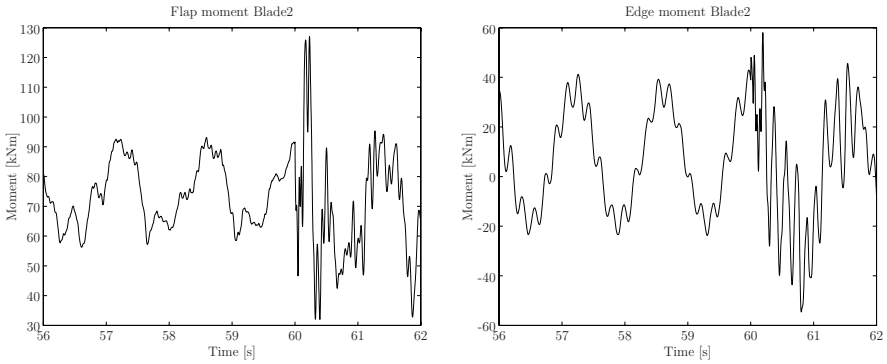

(a) (b)

Figure 5.3: Root flap moment of blade 2, (a). Root edge moment of blade 2, (b).

The tower moment in Figure 5.4 is calculated in the nacelle direction 6.9 m below tower top. The normal operational tower moment, with a mean value of about 230 kNm, is basically the thrust on the rotor. When blade 1 is released, the tower loads increase to a maximum of almost 700 kNm and a minimum of −330 kNm.

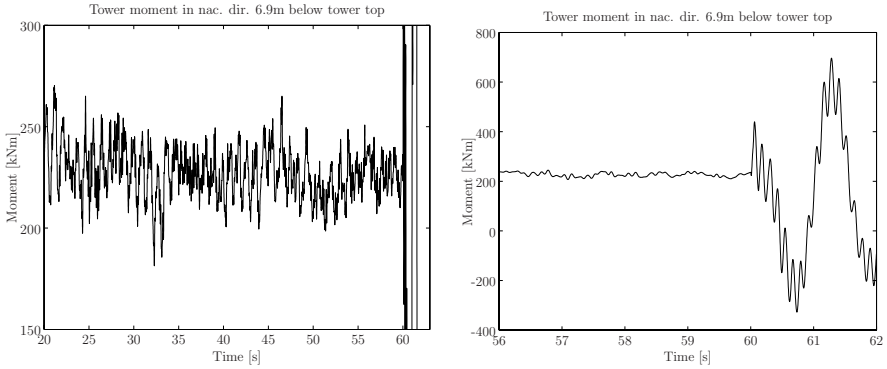

(a) (b)

Figure 5.4: Tower moment in nacelle direction measured 6.7 m below tower top, (a). Magnified tower moment in nacelle direction measured 6.7 m below tower top, (b).

The tower moment in Figure 5.5 is calculated perpendicular to the nacelle direction 6.9 m below tower top. The maximum tower moment is 1270 kNm and the minumum is −1000 kNm.

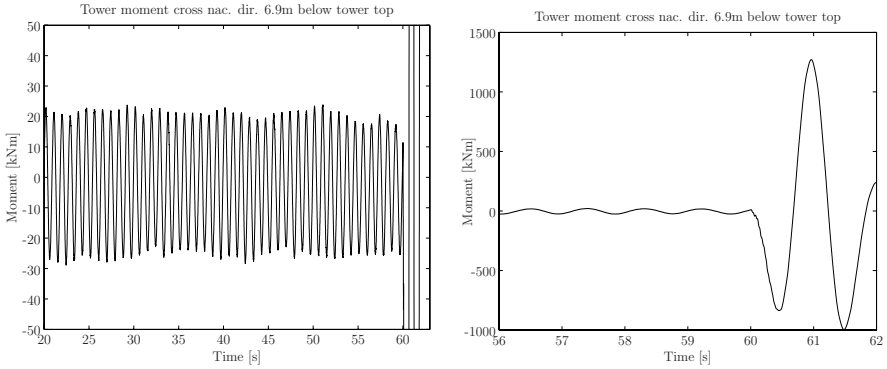

(a) (b)

Figure 5.5: Tower moment perpendicular to nacelle direction measured 6.9 m below tower top, (a). Magnified tower moment in nacelle direction measured 6.9 m below tower top, (b).

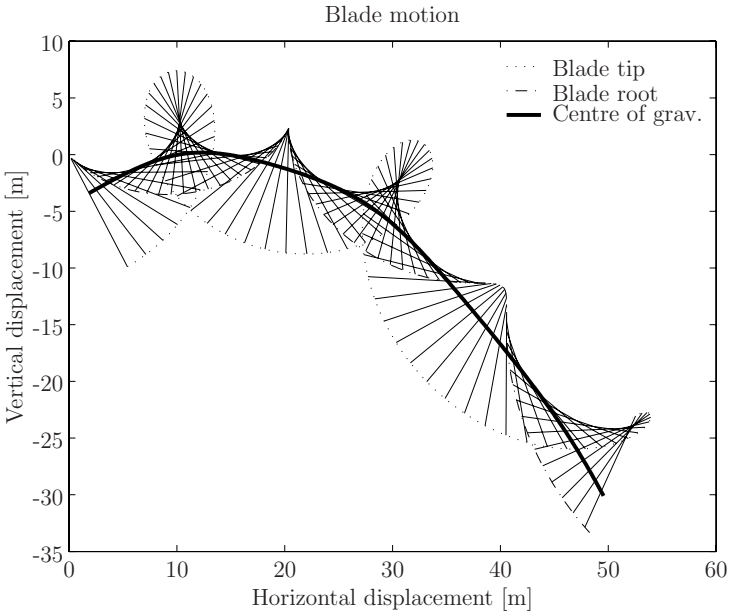

Figure 5.6: Blade motion during blade loss. Only gravity loads are considered.

Figure 5.6 illustrates the trajectory of the free falling blade. A vertical and horizontal coordinate of zero corresponds to the hub centre and a vertical displacement of -30 m corresponds to ground level. The blade travels about 50 m before hitting the ground.

5.1.1.2 Conclusions

The blade loss example demonstrates how the developed code can be used to model special events. The question in Case 1 was whether or not the remaining turbine will collapse after a blade loss. The maximum root flap moment increases from a maximum of 103 kNm in the extreme operational case to 127 kNm shortly after the blade loss. The minimum negative root edge moment decreases from -25 kNm to -55 kNm. The load transients are relatively limited in both cases and the blades will probably withstand the increased loads. The load levels in the tower increase dramatically. From a maximum peak value before the blade loss of 270 kNm in nacelle direction to the maximum 1270 kNm perpendicular to nacelle direction. The tower moment is increased by 5 times the maximum value reached before the blade loss. The load levels are important to know in order to determine possible component or material damage.
Case 2 illustrates the motion of the free falling blade. However, without the aerodynamic forces applied, the motion of the blade's centre of gravity follows a simple projectile motion. However, the main motivation with this particular example was to demonstrate the generality of the developed code.

5.2 Tjæreborg turbine

The Tjæreborg wind turbine was a horizontal axis upwind turbine developed in the late eighties as part of the Wind Energie Große Anlagen (WEGA) programme, [34]. The machine was installed near Esbjerg in Denmark, and was removed in August 2001 due to an accident in the generator, [20]. In December 2001, Elsam erected a Vestas V80, 2 MW prototype turbine on the foundation of the old Tjæreborg turbine. Since the Tjæreborg site was intended for experimental measurements, it was equipped with two meteorological masts, each being of 90 m height, Figure 5.7. The two meteorological masts and the turbine were placed on a line in the dominant wind direction. The distance between the turbine and each mast was 120 m, which corresponded to two rotor diameters, [19].

Figure 5.7: The Tjæreborg wind turbine. Reprinted from [20].

The three-bladed rotor with a diameter of 61.1 m, was connected to a 2 MW enlarged slip induction generator through a three-stage planetary gearbox. The three-degree tilted rotor was running at a constant speed of 22.3 r.p.m., which gave a blade tip speed of 71 m/s. The concrete tower was of 57 m height and shaped as a parabola near the base, gradually turning conical. Some of the basic properties are tabulated in Table 5.2. A more detailed description is given in Paper 2.

Table 5.2: Basic description of the Tjæreborg turbine.

Rotor		**Blades**		**Masses (t)**	
Number of blades	3	Material	GRP	Blades	27.1
Rotor diameter	61.1 m	Blade length	29 m	Hub	22.1
Hub height	61 m	Root chord	3.3 m	Tower	665.0
Rotor speed	22.4 rpm	Tip chord	0.9 m	Towerhead	224.6
Tilt	3°	Blade profiles	NACA 4412–4443	Total weight	889.6

5.2.1 Visualisation and description of an emergency stop of the Tjæreborg turbine

The emergency stop sequence presented aims to clarify Paper 2 and visualises the course of events with some representative plots. The results exemplified are simulated with modified structural data based on the Tjæreborg turbine. Both masses and stiffnesses are scaled equally to 40 % of the original turbine, which mean a lighter and more flexible structure. The scaling procedure is further described in Paper 3. and Section 5.2.2.

In this emergency brake situation, the desired pitch angle is set according to a predefined pitch sequence. Hence, just the inner loop in the control block scheme described in Section 4.3.4 is used. The desired pitch angle sequence is implemented in the simulations in two steps. The first step, with a pitch rate of 16 deg/s, is applied in about 1.8 seconds and a second step with a pitch rate of about 5 deg/s, is applied until the desired pitch angle is reached. The delay time to generator switch off, from when the pitch sequence started, is set to 1.1 s. The idling pitch angle is set to 86 degrees. The emergency braking of the original turbine and a verification with measurements is further presented in Paper 2. The wind conditions during the emergency stop is a mean wind speed of 10.5 m/s and a turbulence intensity of 8 %.

- Time=0, Inc. 7883. Pitching of blades start with an initial pitching rate of 16 deg/s, Figure 5.11. The power production and the root flap moments are rapidly dropping, Figures 5.8 and 5.9, respectively. Figure 5.14 illustrates the wind turbine in the deformed state together with the applied blade loads at the time.
- Time=1.10, Inc. 8066. The generator is turned off and the rotor speed is momentarily increasing before deceleration, Figure 5.13. The blade root flap moments are in this state reduced from an initial 1100 kNm to about 200 kNm.
- Time=1.24, Inc. 8090. The mean flap moment becomes zero and the gravity loads are dominating, Figure 5.15.
- Time=1.92, Inc. 8203. The maximum negative flap and edge moments, Figures 5.9 and 5.10, respectively, are reached and the blades are deflected in the opposite direction, Figure 5.16.
- Time=12.70, Inc. 10000. The blades have reached there final pitching positions and the rotor is idling, Figures 5.11 and 5.12. The gravity load loads are dominating, Figure 5.17.

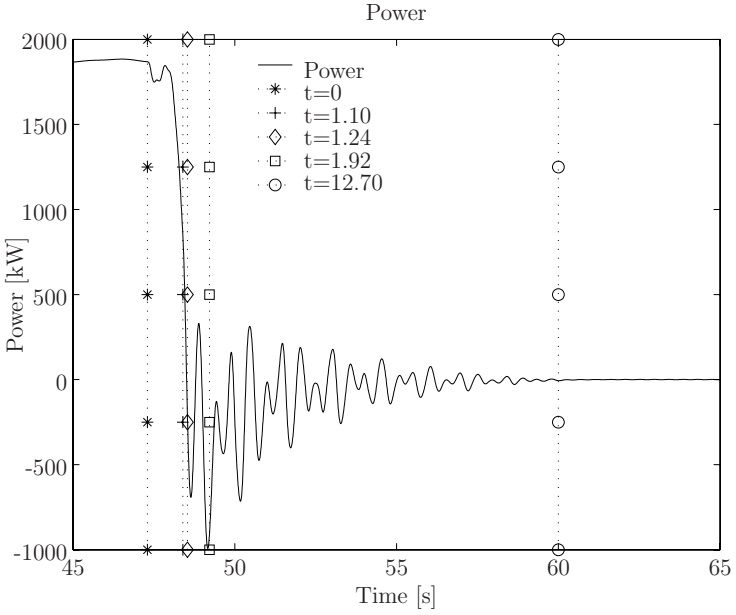

Figure 5.8: Power during emergency braking of the rotor.

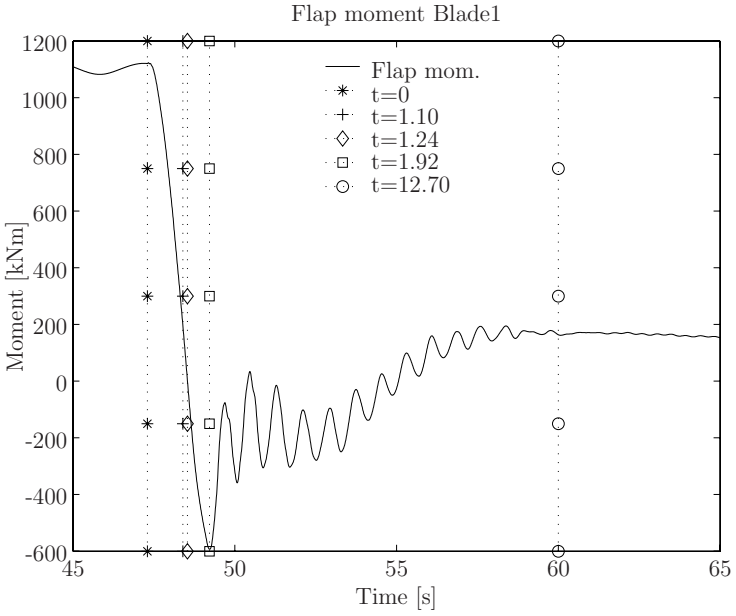

Figure 5.9: Flap moment of blade 1 during emergency braking of the rotor.

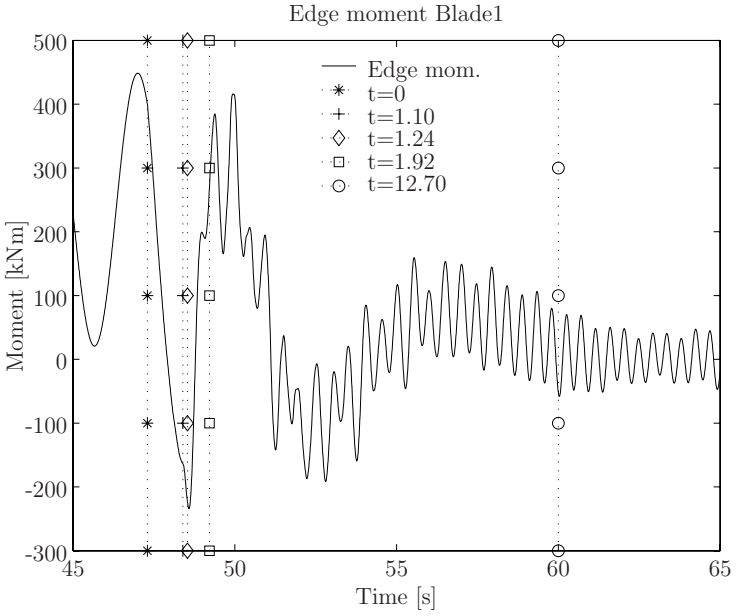

Figure 5.10: Edge moment of blade 1 during emergency braking of the rotor.

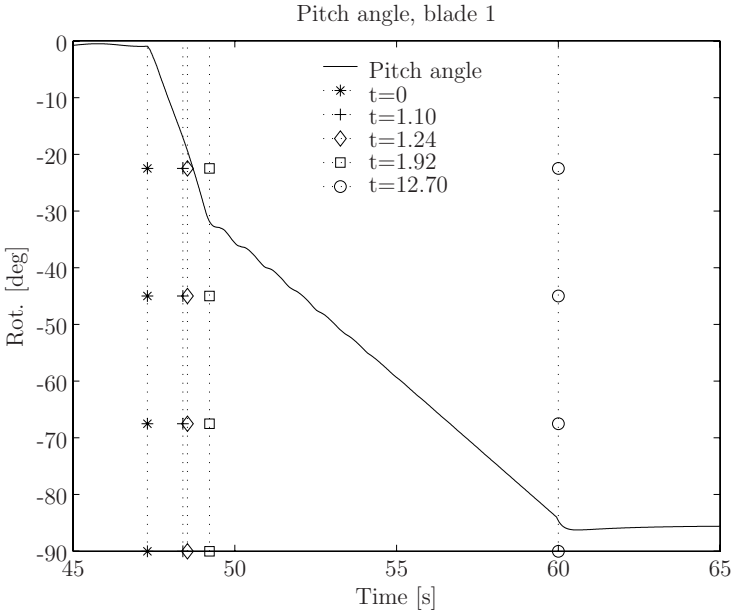

Figure 5.11: Pitch angle of blade 1 during emergency braking of the rotor.

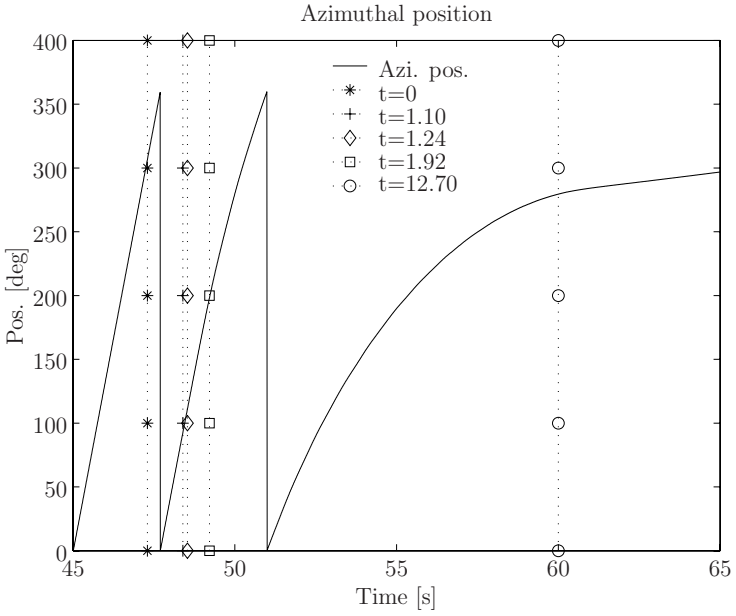

Figure 5.12: Azimuthal rotation of rotor during emergency braking.

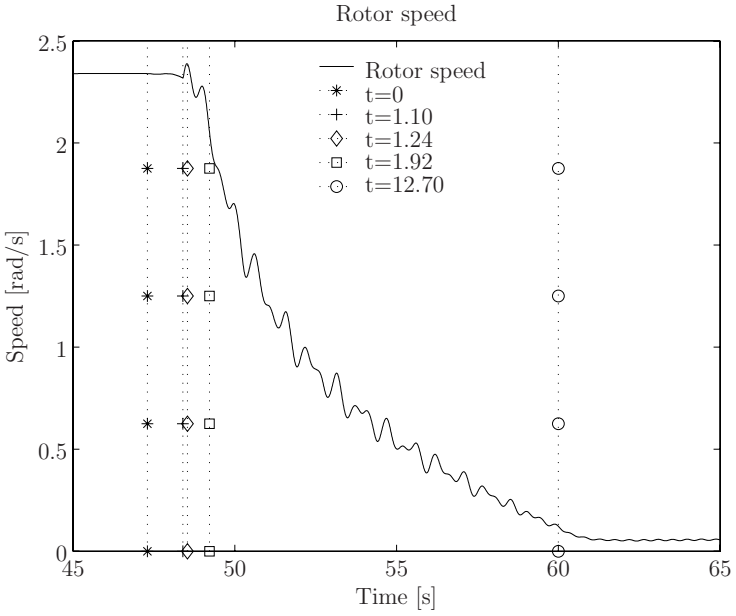

Figure 5.13: Rotor speed during emergency braking.

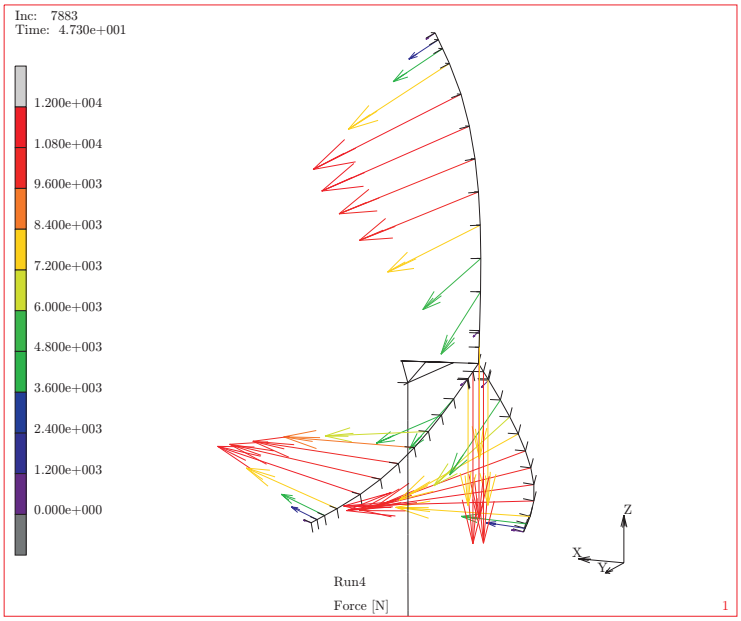

Figure 5.14: Applied loads at $t = 0$, the pitch servo starts operate.

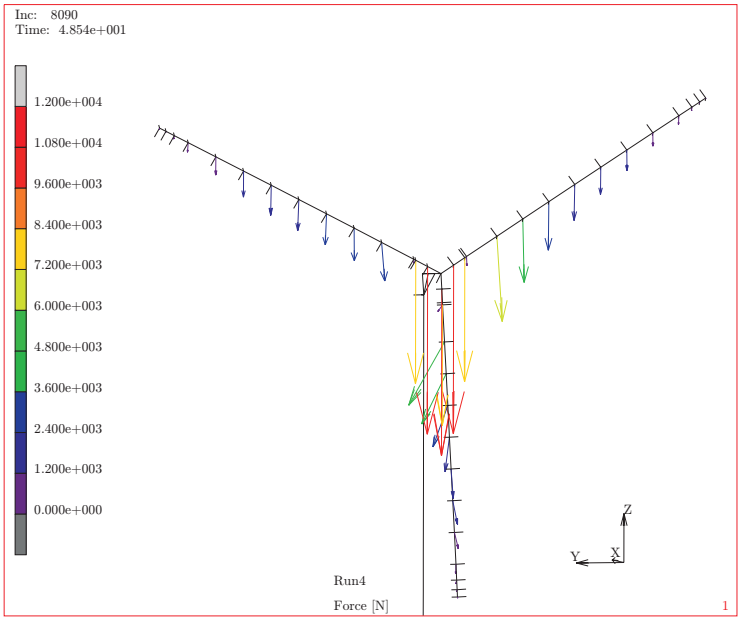

Figure 5.15: Applied loads at $t = 1.24$, the mean flap moment is zero.

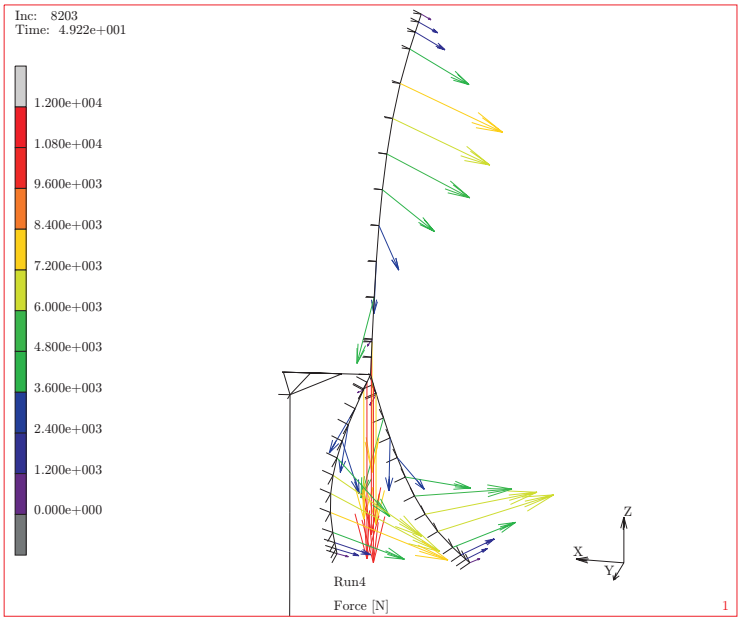

Figure 5.16: Applied loads at $t = 1.92$, the flap moment has reached its maximum negative peak.

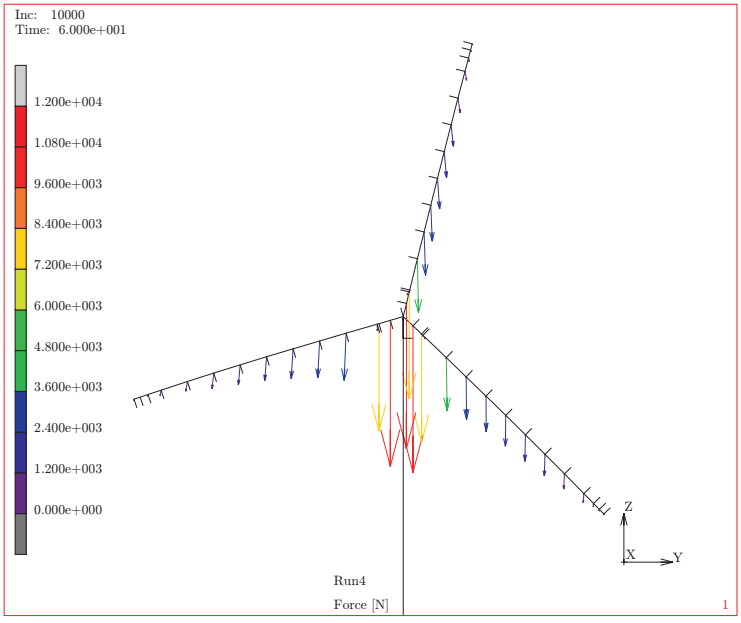

Figure 5.17: Applied loads at $t = 12.70$, the pitch angle has reached its maximum which is almost 90 degrees.

The results presented are, as mentioned, calculated based on a softer turbine compared to the original Tjæreborg turbine presented in Paper 2. Hence, the study is a more dynamical case than is presented in Paper 2. Especially the edge moments are oscillating heavily due to the large blade deflections, compared to the original model. The edgewise oscillations are visible in the rotor speed deceleration as well.

5.2.2 Simulation of emergency brake situations based on a modified Tjæreborg turbine

Paper 3 describes how the loads and power production changes with turbine flexibility during operation in normal conditions. This section aims to give some results associated with large geometrical deformations during an emergency brake of the rotor.

5.2.2.1 Introduction

The basic idea described in Paper 3 and that is used in this section is that by scaling the mass and stiffness properties equally it is possible to change the flexibility of the structure and at the same time keep the initial eigenfrequencies unchanged. The concept can be described by the generalised eigenproblem:

$$(\psi\mathbf{K} - \omega^2\psi\mathbf{M})\mathbf{y} = 0 \tag{5.1}$$

where the nontrivial solution of the eigenproblem gives the circular frequencies ω_i and the corresponding mode shapes $\mathbf{y}_i$. If the mass $\mathbf{M}$ and stiffness $\mathbf{K}$ matrices are scaled equally, by a scaling factor ψ, the eigenvalues remain the same. Practically, the scaling of the mass and stiffness matrices are achieved by scaling densities, elastic moduli, concentrated springs and point masses equally. Results are presented for scaling factors, ψ, in the range 0.2,0.3,...,1.0, where 1.0 is equivalent to the original Tjæreborg turbine.

5.2.2.2 Results

The results presented are calculated in idealised conditions using a constant wind profile with a mean speed of 14 m/s and without any tower shadow effects. The reasons are easy interpretation and comparison of the results, but with a nonphysical description of the wind. Hence, the results presented are mainly aimed for comparison in this particular example. The results are presented as tabulated values just before the emergency stop and in figures. Table 5.3 gives, at each scaling factor ψ, the tip displacement of blade 1, the shaft torque in the low speed shaft, the averaged root flap and edge moments, and the averaged root blade torque. The emergency stop was applied at $t = 47.3$.

Table 5.3: Simulated data at steady state.

ϕ	**Disp. (m)**	**Shaft torqe (kNm)**	**Averaged flap moment (kNm)**	**Averaged torque (kNm)**	**Averaged edge moment (kNm)**
1.0	2.43	874.2	1207.2	−15.6	−332.4
0.9	2.67	872.0	1199.7	−16.8	−328.0
0.8	2.98	857.2	1186.9	−16.6	−324.9
0.7	3.37	853.1	1176.7	−17.7	−315.0
0.6	3.86	843.8	1162.6	−18.9	−297.9
0.5	4.53	834.4	1143.5	−20.8	−278.2
0.4	5.43	813.0	1107.8	−22.7	−255.6
0.3	6.75	775.0	1053.6	−25.2	−250.0
0.2	8.73	698.3	948.6	−27.0	−227.6

Figure 5.18(b) describes the increase in range between the steady state displacements and the first trough located at $t \approx 49.2$. The softest design, with $\phi = 0.2$, makes the blade tip go from a flapwise displacement of 8.7 m to −5.3 m in approximately 1.7 s. The shaft torque is given in Figure 5.19. The flap root moment and blade root torque, Figures 5.20 and 5.21, respectively, are given as the average values for the three blades. Figure 5.22 shows the edge moment of blade 1 and the averaged edge moment, respectively.

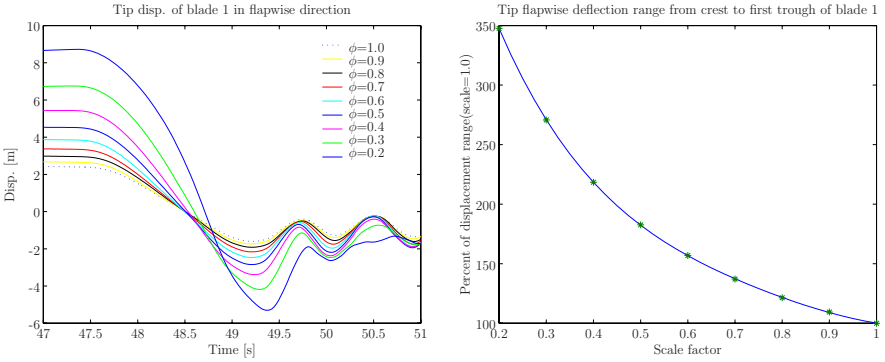

(a) (b)

Figure 5.18: Blade 1, tip deflection in flapwise direction, (a). Increase in displacement range, reaching from crest at $t \approx 47$ to first trough at $t \approx 48.7$, (b).

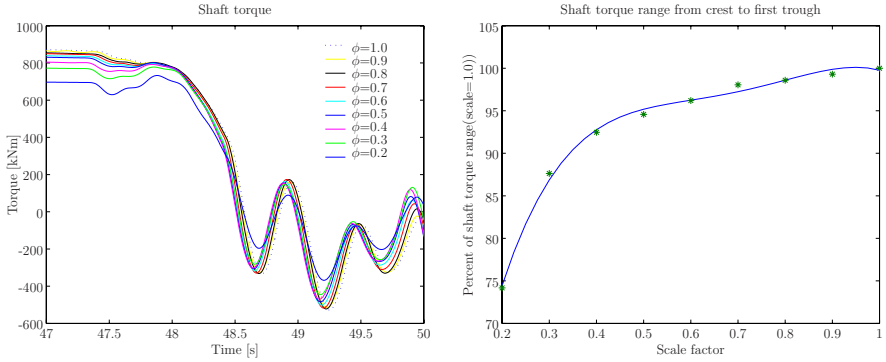

(a) (b)

Figure 5.19: Shaft torque in low speed shaft, (a) and torque range from steady state to first trough, (b).

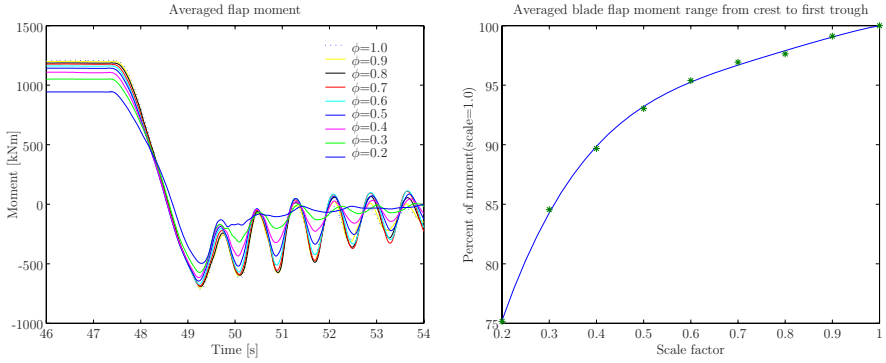

(a) (b)

Figure 5.20: Averaged root flap moment, (a) and averaged flap moment range from steady state to first trough, (b).

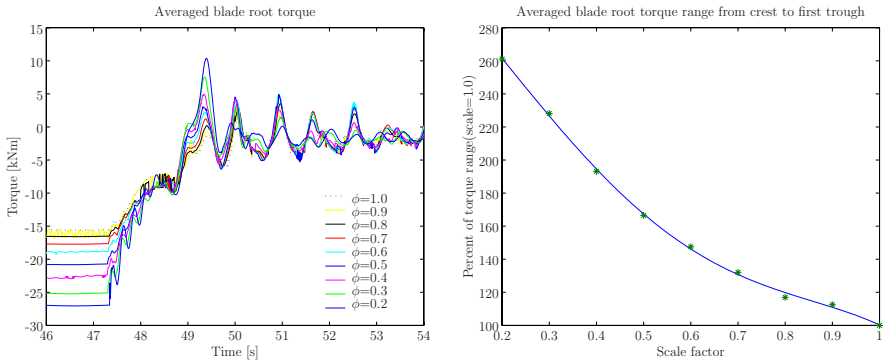

(a) (b)

Figure 5.21: Averaged blade root torque, (a) and averaged blade torque range from steady state to first trough, (b).

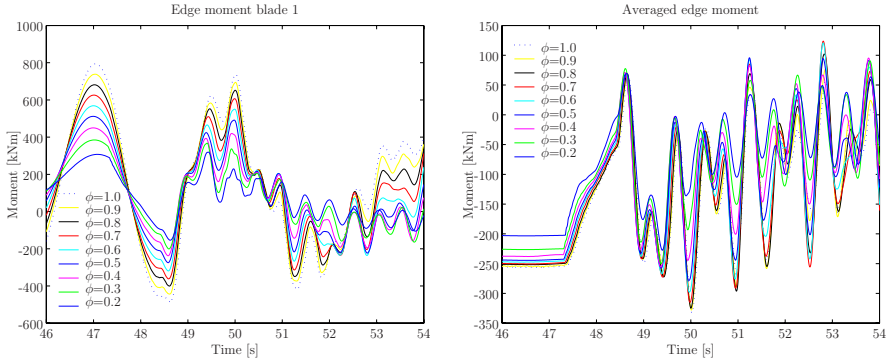

(a) (b)

Figure 5.22: Edge moment of blade 1, (a) and averaged edge moment, (b).

5.2.2.3 Conclusions

The basic idea with a more flexible turbine is to reduce stresses in the structure by transforming them into deformations. Paper 3 shows how the loads were influenced by the flexibility in normal operational conditions. This study follows up with results in the more dynamical case of an emergency stop. As the blades are deflected, their inertia and stiffness with respect to the blade root coordinate system change. This is especially obvious in the case of pitching the blades, as the inertia around the pitch axis increases considerably. In order to achieve an optimum torsional stiffness, the increased torsional torque may be an important design parameter. The increased

inertia gives a large blade root torque increase. In this study the blade root torque more than doubled in the case of using a scaling factor $\phi = 0.2$, compared to the original configuration. This configuration is extremely soft, with a flapwise blade deflection/rotor radius ratio of 30 %. That soft turbines are not likely to be designed. In the more reasonable case, with a flapwise blade deflection/rotor radius ratio of 10 %, corresponding to a scaling factor of about 0.75, the loads are much less influenced. As stated in Paper 3, nonlinearities have a large influence on loads when the flapwise blade deflection/rotor radius ratio exceeds 10 %.

5.3 Comments on simulations

The results presented are examples of possible output data. Depending on what is specified in the input file to MSC.Marc, it is possible to select time steps for which nodal and element solutions shall be saved. Possible outputs are, e.g. nodal displacements, velocities and accelerations. Possible results on the element level are, e.g. stresses, moments, torques and axial forces. The database can then be opened with a post-processor like MSC.Patran or the built in MSC.Mentat, for animation, stress plotting, curve making, etc.

With the discretisation used in the present work (approximately 1200 DOFs) the required computer time was about 48 times the real time on a DELL Xeon 2.4 GHz with 1 GB ram. A typical 600 seconds of simulation would therefore require approximately 8 hours of computer time. Highly deflected blades require some additional iterations to converge, hence the computer time will be a bit longer in those cases. It should be mentioned that the numbers presented are calculated when large amounts of data, approximately 2 GB, were written to files. The computational time is believed to decrease when only data of interest are saved. It is neither practical nor useful to save every increment in an analysis.

Chapter 6

Conclusions and future work

6.1 Conclusions

A tool has been developed for the dynamical simulation of horizontal axis wind turbines. The project has chosen the finite element method as a means to accurately predict the wind turbine loading and response. The primary motivation for the development of the code has been to include nonlinear effects in terms of large displacement assumptions and application of loads on the deformed geometry.

A benefit of the FE-formulation, and especially using a commercial FE-package, is the possibility to relatively easily change properties and different configurations of the model. It is also easy to postprocess the results to study forces, moments, stresses, etc. in the structure. The major drawback is the computational costs, which is high compared to modal formulation models. With the discretisation used in the present work, the required computer time is approximately 48 times the real time for a typical simulation. Hence the model is more suitable for extreme or special load case simulations rather than for certification purpose analyses.

In the thesis, numerical simulations based on models of the Alsvik 180 kW turbine and the 2 MW Tjæreborg turbine, were performed. Verifications with measurements show that the models successfully predict the response in normal as well as in more extreme load cases. Results are also presented, which aimed to verify limitations in codes that assumes small blade deflections. The conclusion is that those codes are believed to be accurate enough in most normal situations and certainly for certification purposes where computational speed is critical. Care must, however, be taken in simulating extreme situations and in the design of even lighter and more flexible machines. In these situations, aeroelastic tools must be used, which are able to properly deal with large blade deflections. No general conclusion can be drawn, but in the presented example it seems like large nonlinearities are to be expected when the blade deflection exceeds 10 % of the blade radius.

6.2 Future research

There are many possible areas to improve or study further.

A natural improvement of today's model is to include a more extensive and realistic control system. These control systems make it possible to model all kind of generators and power regulation types, as variable or constant speed generators during either stall or pitch power regulation. For instance, the implemented pitching system, which includes additional dynamics compared to most other implementations, needs further study. Other areas that need further investigation are the application of damping and blade loads. The blade loads are today applied as nodal forces, but may, with minor modification to the existing code, be distributively applied.

The developed approach gives many possibilities to model extreme events. For example, the blade failure briefly described in Section 5.1 could be interesting to study further. The continuing interest to install large wind turbines offshore is another area of interest. The generality of the developed tool makes it possible to simulate and apply loads to the supporting structure, that can be of any shape. Further studies regarding large blade deflections are also very interesting.
To make the code more convenient to work with, for a wider group of users, a more user-friendly interface may also need to be developed.

Bibliography

[1] A. Ahlström. Simulating Dynamical Behaviour of Wind Power Structures. Technical Report 2002:11, Royal Institute of Technology, Department of Mechanics, Licentiate Thesis, Stockholm, Sweden, 2002.

[2] J. Argyris and H.-P. Mlejnek. *Dynamics of Structures, Volume V.* NORTH-HOLLAND, Amsterdam, 1991.

[3] M. E. Bechly. Studies in Structural Dynamics and Manufacture of Composite Wind Turbine Blades. Technical report, Mechanical Engineering Department, University of Newcastle, Callaghan, NSW, 2308, 1997.

[4] T. Belytschko, W. K. Liu, and B. Moran. *Nonlinear Finite Elements for Continua and Structures.* John Wiley & Sons, Chichester, 2000.

[5] A. Björck. DYNSTALL: Subroutine Package with a Dynamic stall model. Technical Report FFAP-V-110, FFA, Bromma, Sweden, 2000.

[6] A. Björck. Blade-Tower Interaction: Calculations Compared to Wind Tunnel Test Results. Technical Report FFAP-V-107, FFA, Bromma, Sweden, 1999.

[7] A. Björck. AERFORCE: Subroutine Package for unsteady Blade-Element/Momentum Calculations. Technical Report TN 2000-07, FFA, Bromma, Sweden, 2000.

[8] T. Burton, D. Sharpe, N. Jenkins, and E. Bossanyi. *Wind Energy Handbook.* John Wiley & Sons, Chichester, 2001.

[9] I. Carlén. SOSIS-W Version 1.3. Technical report, Teknikgruppen AB, Sollentuna, Sweden, 2000.

[10] J. Chung and G. M. Hulbert. A family of single-step Houbolt time integration algorithms for structural dynamics. *Computer Methods in Applied Mechanics and Engineering*, 118:1–11, 1994.

[11] Compaq Fortran. Language Reference Manual. Technical Report AA-Q66SD-TK, Compaq Computer Corporation, Houston, Texas, 1999.

[12] A. Crispin, editor. *Wind Directions—How many blades is best?* Arthouros Zervos, Magazine of the European wind energy association, Hockpitt Farm, Nether Stowey, Bridgwater, Somerset, March 2000.

[13] Danish Wind Turbine Manufacturers Association. The Wind Energy Pioneer — Poul la Cour.
Internet online, 23 April 2000.
http://www.windpower.dk/pictures/lacour.htm.

[14] Danish Wind Turbine Manufacturers Association. The Wind Turbine Yaw Mechanism.
Internet online, 20 June 2000.
http://www.windpower.dk/tour/wtrb/yaw.htm.

[15] Danish Wind Turbine Manufacturers Association. Wind Turbine Generators.
Internet online, 29 Maj 2000.
http://www.windpower.dk/tour/wtrb/electric.htm.

[16] E. Djerft and H. Mattson. Evaluation of the Software Program WindFarm and Comparisons with Measured Data from Alsvik. Technical Report TN 2000-30, FFA, Bromma, Sweden, 2000.

[17] L. Donghoon, D. H. Hodges, and M. J. Patil. Multi-flexible-body Dynamic Analysis of Horizontal Axis Wind Turbines. *Wind Energy*, 5:281–300, 2002.

[18] R. Edinger and S. Kaul. *Renewable Resources for Electric Power: Prospects and challenges*. Quorum, Westport, 2000.

[19] ELSAMPROJECT A/S. The Tjæreborg Wind Turbine - Final Report. Technical Report EP92/334, CEG, DG XII contract EN3W.0048.DK, Fredericia, Denmark, 1992.

[20] ELSAMPROJECT A/S. The Tjæreborg Wind Turbine.
Internet online, 31 August, 2004. http://www.afm.dtu.dk/wind/tjar.html.

[21] Enercon. Enercon E-40.
Internet online, 4 June 2000.
http://www.enercon.de/englisch/produkte/e_40_daten.html.

[22] Energy Engineering Board-Commission on Engineering and Technical Systems. Assessment of research needs for wind turbine rotor materials technology. Technical report, National Research Council, Washington, D.C., 1991.

[23] F. Enoksson, J. Olsson, Å. Persson, M. Ringkvist, and C. Wagner. Vindkraft till havs. Technical report, Projektlinjen i matematik, Fysikum Stockholms Universitet, Stockholm, 1999.

[24] European Wind Energy Association. *A plan for action in Europe: Wind Energy—The Facts*. Office for Official Publications of the European Communities, Luxembourg, 1999.

[25] H. Ganander and B. Olsson. VIDYN simuleringsprogram för horisontalaxlade vindkraftverk. Technical Report TG-R-98-14, Teknikgruppen AB, 1998.

[26] Garrad Hassan and Partners. BLADED for Windows, A design Tool for Wind Turbine Performance and Loading.
Internet online, 27 Mars 2001.
http://www.garradhassan.com/bladed/index.htm.

[27] P. Gipe. *Wind energy comes of age*. John Wiley & Sons, New York, 1995.

[28] M. Géradin and D. Rixen. *Mechanical Vibrations—Theory and Applications to Structural Dynamics, 2nd ed.* John Wiley & Sons, New York, 1997.

[29] A. Grauers. Design of Direct-driven Permanent-magnet Generators for Wind Turbines. Technical report, Chalmers, Department of Electric Power Engineering, Techical Report No. 292, Göteborg, Sweden, 1996.

[30] A. C. Hansen and D. J. Laino. USER's GUIDE: YawDyn and AeroDyn for ADAMS. Technical report, Mechanical Engineering Department, University of Utah, Salt Lake City, UT 84112, 1998.

[31] O. L. Hansen. Basic Rotor Aerodynamics applied to Wind Turbines. Technical report, Department of Energy Engineering, Fluid Mechanics, Technical University of Denmark, 1998.

[32] R. Harrison, E. Hau, and H. Snel. *Large wind turbines*. John Wiley & Sons, Chichester, 2000.

[33] E. Hau. *Windturbines: Fundamentals, Technologies, Application and Economics*. Springer, München, 2000.

[34] E. Hau, J. Langenbrinck, and W. Palz. *WEGA Large Wind Turbines*. Springer, Berlin, 1993.

[35] R. L. Hills. *Power from wind: a history of windmill technology*. Cambridge University Press, Cambridge, 1994.

[36] J. Holmqvist. Optimization of Wind Turbine Rotors. Technical Report TN 1998-19, FFA, Bromma, Sweden, 1998.

[37] INTEGRATED ENERGIES. Airfoil Lift Theory Revisited.
Internet online, 11 July 2002.
http://home.inreach.com/integener/IE010309AG/.

[38] Jyllands-Posten. Vindmølle løb løbsk.
Internet online, 5 Januari, 2005.
http://www.jp.dk/indland/artikel:aid=2837638/.

[39] M. Kuhn and W. Bierbooms. Delft University Wind Energy Converter Simulation Program.
Internet online, 27 Mars 2001.
http://www.ct.tudelft.nl/windenergy/resduwec.htm.

[40] G. C. Larsen, M. H. Hansen, A. Baumgart, and I. Carlén. Modal Analysis of Wind Turbine Blades. Technical Report Risø-R-1181, Risø National Laboratory, Roskilde, Denmark, 2002.

[41] T. J. Larsen and A. M. Hansen. Aeroelastic effects of large blade deflections for wind turbines. In Delft University of Technology, editor, *The Science of making Torque from Wind*, pages 238–246, Roskilde, Denmark, 2004.

[42] Å. Larsson. Vindkraft i lokala och regionala nät—elektriska egenskaper och elkvalitet. Technical report, Elforsk Rapport 98:20, Elforsk AB, Stockholm, 1998.

[43] G. Larsson. SOLVIA, Finite Element System Version 99.0. Technical Report Report SE 99-6, SOLVIA Engineering AB, Västerås, Sweden, 2000.

[44] C. Lindenburg and T. Hegberg. PHATAS-IV user's manual. Program for Horizontal Axis wind Turbine Analysis and Simulation. Version IV. Technical Report ECN-C−99-093, Netherlands Energy Research Foundation ECN, Petten, 2000.

[45] LM Glasfiber A/S. Rotor Blades Development, Vortex Generators. Technical Brochure, June 2000. Denmark.

[46] LM Glasfiber A/S. Photo archive.
Internet online, 21 Januari, 2005.
http://www.lm.dk/UK/News/PressKit/Image+gallery.htm.

[47] J. F. Manwell, J. G. McGowan, and A. L. Rogers. *Wind Energy Explained*. John Wiley & Sons, Chichester, 2002.

[48] Mathworks. Matlab manual.
Internet online, 17 June 2002. http://www.mathworks.com/.

[49] D. Molenaar. State-of-the-Art of Wind Turbine Design Codes: Main Features Overview for Cost-effective Generation. *Wind engineering*, 23:295–311, 1999.

[50] MSC Software Corporation. Features of MSC.Marc.
Internet online, 20 Januari, 2003.
http://www.marc.com/Support/Library/Features_of_Marc_2001.pdf.

[51] MSC Software Corporation. MSC.Marc Volume A, Theory and User Information. Technical Report MA*V2003*Z*Z*Z*DC-VOL-A, 2003.

[52] MSC Software Corporation. MSC.Marc Volume D, User Subroutines and Special Routines. Technical Report MA*V2003*Z*Z*Z*DC-VOL-D, 2003.

[53] Nordex AG. Products and service.
Internet online, 23 April 2000.
http://www.nordex-online.com/_e/produkte_und_service/index.html.

[54] NREL. NREL 10-m Wind Turbine Testing in NASA Ames 80'x120' Wind Tunnel.
Internet online, 21 Januari, 2005. http://wind.nrel.gov/amestest/.

[55] S. Øye. FLEX4, Simulation of Wind Turbine Dynamics. In B. Maribo Pedersen, editor, *State of the Art of Aerolastic Codes for Wind Turbine Calculations*, pages 71–76, Lyngby, Denmark, 1996.

[56] W. D. Pilkey. *Elastic Beams*. John Wiley & Sons, New York, 2002.

[57] Professional Services Group. ADAMS/WT 2.0 User's Guide. Technical report, Mechanical Dynamics, 6530 E. Virginia St. Mesa, AZ 85215, 1998.

[58] D. C. Quarton. Wind turbien design calculations the state of the art. In A. Zervos, H. Ehmann, and P. Helm, editors, *European union wind energy conference 1996*, pages 10–15, Göteborg, Sweden, 1996.

[59] D. C. Quarton. The Evolution of Wind Turbine Design Analysis – A Twenty Year Progress Review. *Wind Energy*, 1:5–24, 1998.

[60] M. Rapolder and W. Wunderlich. Adaptive integration algorithms for the dynamic analysis of contact and plasticity. In *European Congress on Computational Methods in Applied Sciences and Engineering ECCOMAS 2000*.

[61] F. Rasmussen and M. H. Hansen. Present Status of Aeroelasticity of Wind Turbines. *Wind Energy*, 6:213–228, 2003.

[62] J. G. Schepers. Verification of European wind turbine design codes, VEWTDC : final report. Technical Report ECN-C−01-055, Netherlands Energy Research Foundation ECN, Petten, 2002.

[63] T. Soerensen and M. H. Brask. Lightning protection of wind turbines. Technical report, DEFU, Risoe, Denmark, 1999.

[64] D. A. Spera. *Wind turbine technology: fundamental concepts of wind turbine engineering*. ASME PRESS, New York, 1994.

[65] Statens Kärnkraftinspektion. Kärnkraft.
Internet online, 24 May 2000. http://www.ski.se/.

[66] Stentec B.V. Wind Energy. TWISTER.
Internet online, 28 Mars 2001. http://www.stentec.com/windframe.html.

[67] H. Stiesdal. Bonus Energy A/S, The wind turbines components and operation. Technical Brochure, 2000. Denmark.

[68] J. Svensson. Grid-Connected Voltage Source Converter-Control Principles and Wind Energy Applications. Technical report, Chalmers, Department of Electric Power Engineering, Techical Report No. 331, Göteborg, Sweden, 1998.

[69] United States Department of Energy Wind Energy Program. History of Wind Energy Use.
Internet online, 19 April 2000. http://www.eren.doe.gov/wind/history.html.

[70] V. A. Vasilis and S. G. Voutsinas. GAST: A General Aerodynamic and Structural Prediction Tool for Wind Turbines. In *European union wind energy conference 1997*, Dublin, Ireland, 1997.

[71] Vattenfall Utveckling AB. Nordic 1000 Utvecklingen av ett vindkraftverk enligt den svenska linjen. Technical report, Vattenfall Utveckling AB, Älvkarleby, 1997.

[72] Vestasvind Svenska AB. Teknisk beskrivning av Optislip® i Vestas vindkraftverk.
Brochure, 30 Mars 2000. Item Nr 947525.R2.

[73] B. Visser. The aeroelastic code FLEXLAST. In B. Maribo Pedersen, editor, *State of the Art of Aeroelastic Codes for Wind Turbine Calculations*, pages 161–166, Lyngby, Denmark, 1996.

[74] J. Walker and N. Jenkins. *Wind energy technology*. John Wiley & Sons, Chichester, 1997.

[75] B. Wilson. FAST_AD advanced dynamics code. Technical Report OSU/NREL REPORT 99-01, NREL, Oregon State University, Corvallis, Oregon, 2000.

[76] B. Wilson. An aerodynamics and dynamics analysis code for horizontal-axis wind turbines.
Internet online, 27 Mars 2001. http://wind2.nrel.gov/designcodes/fastad/.

[77] Wind Power Monthly. Wind energy facts and figures from Windpower Monthly.
Internet online, 9 November 2004.
http://windpower-monthly.com/spis/runisa.dll?WPM:WINDICATOR:910351.

Appendix A

Airfoil data

A.1 Lift and drag profiles of the Alsvik 180 kW wind turbine

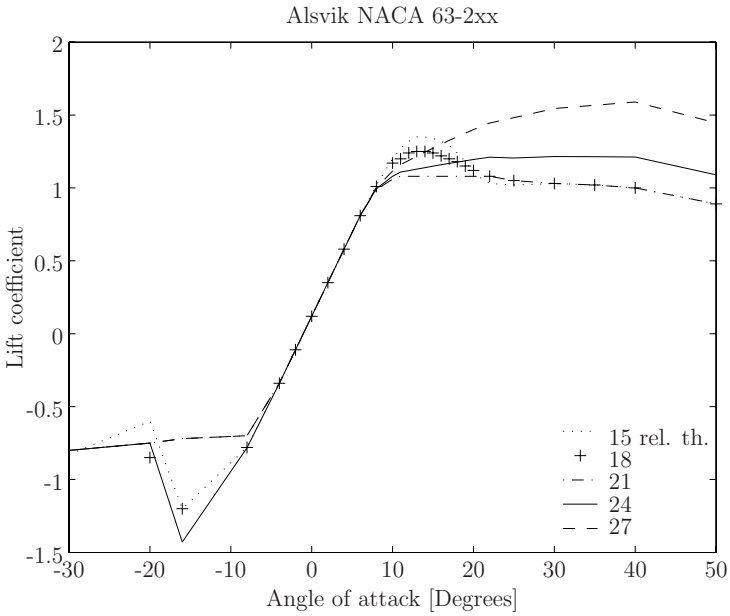

Figure A.1: Lift coefficient as function of the angle of attack for the Alsvik turbine with airfoils corresponding to blade sections referenced to relative thicknesses.

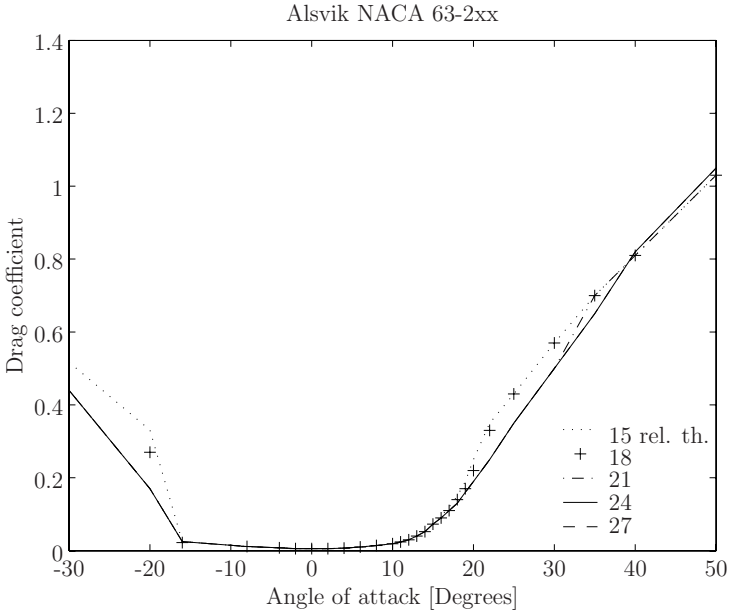

Figure A.2: Drag coefficient as function of the angle of attack for the Alsvik turbine with airfoils corresponding to blade sections referenced to relative thicknesses.

A.2 Lift and drag profiles of the Tjæreborg 2 MW wind turbine

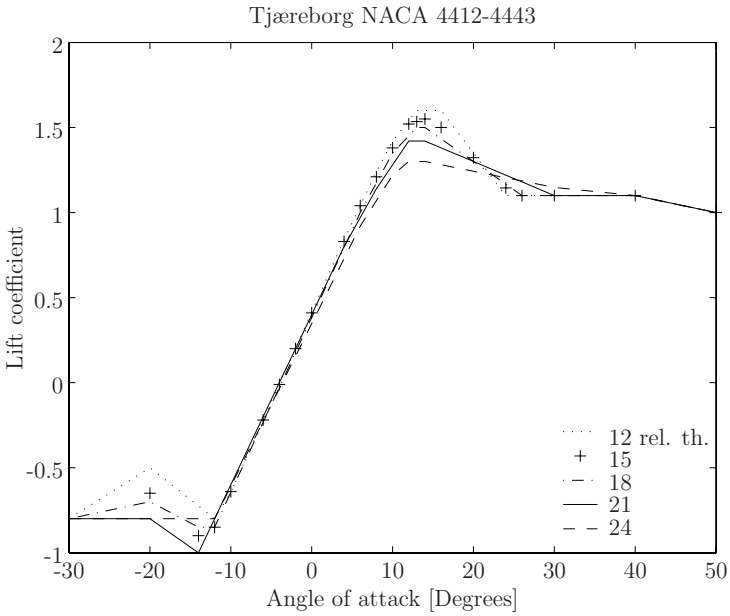

Figure A.3: Lift coefficient as function of the angle of attack for the Tjæreborg turbine with airfoils corresponding to blade sections referenced to relative thicknesses.

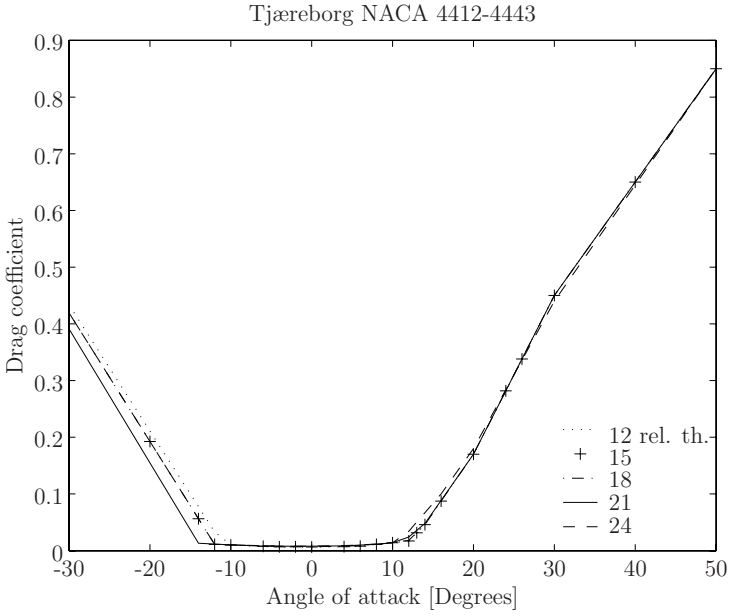

Figure A.4: Drag coefficient as function of the angle of attack for the Tjæreborg turbine with airfoils corresponding to blade sections referenced to relative thicknesses.

Appendix B

Input files

B.1 Example of SOSIS-W input file

```
# DEMONSTRATION INPUT DATA FILE FOR SOSIS-W VERSION 1.3
#
# RUN PARAMETERS:
# ID OF RUN
#
   demo
#
# GRID PARAMETERS:
# HUB HEIGHT , WIND SPEED AT HUB HEIGHT , INCLINATION , POWER
#
     35.0              10.0                10.0        0.2
#
# NUMBER OF GRID POINTS , GRID SIZE
#
          144                2.0
#
# SIGNAL PARAMETERS:
# TIMESTEP (s) , LENGTH OF SIGNALS (s) , SPECFLAG
#
     0.1                600.0              1
#
# STANDARD DEVIATIONS OF TURBULENCE (AMBIENT AND WAKE):
# STANDARD DEV u  ,  STANDARD DEV v  ,  STANDARD DEV w
#
     1.5  1.5           1.2   1.2          0.75   0.75
#
# LENGTH SCALES OF TURBULENCE (AMBIENT AND WAKE):
#       Lu        ,       Lv          ,     Lw
#
  350.0   350.0       50.0   50.0       12.2  12.2
```

```
#
# COHERENCE DECAY FACTORS AND LENGTH SCALE:
# U-COMPONENT , V-COMPONENT , W-COMPONENT , LENGTH SCALE
#
      8.8           8.8           8.8         10000.0
#
# WAKE PARAMETERS:
#  DIAM    ,   DEFICIT   ,  YOFF  ,  ZOFF  ,  SIGMAY   ,  SIGMAZ
#
   37.0          0.001        0.0     -0.0       0.4        0.37
#
# SEED     CORRECTION1  CORRECTION2   OUTFLAG
#
  890505       0.1          0.5          4
#
```

B.2 The Alsvik input file

```
# Turbine name
  Alsvik
# Rotor coning angle beta (deg) and tilt angle tau (deg)
                     0.0                          0.0
# a check number 888.88 should be on next line
  888.88
# Blade tip radius and rot radius
# hub height and "overhang", xh
#
# th=z for tower top, xh=x for hub position. Positive
# for upwind turbines
# rtip       rrot      th      xh
  11.6       1.0       29.7    1.477
# ================= BLADE DATA ====================================
# if isetarea=0 the areas from the tabulated values will be used
  0
# Radius  Chord     Area     Twist    rel, th.   profile1 profile2
# m       m         m2       deg      -          -        -
  1.05    0.68      0.44     20.5     30         5        0
  2.1     1.35      1.07     20.1     35         5        0
  3.3     1.39      1.64     12.1     31         5        0
  4.5     1.27      1.60     6.04     27         5        0
  5.7     1.15      1.45     3.04     22.5       4        0
  6.9     1.03      1.31     1.33     19         3        2
  8.1     0.91      1.16     0.42     17         2        1
  9.3     0.79      1.02     0.11     15         1        0
  10.2    0.7       0.67     0        15         1        0
```

```
  11.3    0.59      0.71     0        15         1        0
# End blade data
# ====Dynamic stall method. common for all airfoils=================
# If lcncl=0 static profile data will be used. All other parameters
# in the dynamic stall model will then be disregarded
#-------------------------------------------------------------------
# lcncl   lpotmeth  lfmeth  lvormeth  lcddyn  ldut
  2       4         4       2         2       0
#-------------------------------------------------------------------
# coeffa1     coeffa2      coeffb1     coeffb2
  0.3         0.7          0.13        0.53
# Number of airfoils (1 row)
  5
# ++++++++++++ New profile ++++++++++++++++++++++++++++++++++++++++
# File name with "sep-data" (1 row)
  D:\vindverket\profildata\alvid15v1_360.cla
# airfoil number
  1
# rel thickness
  15
# tf data (3 rows)
  0.0  0.5  0.1
  5
  0
# -------------------------------------------------------------------
# vortex parameters (1 row)
# tv, tvl, tvs, cn1pos, cn1neg
  2   1    1    2       -1
# ++++++++++++ New profile ++++++++++++++++++++++++++++++++++++++++
# File name with "sep-data" (1 row)
  D:\vindverket\profildata\alvid18v1_360.cla
# airfoil number
  2
# rel thickness
  18
# tf data (3 rows)
  0.0  0.5  0.1
  5
  0
# -------------------------------------------------------------------
# vortex parameters (1 row)
# tv, tvl, tvs, cn1pos, cn1neg
  2   1    1    2       -1
# ++++++++++++ New profile ++++++++++++++++++++++++++++++++++++++++
# File name with "sep-data" (1 row)
  D:\vindverket\profildata\alvid21v1_360.cla
```

```
# airfoil number
  3
# rel thickness
  21
# tf data (3 rows)
  0.0  0.5  0.1
  5
  0
# ------------------------------------------------------------------
# vortex parameters (1 row)
# tv, tvl, tvs, cn1pos, cn1neg
  2   1    1    2       -1
# ++++++++++++ New profile ++++++++++++++++++++++++++++++++++++++++
# File name with "sep-data" (1 row)
  D:\vindverket\profildata\alvidnr4_360.cla
# airfoil number
  4
# rel thickness
  24
# tf data (3 rows)
  0.0  0.5  0.1
  5
  0
# ------------------------------------------------------------------
# vortex parameters (1 row)
# tv, tvl, tvs, cn1pos, cn1neg
  2   1    1    2       -1
# ++++++++++++ New profile ++++++++++++++++++++++++++++++++++++++++
# File name with "sep-data" (1 row)
  D:\vindverket\profildata\alvidnr5_360.cla
# airfoil number
  5
# rel thickness
  27
# tf data (3 rows)
  0.0  0.5  0.1
  5
  0
# ------------------------------------------------------------------
# vortex parameters (1 row)
# tv, tvl, tvs, cn1pos, cn1neg
  2   1    1    2       -1
# ======== End of profile data ====================================
# For constants and choice of method. See AERFORCE-manual
#
# default: at1=0.32
```

```
# luitan=1
# time-const int-method luitan
# at1,     con_vec(1),    lval(2), lval(1)
  0.32     .2             1        1
#
# =========== Wind, mech, etc. ======================================
# Air density (rho)
  1.225
# gridpo: Number of gridpoints along an edge, must be the same
# number as specified in SOSIS. N=gridpo*gridpo e.g. 144=12*12
# grsteps: Grid size in meters
# gridpo grstep
  12      2
# =========== Tower data for shadow wake effects====================
# Tower data is used if ltornskugga=1
# ntornin (number of heights were the tower radius is given)
  2
# ztorn rtorn   (z is height over surface)
  0     1.1
  29.8  0.63
# ---------------------
# One row with 7 integer
# Two rows with 7 real
# ltorskugga = 0 => no tower shadow effects
# See AERFORCE-manual for further description
# ltornskgga  luitower lupmeth  int_dum   int_dum   int_dum int_dum
  1           1        1        0         0         0       0
# ytornlimit  cd_bp1   cd_bp2   re_bp1    re_bp2 bvak_bp1  bvak_bp2
  50          .4       1.2      0.2       0.4    2         5
# coeff_bp1 coeff_bp2 vakvinkel_bp1 vakvinkel_bp2 delta dummy
  1.5       1.3       1             100           0     0
# If ytornlimit is >100, then standard (default) values will be
# used and values for all _bpx-values set in the input file will
# be ignored.
# Re_bpx should be given in millions (Re=V,tower*d,tower/ny)
# vakvinkel_bp1 i grader
#
# If cd_bp2 is 888.0, then values for Cd_bp1, bvak_bp1 and coeff_bp1
# will be used for all Re,tower
#
#=======================END TOWERDATA==============================
# a check-number 888.88 should be on next line
  888.88
#-------------------------------------------------------------------
```

Paper 1

Aeroelastic FE modelling of wind turbine dynamics

By Anders Ahlström
Department of Mechanics, KTH, SE-100 44 Stockholm, Sweden

Submitted to Computers & Structures

Summary By designing wind turbines with very flexible components it is possible to reduce loads and consequently the associated cost. As a result, the increased flexibility will introduce geometrical nonlinearities. Design tools that can cope with those nonlinearities will therefore be necessary at some stage of the design process. The developed model uses the commercial finite element system MSC.Marc, which is an advanced finite element system focused on nonlinear design and analysis, to predict the structural response. The aerodynamic model named AERFORCE, used to transform the wind to loads on the blades, is a Blade-Element/Momentum model, developed by The Swedish Defence Research Agency (FOI, previously named FFA). The paper describes the developed model with focus on component modelling to allow for geometrical nonlinearities. Verification results are presented and discussed for an extensively tested Danwin 180 kW stall-controlled wind turbine. Code predictions of mechanical loads, fatigue and spectral properties, obtained at normal operational conditions, have been compared with measurements. The simulated results correspond well with measurements. Results from a blade loss simulation are presented to exemplify the versatility of the developed code.

Key words: wind turbine; structural dynamics; aeroelasticity; finite element, nonlinear analysis

1 Introduction

Designing long-lasting, fatigue-resistant wind turbines at minimal cost is a major goal of the wind turbine industry and their customers. To achieve this goal, it is important to use reliable tools in the design process. There are many design codes available today, which have been proved to perform well in comparison tests, e.g. Bladed, Flex5, Phatas, Vidyn and Hawc [1–5]. There are noticeable differences between the codes in use, e.g. that all codes do not include torsional blade deflections. Most of them assume that deflections are small and that the aerodynamic loads can be applied to the un-deformed structure [6]. In reference [6] it is also concluded that these assumptions are being exceeded with the present development towards flexible turbines.

The main motivation of the developed code was to include effects due to geometrical nonlinearities particularly introduced by large blade deflections.

The model presented is based on the commercial FE package MSC.Marc, [7], which focuses on nonlinear design and analysis. The many rotations together with the extreme number of time steps required in a dynamic analysis, put great demands upon the software. Further must the system be able to communicate with other softwares. MSC.Marc offers the possibility to link user-written FORTRAN subroutines into the FE code. This is a requirement since the aerodynamic loads must be calculated and updated in each increment.

The objective with the presented work is to describe how a commercial software can be adopted to wind turbine applications. Special emphasis will be put on component modelling and the application of loads with respect to large displacements. Further are numerical examples presented in normal wind conditions and in the transient case of a blade failure, leading to loss of one blade. The results under normal conditions are compared with experimental data from the Swedish experimental wind farm at Alsvik, on a three-bladed, stall controlled Danwin 180 kW. The relatively stiff turbine will not cause any significant deflections of the blades during normal operation. Hence, the effects of geometrical nonlinearities due to large deflections are small. However, the well defined conditions on the site, together with the large number of measurements, of which some are described in [8], makes the turbine a good candidate for initial comparison. The blade loss example, performed on the same turbine, is a transient load case that is used to show how the developed code can be utilised to model events that are normally not possible to simulate with the present aeroelastic codes.

2 Structural model

2.1 Program structure

The wind turbine simulating tool consists of three main parts: The MSC.Marc finite element program for modelling the structural dynamics, AERFORCE for the calculation of the aerodynamic loads and SOSIS-W for the generation of the turbulent wind fields. The idea with using a commercial FEM program is to take advantage of the stability and versatility an extensively tested, well documented, program offers. Another advantage is that the software may be used as a tool throughout the complete design process. For instance to dimension specific parts of the structure, or to include effects from waves etc. The generality makes it possible to model special events like, e.g. the presented blade loss example.

2.2 Structural modelling

MSC.Marc allows modelling of linear and nonlinear problems involving, e.g. contacts, nonlinear material effects and structural dynamics, [7]. A main advantage with MSC.Marc is the subroutine feature that allows user to substitute existing subroutines with subroutines adopted to the specific problem. Subroutines for implementation of loads, tying constraints and local coordinate systems are especially useful in wind turbine applications. The user-supplied load was defined as a nodal load type. User-supplied routines for nonuniform distributed loads are present but are currently not implemented. The user-supplied loads were evaluated in each time step and in each iteration. These loads were added to the global load vector normally established in the response calculation for the time steps. The user-supplied loads can be calculated based on a number of different nodal parameters. Typical parameters used were e.g. information about nodal displacements and velocities.

The subroutines, [9], used in the present model were *forcdt* for inputting time dependent nodal quantities as nodal forces, prescribed displacements, et cetera. *utrans* for implementation of local coordinate systems. The systems were updated in each iteration by updating the rotation matrix from the local to global coordinate system. *uforms* for defining constraint conditions (tying). The tying subroutine was used to apply constraints between nodal displacements in global or local coordinate systems. Subroutines were also used to write nodal and element quantities to file.

All Fortran subroutines as well as MSC.Marc were written in double precision. The user subroutines were linked with the MSC.Marc library and a new executable was created using *Compaq Visual Fortran Standard Edition 6.6.B* [10].

2.3 Aerodynamic modelling

For the calculation of the aerodynamic forces acting on the blades of the wind turbine, a subroutine package named AERFORCE, [11], was used. The aerodynamic model is based on the blade element momentum (BEM) method, which today is the most common method in aeroelastic codes. In order to get better results, the BEM model needs to be extended. In AERFORCE the BEM method is extended to incorporate:

- Dynamic inflow: unsteady modelling of the inflow for cases with unsteady blade loading or unsteady wind.
- Extensions to BEM theory for inclined flow to the rotor disc (yaw model).
- Unsteady blade aerodynamics: the inclusion of 2D attached flow, unsteady aerodynamics and a semi-empirical model for 2D dynamic stall.

In spite of a number of limitations in the method itself, the BEM method is still the best tool available, within reasonable computation time, for getting good first order predictions of thrust, torque and efficiency for turbine blades under a large range of operating conditions.

All properties related to structural geometry and kinematics, such as blade velocities, blade element lengths, etc. were calculated and inputted in the deformed state.

In the package, additional models are included for the modelling of tower shadow effects and dynamic stall. The models are described in [12, 13], respectively.

2.4 Wind field simulation

SOSIS-W is an artificial wind data generator, [14]. The program is separated from the aeroelastic code and is used as a stand alone program for providing the pseudo-random wind field series, in three global directions, to use in the structural simulation. The results presented in the verification examples were calculated by SOSIS-W.

2.5 Calculation scheme

The section aims to give a brief insight into the calculation steps performed through FORTRAN subroutines and data read as input, in a simulation. The wind turbine model itself is determined in the MSC.Marc input file by giving node coordinates, element types and connections, stiffness and mass properties, constraint equations, etc. Input and parameters are further described in the numerical example. The main effort in developing the aeroelastic tool has been to implement routines for adaption of the structural model to the aerodynamic code, [15]. As the loads are varying

over time and space the equations of motion are solved numerically in a step-by-step manner using an implicit integration scheme. During the step-by-step response calculation, the aerodynamic loads are evaluated in each iteration and time step.

The following sequence is called by MSC.Marc in each iteration:

1. Save x,y,z displacement components for nodes of interest, e.g. blade nodes and orientation nodes.
2. Save x,y,z velocity components for each blade node and the rotational speed of the rotor.
3. Derive the transformation matrices, $\mathbf{S}_{\text{gr}}$ (between the global and the rotor system) and $\mathbf{S}_{\text{ge}}$ (between the global and each blade element system), based on the x,y,z components saved at step 1. Calculate the transformation matrix between the rotor and the global system, $\mathbf{S}_{\text{re}}$.
4. Read input data and calculate aerodynamic forces.
   (a) Read data from input file, e.g. blade information such as chord length, thickness, area, twist, pitch, profile number, etc. Step 4(a) is only performed at the first time step since the values are not time dependent.
   (b) Process the data read at step 4(a) For instance interpolate data between input airfoil tables and modify $\mathbf{S}_{\text{re}}$ to include the contributions from twist and pitch.
   (c) Calculate the wind speed acting on each blade element depending on the rotor position.
   (d) Input necessary parameters to AERFORCE and calculate the forces acting on each blade element.
5. Transform blade element forces to the global load vector.
6. Calculate generator moment and write result to the global load vector.

The data are then transferred back to MSC.Marc, where the equilibrium iterations of the time step are performed. The scheme described above should be seen as a very general description of what steps are performed in a simulation. To allow for large deformations, all tying constraints and springs must follow the deformed geometry. That was achieved by specifying local coordinate systems that were updated in each iteration. In addition to the coordinate systems mentioned above, systems were used for the non-rotating rotor shaft and the yaw system.

2.6 Derivation of transformation matrices

Transformation matrices were used for specifying local coordinate systems and for transforming the aerodynamic loads to the global system. All transformation matrices were, in the present implementation, based on the position of an additional

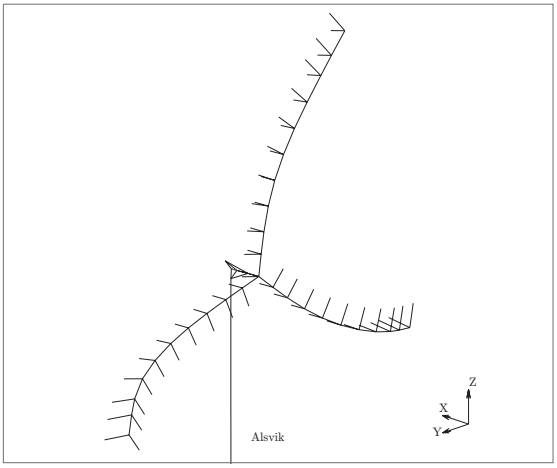

Figure 1: Element configuration on a rotor divided in ten elements/blade.

element configuration. For instance, to find the transformation matrix between the global system and a system attached to the deformed blade, two help nodes and two elements were used. The first element was connected to the blade node and a help-node perpendicular to the blade node in the Y-Z plane, Figure 1. The second element was connected to the blade node and a help-node perpendicular to the blade element in the X-direction, Figure 1. The two help nodes are then forced to follow the blade's node motion when elastic deformation and rigid motion is present. With the information available about the coordinates of the two help nodes and the rotor node, two base vectors were calculated. After normalising the vectors, the third direction vector was calculated as the vector product between the two base vectors. The elements used for keeping track of the position of the blades were modelled with zero mass to avoid influences on the results due to forces introduced by inertia effects. An alternative way to calculate the transformation matrices is to use a rigid link configuration, but this does not seem possible in large rotation analysis in the current version of MSC.Marc. The main benefit with using rigid links compared to beam elements for this purpose is to reduce the number of DOFs.

2.7 Numerical methods, tolerances and damping

The finite element equations are formulated with the updated Lagrangian formulation, which means that all static and kinematic variables are referred to the current configuration, [16]. The full Newton-Raphson was used in the simulations for equilibrium iterations in each time increment, together with a sparse direct solver. The Single Step Houbolt (SSH) method, which introduces numerical damping, has been used in the present work, [17]. Displacement checking was used as the criterion for convergence. The ratio of iterative change to increment in displacements, $\| \delta u \|_\infty$ / $\| \Delta u \|_\infty < tol_1$, was set to 10^{-4}. Here, Δu is the displacement increment

vector and δu the correction to incremental displacement vector. With this method, convergence is satisfied if the maximum displacement of the last iteration is small compared to the actual displacement change of the increment.

Proportional damping, [18], was used to damp tower motions. The tower mass contributions to the global mass matrix were scaled with 0.5, which corresponds to a logarithmic decrement of 2.5 %, to form the tower's contribution to the damping matrix. Blade damping was introduced to each blade element by dashpots formulated in the co-rotational blade root system. The damping is thereby referred to the blade root system and the damping properties can be set independently in flap, edge and torsional direction. The dashpots were set to give a logarithmic decrement of 4 % in both flapwise and edgewise direction.

3 Description of the wind farm, collected data and assumptions

3.1 Site details

The Swedish experimental wind farm at Alsvik is located on the west coast of the island of Gotland in the Baltic sea. The wind farm is specifically designed for the purpose of experimental measurements and it consists of four strategically placed Danwin 180 kW wind turbines, Figure 2, [19]. Three of the turbines stand on a line that runs along the shoreline in a NNW-SSE direction. The fourth turbine is located to the east of this row, thus deliberately subjected to wind turbine wakes during westerly winds. The northeast land behind them is low and flat, consisting mainly of grazed grasslands and a low growing pine forest.

3.2 Data acquisition and anemometry

Since the Alsvik wind farm was intended for experimental measurements, it was equipped with two meteorological masts, each being 52 m high. Equipments on the masts measure the wind speed and the direction on seven elevations above ground. Mast 1 is placed between Machine 1 and 2 and Mast 2 is located just to the south west of Machine 4. Machine 4 has been equipped with a number of sensors and strain gauges to allow loading measurements of the major loading components. In the experiments utilised in the present project, the following signals were recorded with a sampling frequency of 31.25 Hz:

- Root flapwise and edgewise bending moment on all three blades
- Tower bending and torsional moments at two elevations
- Acceleration along and across nacelle direction

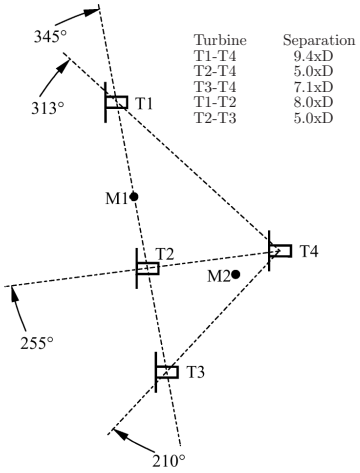

Figure 2: Layout of the wind farm at Alsvik, with turbines T1-T4 and masts M1, M2. Reproduced by permission of [19].

- Angular acceleration of nacelle
- Nacelle direction relatively north
- Rotor azimuthal position
- Wind speed on top of the nacelle (disturbed)
- Electrical power

The meteorological masts are equipped with cups and vane anemometers at heights of 2.8, 9.9, 18.4, 24.4, 30.8, 35.6 and 40.7 m. The speed and direction of the wind were sampled at 2 Hz. The collected data were recorded in the early nineties by The Swedish Defence Research Agency (FOI, previously named FFA) and constitutes a comprehensive database of high quality measurements. The database has been used in many studies, e.g. [19, 20].

3.3 Description of studied campaigns

The campaigns used for comparisons, campaigns 1–2, were deliberately chosen to be unaffected by wake effects from the other turbines. Campaign 3 was synthetically generated by SOSIS-W and used in the blade failure example.

- **Campaign 1, low wind speed** The first campaign selected for comparison was a 600 s long sequence with a mean wind speed of 9.8 m/s and turbulence intensity of 10.6 %.

- **Campaign 2, high wind speed** Campaign 2 also had a duration of 600 s. The relatively high mean wind speed of 14.9 m/s makes the turbine work mostly in the stall region. The turbulence intensity is 11.8 %.
- **Campaign 3, blade loss** Campaign 3 has a mean wind speed of 25.0 m/s and a turbulence intensity of 6.0 %.

3.4 Modification and processing of the measured data

There are two types of errors in the measurements: errors related to wind speed and direction, and blade moment errors. The errors were corrected for, based on modifications derived in, [19]. The exponential wind profiles were determined based on the five wind series. The measured winds at hub height were then spatially distributed in space with statistically correct coherent turbulence components in all three directions. The generated wind series were derived based on a random seed.

3.5 Blade loss presumptions

To demonstrate the versatility of the developed code, an example is presented where one blade comes loose. The aerodynamic loads act on all three blades. This assumption is valid until and shortly after the blade is released. The limitation is, in the current implementation of the BEM method, averaging of e.g. the induction factor. Hence, loads and displacements are believed to be reasonably correct during the failure and shortly after. The time step was reduced from 6 ms to 2 ms, in order to better capture the transients at the blade loss.

4 Analysis and modelling of the Alsvik wind farm

The goal with the numerical example was to model the Danwin turbine as closely to reality as possible based on available data.

4.1 Machine parameters

The basic machine parameters are tabulated in Table 1. The turbine is a three bladed stall controlled Danwin with a rated power of 180 kW and a rated wind speed of 12 m/s. The cut-in speed is 5 m/s and the cut-out speed is 25 m/s. Five airfoil tables, covering the full 360 degrees range of angle of attack, were used in the calculations.

Table 1: Basic description of the Alsvik turbine.

Rotor		Blades		Masses (kg)	
Number of blades	3	Material	GRP	Blade	700
Rotor diameter	23.2 m	Blade length	10.52 m	Rotor and hub	2990
Hub height	30.0 m	Root chord	1.45 m	Nacelle without rotor	5880
Rotor speed	42.8 rpm	Tip chord	0.59 m	Tower	10400
Tilt	5°	Blade profiles	NACA 63-2xx series	Total weight	19300

4.2 Rotor

The rotor was modelled with rectangular six degree-of-freedom elastic Euler-Bernoulli beam elements. Shear centre, mass centre and pitch axis were assumed to coincide in the current work. Each blade was modelled by twenty elements to which additional massless elements were attached. The massless elements were used to calculate the transformation matrices needed in the simulations to keep track of the position and torsion of the blades according to Section 2.6. Structural data can be found together with the blade coordinates and the stiffness properties in Appendix A, Table 6.

4.3 Tower

The tower was modelled with circular hollow six degree-of-freedom elastic Euler-Bernoulli beam elements. The tower was discretised into fourteen elements and was rigidly connected to the ground. The connection between tower-top and bedplate was described by a combination of springs and constraint equations. The mass properties were calculated based on the geometrical data and the density of steel, 7850 kg/m^3, specified in the MSC.Marc input file. A concentrated mass of 950 kg was also applied at the tower top. The tower data can be found in Appendix A, Table 7. The tower elements were given a mass scaled damping property, $\alpha = 0.5$, according to the definition in Section 2.7.

4.4 Bedplate and drivetrain

The bedplate and drivetrain were, in principle, modelled as described by Figure 3. The bedplate, with corner nodes n2, n4, n6 and n8 in the figure, was modelled relatively rigid with six degree-of-freedom elastic beam elements. The mass of the bedplate was applied, in all three directions, as a point mass of 6500 kg at the centre of gravity. At the same point were the moments of inertia, 1760, 5405 and 4729 kgm^2, applied for each rotational degree of freedom.

The drive train was made up by the rotor shaft, between the hub centre, node n10

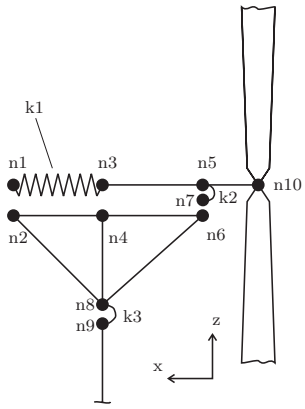

Figure 3: Bedplate and drive train.

and node n3, and the spring-damper configuration between nodes n1 and n3, Figure 3. Further was node n10 given a concentrated mass of 900 kg and a concentrated moment of inertia of 2000 kgm^2, about the rotating shaft, representing the mass properties of the hub. The generator moment of inertia, applied to node n1, was set to 2548 kgm^2.

The connection between rotor and bedplate was achieved by using constraint equations on nodes n1–n2, n3–n4 and n5–n6–n7. These equations ensured that all displacements were equal between node pairs. In the figure, the node sets n1–n2, n3–n4, n5–n6–n7 should in fact be located at the same coordinates, but for illustrative reasons the axle is shown above the bedplate. The nodes were used to specify constraint equations expressing slave (dependent) degrees of freedom as linear combinations of master (independent) degrees of freedom. Nodes n1–n2 and n3–n4 were constrained in x, y, z translations and y, z rotations, where the x-axis coincide with the shaft direction. The n5–n6–n7 configuration was arranged so that n7 acted as a master node constrained to n5 and n6 as x, y, z, ϕ_x and x, y, z, ϕ_y, ϕ_z, respectively. The spring constant k2, according to Figure 3, was set as a rotational spring acting in tilt and yaw directions. The connection between bedplate and tower, n8–n9, was achieved by springs and constraint equations. The nodes were constrained to represent a pin joint connection between the parts. The spring constants in the connection decides the rotational stiffness. The stiffness and damping properties are shown in Table 2. All constraint equations and springs used were specified in local coordinate systems, which mean that the turbine may deflect without affecting the behaviour of one or other. The blade loss example was carried out by using the possibility to change tying constraints in time by using a subroutine. At a specific time, the constraints that were keeping the blade in normal position were turned off, hence the blade was released from the hub.

The generator was modelled as an asynchronous generator. The model used in the simulations was calculated based on approximately 2% slip and a rotational velocity

Table 2: Spring stiffness of k1, k2, k3 in Figure 3.

Stiffness	**k (Nm/rad)**	**Associated damper (Nms/rad)**	**Comment**
$k1_x$	$1.96{\cdot}10^6$	2500	Primary shaft torsion
$k2_y$	$2.08{\cdot}10^7$	$80{\cdot}10^5$	Primary shaft and bearing tilt
$k2_z$	$1.0{\cdot}10^8$	$80{\cdot}10^5$	Primary shaft and bearing yaw
$k3_x$	$1.0{\cdot}10^9$	0	Yaw bearing roll
$k3_y$	$4.0{\cdot}10^8$	0	Yaw bearing tilt
$k3_z$	$3.75{\cdot}10^7$	0	Yaw system system

of approximately 4.43 rad/s:

$$M_{\text{gen}} = 457000(\omega_{\text{rot}} - 4.43) \tag{1}$$

where ω_{rot} is the generator rotational velocity, measured in each time iteration. The expression introduces a penalty moment, striking towards the correct rotational speed. The generator moment was transformed to act around the shaft, independently of the total deflection or yaw of the turbine.
Equation (1) was modified with a time variable t to be used at startup to prevent overloading. The modified equation was in use the first 20 seconds of simulation and gives a softer startup sequence:

$$M_{\text{gen}} = 457000\left(\omega_{\text{rot}} - \frac{4.43t}{20}\right) \tag{2}$$

4.5 Tuning of model parameters based on experimental data

As mentioned earlier, the Alsvik wind farm has been the subject of many reports and projects. Holm [21], performs a frequency analysis on some of the stand still campaigns. Six campaigns are studied, 'fcam949', 'fcam338', 'fcam827', 'fcam500', 'fcam722' and 'fcam00'. The campaigns are, between 35 to 60 minutes long except for 'fcam00', which is 10 minutes. The result of the analysis is presented in Table 3 and some of the mode shapes are illustrated in Figures 4 (a–d). The last column in Table 3 shows the tuned frequencies of the numerical model. The tuned coupling stiffnesses are shown in Table 2 and are used in the sequel.

5 Results obtained from the numerical simulations

The results are mainly presented in figures and tables. If different colours have been used in the figures, the grey line indicates simulated data and the black line measured.

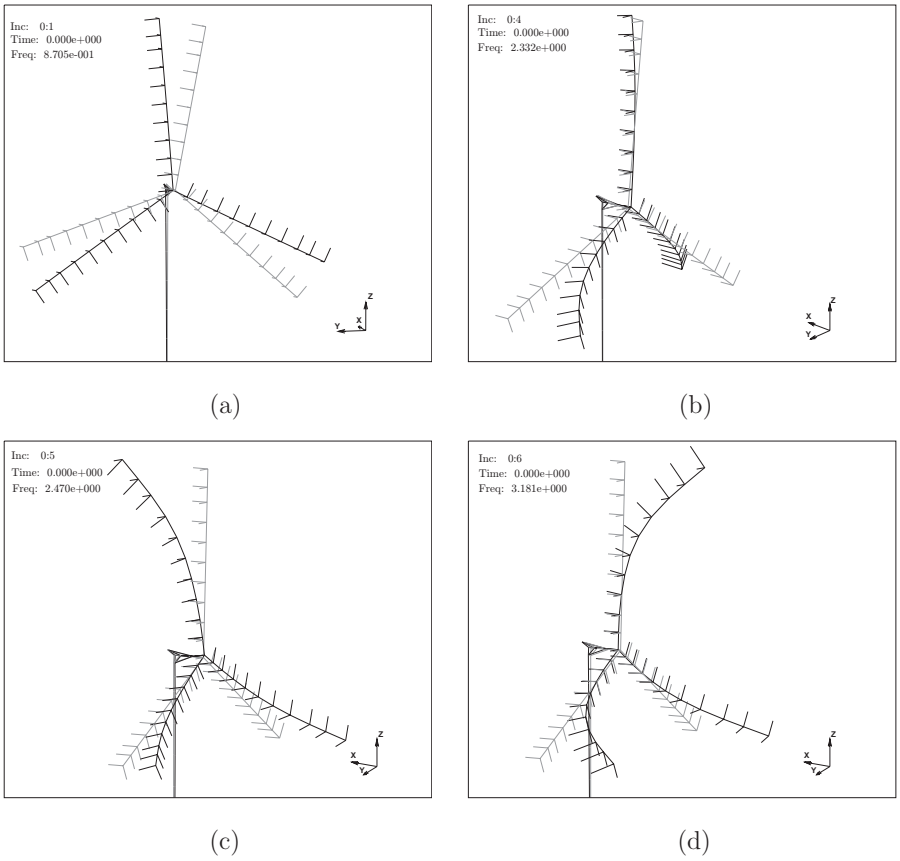

Figure 4: Some of the mode shapes. Mode1, shaft torsion mode (a). Mode 4, yaw and asymmetrical rotor mode, (b). Mode 5, flapwise symmetrical rotor mode, (c). Mode 6, edgewise mode, (d).

Table 4 and 5 show the basic statistical variations of campaign 1 and 2 for some of the time series available. The description of each series is presented in Section 3.2. An empty cell in the table denotes that the mean value was, or was close to, zero. The powers presented in the table are not directly comparable as the simulated power was derived from the torsional moment in the turbine axle while the measured power is the electrical output. Some representative plots are given in Figures 6 (a–f) and Figures 7 (a–d) for campaign 1 and 2, respectively. Figures 7 (e–f) illustrates the edgewise blade root moment of blade 3 in the case of low structural damping leading to edgewise vibrations.

A rainflow counting algorithm was used to compare the influence of the simulated versus the measured load in a fatigue manner. In order to compare the simulated and measured results, it is convenient to evaluate the fatigue impact as an equivalent

Table 3: Identified eigenfrequencies of the Alsvik turbine.

Mode	**fcam 949 (Hz)**	**fcam 338 (Hz)**	**fcam 827 (Hz)**	**fcam 500 (Hz)**	**fcam 722 (Hz)**	**fcam 00 (Hz)**	**Model (Hz)**
1^{st} tower bending mode in nacelle direction	1.08	1.08	1.08	1.08	1.08	1.06	1.09
1^{st} tower bending mode perp. to nacelle direction	1.12	1.12	1.12	1.12	1.12	1.06	1.12
Shaft torsion mode	0.87	0.87	0.87	0.91	0.55	1.24	0.87
Combined yaw and asymmetrical rotor mode	2.35	2.35	2.35	2.35	2.35	2.26	2.33
Tilt mode, 1^{st} asymm. rotor mode and 2^{nd} tower bending mode	2.47	2.47	2.47	2.47	2.47	2.40	2.47
Symmetrical rotor mode in flapwise direction	3.18	3.18	3.18	3.18	3.18	3.20	3.18
Edgewise mode without shaft torsion response	5.28	5.28	5.21	5.21 5.40	5.30	—	5.43
Edgewise mode with shaft torsion response	—	—	—	—	6.25	5.32 5.40	6.41

load range R_{eq}, [22, 23]. The equivalent load range is defined as:

$$R_{\text{eq}} = \left(\frac{\sum n_i R_i^m}{n_{\text{eq}}} \right)^{1/m} \tag{3}$$

where R is the load range, n the number of loads in the range and m describes the slope of the fatigue curve. The equivalent loads were evaluated for m=12. The differences between measured and simulated equivalent loads were for the blade loads as well as for the tower bending moments within 10 % when simulating campaign 1. The equivalent loads of campaign 2 were within 7 % for the blade loads and within 12 % for the tower loads.

The power curve has been calculated and is shown in Figure 5. The simulated curve has been multiplied by 0.97 to reflect the efficiency losses in the gearbox, etc. The fluctuating parts are caused by tower shadow effects.

Results of the blade loss example are presented in Figures 8 (a–f). The root flap and edge moments of one blade, together with the tower moment 6.9 m below tower top are presented. The maximum root flap moment increases from a maximum of 103 kNm in the extreme operational case to 127 kNm shortly after the blade loss. The minimum negative root edge moment decreases from −25 kNm to −55 kNm. The load levels in the tower increase from a maximum peak value before the blade loss of 270 kNm in nacelle direction to the maximum 1270 kNm cross nacelle direction.

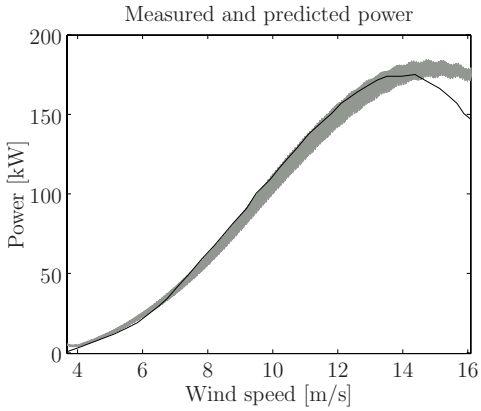

Figure 5: Measured and predicted power performance.

Table 4: Tabulated results, campaign 1, ambient wind speed 7.7 m/s, turbulence intensity 21.0 %.

Series	**Mean exp.**	**Mean sim.**	**Mean err.**	**Std exp.**	**Std sim.**	**Std err.**
Flap1 (kNm)	45.0	44.9	−0.3	5.9	6.3	6.9
Edge1 (kNm)	9.2	7.4	−19.5	17.7	17.7	−0.3
Flap2 (kNm)	43.3	44.8	3.4	6.0	6.4	5.0
Edge2 (kNm)	9.2	7.4	−20.0	17.9	17.5	−2.5
Flap3 (kNm)	42.1	44.8	6.3	6.1	6.1	−0.4
Edge3 (kNm)	9.2	7.4	−20.0	17.5	17.7	9.0
TM1 (kNm)	—	—	—	14.5	15.8	5.7
TM2 (kNm)	—	—	—	10.6	12.7	19.5
Acc1 (m/s^2)	—	—	—	0.094	0.105	11.8
Acc2 (m/s^2)	—	—	—	0.087	0.098	13.0
Acc3 (m/s^2)	—	—	—	0.060	0.108	82.3
Pow. (kW)	110.5	108.6	−1.7	26.5	24.5	−19.0

6 Discussion

The aim with the presented results was to give examples on how the developed code can be used in wind turbine simulations in both ordinary and special conditions. A complete verification is based on a statistical basis which would require hundreds of simulations in different wind conditions. Hence the presented results in normal conditions, due to the stochastic nature of the loads, are not sufficient to verify the aeroelastic model. However, the results show that the methods used in the study were suitable for the application and that the dynamics were captured very well. The chosen time integration method, together with the chosen time step of 6 ms, gives a good correspondence of the PSD plots below rated speed for both the root flap and edge moments up to approximately 14 Hz, which corresponds to second and

Table 5: Tabulated results, campaign 2, ambient wind speed 15.1 m/s, turbulence intensity 10.8 %.

Series	Mean exp.	Mean sim.	Mean err.	Std exp.	Std sim.	Std err.
Flap1 (kNm)	61.0	59.4	−2.7	8.1	8.7	7.6
Edge1 (kNm)	14.5	12.7	−12.4	18.4	18.7	1.9
Flap2 (kNm)	59.1	59.3	0.4	8.3	8.4	1.6
Edge2 (kNm)	14.8	12.6	−14.5	18.9	18.7	−0.8
Flap3 (kNm)	58.7	59.3	1.0	8.0	8.4	4.7
Edge3 (kNm)	16.3	12.5	−23.0	18.4	18.7	1.9
TM1 (kNm)	—	—	—	16.3	15.6	−4.7
TM2 (kNm)	—	—	—	12.5	13.0	4.2
Acc1 (m/s^2)	—	—	—	0.229	0.139	−39.3
Acc2 (m/s^2)	—	—	—	0.177	0.112	−39.7
Acc3 (m/s^2)	—	—	—	0.148	0.139	−6.6
Pow. (kW)	192.2	187.2	−2.6	15.9	10.7	−32.4

third order coupled modes. However, as the studied turbine in stall operates near instability, care must be taken in the choice of time step and structural damping. If the simulations are performed without structural damping, edgewise instabilities develop above rated wind speeds due to the reduction of aerodynamic damping associated with operation in stall. The phenomenon is illustrated in Figures 7 (e–f), where the low structural damping gives rise to stall-induced vibrations. The vibrations were almost under control when the logarithmic damping in edgewise direction was set to 2 %, but dramatically increased with no additional damping applied.

The blade loss example is a very dramatic load case, that fortunately happens very rarely. The aim with the simulation was to exemplify the strengths of the developed tool in an unusual load case. The feature that makes it possible to model this special case, as well as ordinary cases, is the implementation of subroutines. The subroutines can be updated in each iteration, for constraints, springs and dampers in local coordinate systems. The implementation makes it possible to allow for large deformations of the hole wind turbine, which was the main objective in developing another aeroelastic tool.

7 Conclusions

An aeroelastic tool aimed for wind turbine time simulations has been developed. The tool uses the commercial system MSC.Marc, to which subsystems for aerodynamics and wind generation, have been adopted. The main objective in the development of the code has been to consider large deformations of the blades as well as for tower and subcomponents. All loads were calculated based on and applied to the deformed geometry. Further were all tying constraints, dampers and springs implemented to allow for large deformations.

Two campaigns were studied for comparison with measured data, one campaign below rated wind speed and one above. The simulated results were compared to the measured data and the comparison shows that the code predicts loads, power spectra and fatigue loads well in this particular study. Results were also presented for the case of blade failure leading to loss of one blade.

Even though the study is limited with respect to compared campaigns, the results show that a commercial software can be adapted for wind turbine dynamic simulations. The blade loss example presented, shows the versatility of the code, which together with the large displacement assumption are two of the major advantages with the developed code. The drawback is long computational times: about 8 hours for 600 seconds of simulation, compared to modal formulation models. However, the code is primarily intended for research areas to study specific phenomena as e.g. the exemplified blade loss example and not for verification purposes where hundred of simulations are needed.

8 Further research

Although the developed model has been shown very effective in the scrutinised example, there are many possible areas for further studies. A natural step is to broaden the study from operational loads to more severe load cases where the developed model's ability to deal with nonlinearities is utilised. Typical situations are extreme wind conditions and effects from ice accretion etc. Other types of situations are in the case of technical malfunctions, leading to rotor emergency stop. The abrupt deceleration of the rotor results in extraordinary loading situations and deflections which in the worst case increases stresses up to the strength limit. Another study that would be of great interest for wind turbine producers, is to determine in which cases nonlinear finite element models are needed and in which cases faster methods, like e.g. modal approaches, are sufficient to determine the turbine's dynamical behaviour.

9 Acknowledgement

Thanks go to Jan-Åke Dahlberg at FOI for help and interpretation of the experimental data. Thanks also to Anders Björck at NWP for explanations and advise regarding the aerodynamic model. Many grateful thanks to Ingemar Carlén and Hans Ganander at Teknikgruppen AB, for the structural properties of the studied turbine and for explaining all kinds of wind turbine orientated questions.

Support from The Swedish Energy Administration is gratefully acknowledged. Contract/grant number: P12020-1.

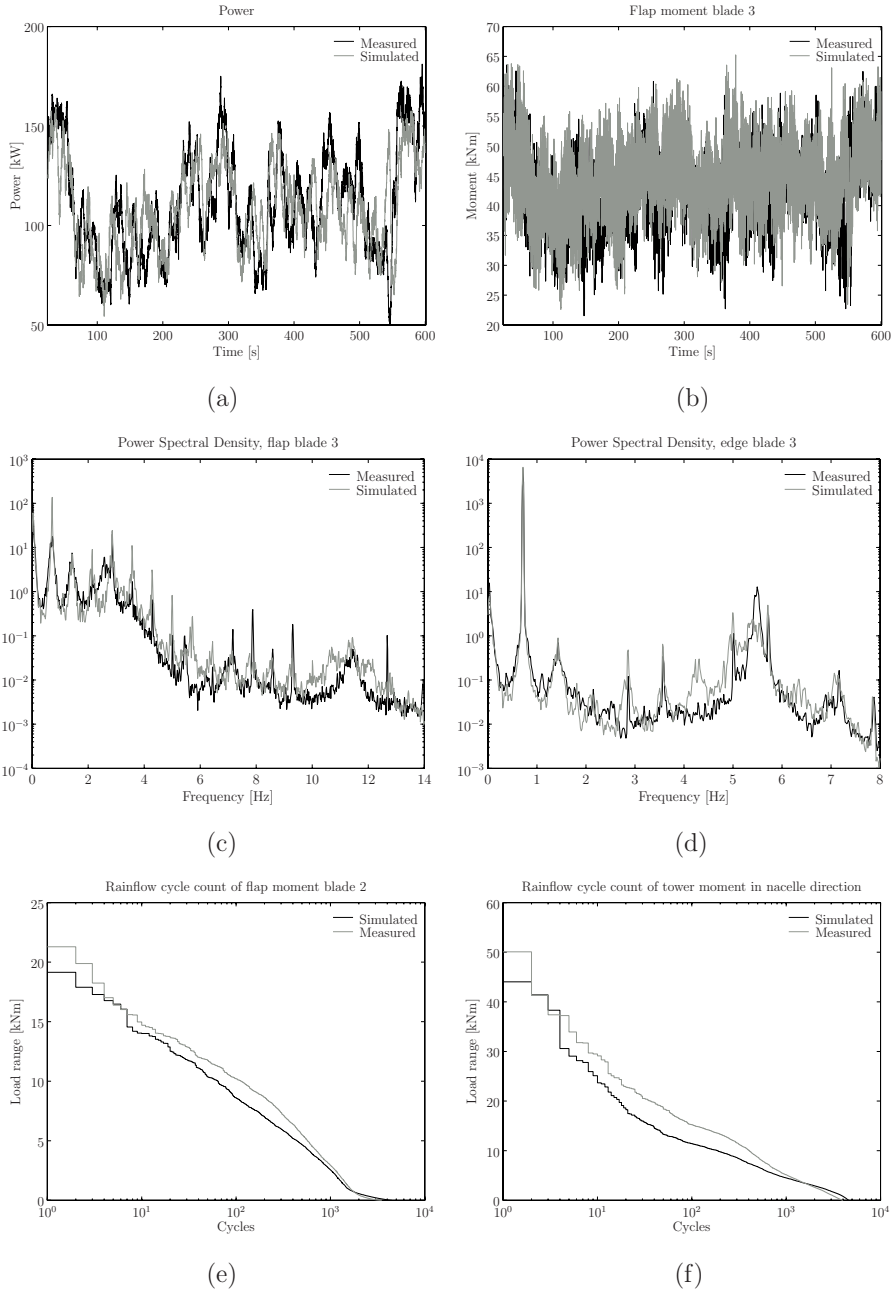

Figure 6: Campaign 1: Electrical power, (a). Flap moment blade 1, (b). Power spectrum flap moment blade 3, (c). Power spectrum edge moment blade 3, (d). Rainflow cycles flap moment blade 2, (e). Rainflow cycles tower moment, (f).

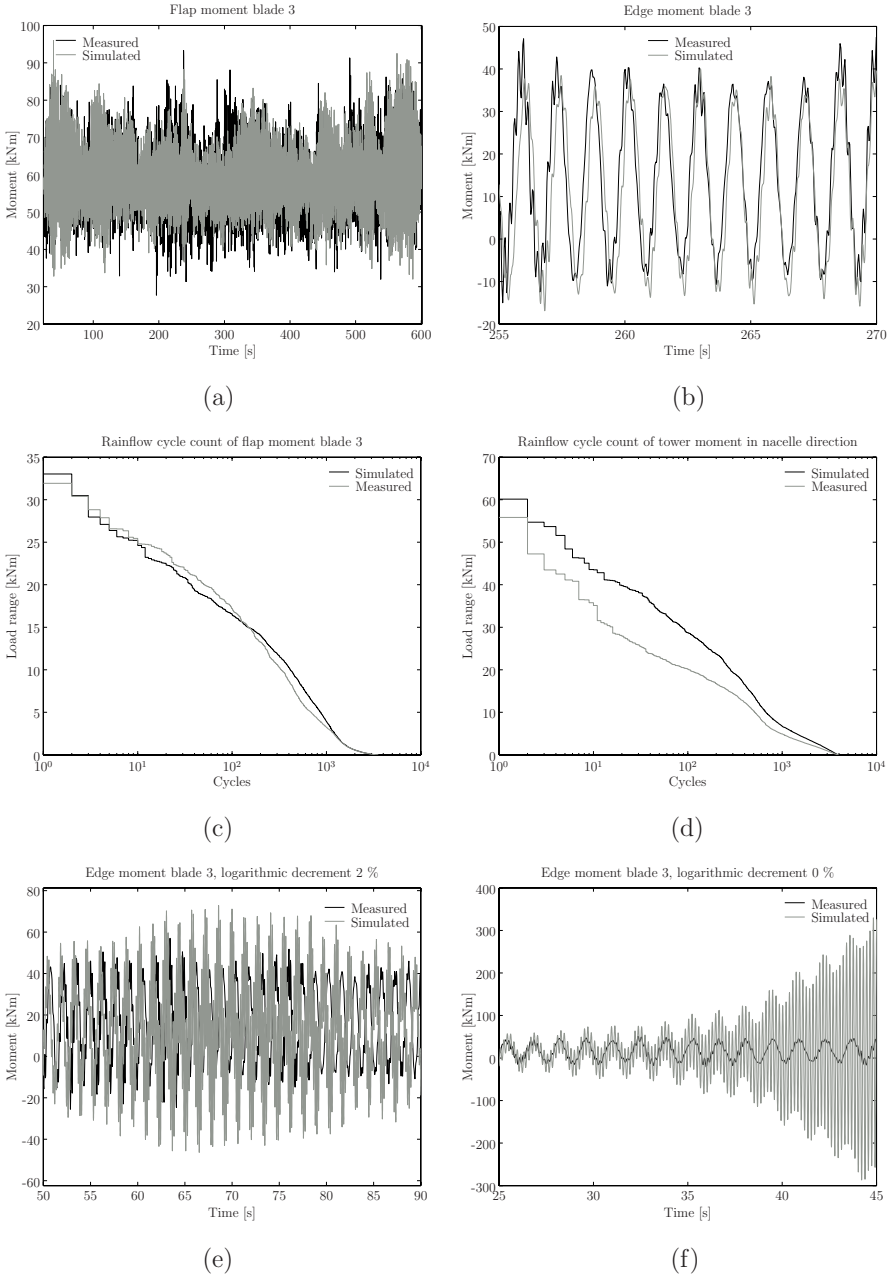

Figure 7: Campaign 1: Flap moment blade 3, (a). Edge moment blade 3, (b). Rainflow cycles flap moment blade 3, (c). Rainflow cycles tower moment, (d). Edge moment blade 3 partly stable, (e). Edge moment blade 3 unstable, (f).

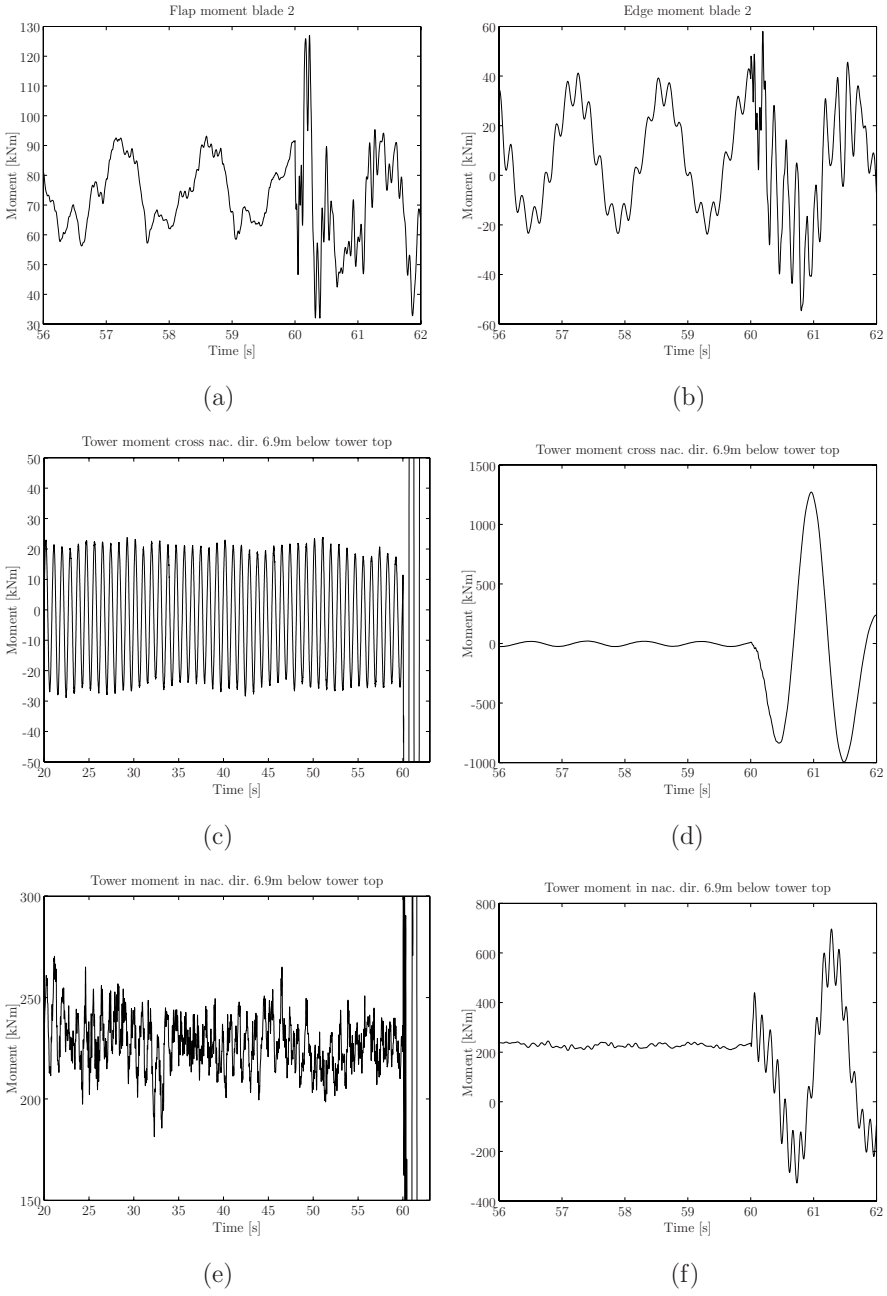

Figure 8: Root flap moment of blade 2, (a). Root edge moment of blade 2, (b). Tower moment cross nacelle direction measured 6.7 m below tower top, (c). Magnified tower moment in nacelle direction measured 6.7 m below tower top, (d). Tower moment in nacelle direction measured 6.7 m below tower top, (e). Magnified tower moment in nacelle direction measured 6.7 m below tower top, (f).

REFERENCES

1. Garrad Hassan and Partners. BLADED for Windows, A design Tool for Wind Turbine Performance and Loading.
   Internet online, 2001. http://www.garradhassan.com/bladed/index.htm.

2. Øye S. FLEX4, Simulation of Wind Turbine Dynamics. In BM Pedersen, ed., State of the Art of Aerolastic Codes for Wind Turbine Calculations. Lyngby, Denmark, 1996; 71–76.

3. Lindenburg C, Hegberg T. PHATAS-IV user's manual. Program for Horizontal Axis wind Turbine Analysis and Simulation. Version IV. Technical Report ECN-C−99-093, Netherlands Energy Research Foundation ECN, Petten, 2000.

4. Larsen TJ, Hansen AM. Aeroelastic effects of large blade deflections for wind turbines. In Delft University of Technology, ed., The Science of making Torque from Wind. Roskilde, Denmark, 2004; 238–246.

5. Ganander H. The Use of a Code-generating System for the Derivation of the Equations for Wind Turbine Dynamics. Wind Energy 2003;6:333–345.

6. Rasmussen F, Hansen MH. Present Status of Aeroelasticity of Wind Turbines. Wind Energy 2003;6:213–228.

7. MSC Software Corporation. Features of MSC.Marc.
   Internet online, 20 Januari, 2003.
   http://www.marc.com/Support/Library/Features_of_Marc_2001.pdf.

8. Adams BM. Dynamic Loads in Wind Farms II. Technical report, Final Report, JOULE II, (JOU2-CT92-0094), Techical Report No. 286/R/1, 1996.

9. MSC Software Corporation. MSC.Marc Volume D, User Subroutines and Special Routines. Technical Report MA*V2003*Z*Z*Z*DC-VOL-D, 2003.

10. Compaq Fortran. Language Reference Manual. Technical Report AA-Q66SD-TK, Compaq Computer Corporation, Houston, Texas, 1999.

11. Björck A. AERFORCE: Subroutine Package for unsteady Blade-Element/Momentum Calculations. Technical Report TN 2000-07, FFA, Bromma, Sweden, 2000.

12. Björck A. DYNSTALL: Subroutine Package with a Dynamic stall model. Technical Report FFAP-V-110, FFA, Bromma, Sweden, 2000.

13. Björck A. Blade-Tower Interaction: Calculations Compared to Wind Tunnel Test Results. Technical Report FFAP-V-107, FFA, Bromma, Sweden, 1999.

14. Carlén I. SOSIS-W Version 1.3. Technical report, Teknikgruppen AB, Sollentuna, Sweden, 2000.

15. Ahlström A. Simulating Dynamical Behaviour of Wind Power Structures. Technical Report 2002:11, Royal Institute of Technology, Department of Mechanics, Licentiate Thesis, Stockholm, Sweden, 2002.

16. Belytschko T, Liu WK, Moran B. Nonlinear Finite Elements for Continua and Structures. Chichester: John Wiley & Sons, 2000.

17. Chung J, Hulbert GM. A family of single-step Houbolt time integration algorithms for structural dynamics. Computer Methods in Applied Mechanics and Engineering 1994;118:1–11.

18. Géradin M, Rixen D. Mechanical Vibrations—Theory and Applications to Structural Dynamics, 2nd ed. New York: John Wiley & Sons, 1997.

19. Djerft E, Mattson H. Evaluation of the Software Program WindFarm and Comparisons with Measured Data from Alsvik. Technical Report TN 2000-30, FFA, Bromma, Sweden, 2000.

20. Björck A, Dahlberg J-Å, Carlén I, Ganander H. Load Prediction of Stall Regulated Wind Turbines. In 1996 European Union Wind Energy Conference. Göteborg, Sweden, 1996; 829–833.

21. Holm R. Frekvensanalys av stilleståndskampanjer på Danwin 180 kW aggregatet i Alsvik. Technical Report FFAP-V-063, FFA, Bromma, Sweden, 2000. (In Swedish).

22. Sutherland HJ. Fatigue Analysis of Wind Turbines. Technical Report SAND99-0089, Sandia National Laboratories, Albuquerque, New Mexico, 1999.

23. Thomsen K. The Statistical Variation of Wind Turbine Fatigue Loads. Technical Report Risø-R-1063, Risø National Laboratory, Roskilde, Denmark, 1998.

A Detailed description of the Alsvik 180 kW wind turbine

A.1 Blade properties

Table 6: Geometrical and structural data of the Alsvik turbine blades.

Radial pos. (m)	**Chord (m)**	**Area (m)**	**Twist (deg.)**	**Mass (kg)**	**EI flap (MNm^2)**	**EI edge (MNm^2)**
1.05	0.68	0.34	20.5	137	60	60
1.55	1.05	0.52	20.6	77.2	60	60
2.1	1.35	0.81	20.1	64.6	50	65
2.7	1.47	0.88	17.0	50.7	35	68
3.3	1.39	0.83	12.1	42.7	25	50
3.9	1.33	0.80	8.47	37.2	17	37
4.5	1.27	0.76	6.04	34.8	11	31
5.1	1.21	0.72	4.37	32.0	7.0	25
5.7	1.15	0.69	3.04	28.8	4.5	22
6.3	1.09	0.65	2.05	26.7	3.4	18
6.9	1.03	0.62	1.33	24.9	2.4	16
7.5	0.97	0.58	0.78	23.7	1.7	13
8.1	0.91	0.54	0.42	22.2	1.1	11
8.7	0.85	0.51	0.22	21.0	0.8	9.1
9.3	0.79	0.47	0.11	18.2	0.65	6.5
9.8	0.74	0.29	0	14.0	0.65	5.3
10.2	0.70	0.28	0	13.5	0.65	4.9
10.7	0.65	0.39	0	16.0	0.65	4.6
11.3	0.59	0.35	0	16.2	0.65	4.5

A.2 Tower properties

Table 7: Geometrical and structural data of the Alsvik tower.

Height (m)	**Outer diameter (m)**	**Thickness (m)**	**Height (m)**	**Outer diameter (m)**	**Thickness (m)**
1.0	2.200	0.01	16.0	1.715	0.008
2.0	2.168	0.01	18.0	1.651	0.008
4.0	2.103	0.01	20.0	1.586	0.008
6.0	2.038	0.01	22.0	1.522	0.006
8.0	1.974	0.01	24.0	1.457	0.006
10.0	1.909	0.01	26.0	1.392	0.006
12.0	1.845	0.008	28.0	1.327	0.006
14.0	1.780	0.008	29.8	1.262	0.006

Paper 2

Emergency stop simulation using a FEM model developed for large blade deflections

By Anders Ahlström
Department of Mechanics, KTH, SE-100 44 Stockholm, Sweden

Accepted for publication in Wind Energy

Summary Predicting the load in every possible situation is necessary in order to build safe and optimised structures. A highly dynamical case, where large loads are developed, is an emergency stop. Design simulation tools that can cope with the upcoming nonlinearities will be especially important as the turbines get bigger and more flexible. The developed model uses the advanced commercial finite element system MSC.Marc, focused on nonlinear design and analysis, to predict the structural response. The aerodynamic model named AERFORCE, used to transform the wind to loads on the blades, is a Blade-Element/Momentum model. A comparison is made between measured and calculated loads for the Tjæreborg wind turbine during emergency braking of the rotor. The simulation results correspond well with measured data. The conclusion is that the aeroelastic tool is likely to perform well when simulating turbines that are more flexible.

Key words: wind turbine; structural dynamics; aeroelasticity; finite element; simulation; emergency stop

1 Introduction

Designing long-lasting, fatigue-resistant wind turbines at minimal cost is a major goal of the wind turbine industry and their customers. Work has led to larger and more flexible turbines that efficiently capture the energy in the wind. The trend to lighter and more optimised structures will continue and the need for reliable design tools that are able to simulate and predict the enlarged effects from primarily geometrical nonlinearities will increase. The aeroelastic tools available in the design process today, e.g. Bladed, Flex5, Phatas, Vidyn and Hawc [1–5], are generally based on modal analysis or a finite element (FE) representation. The general approach is to assume small displacements and application of the aerodynamic loads in the undeflected state. The main objective with the developed tool was to include large deformation assumption and application of loads on the deformed geometry. A typical situation where geometrical nonlinearities are likely to occur is, e.g., operation in extreme wind conditions leading to large blade deflections. Other situations are in the case of technical malfunctions, leading to a rotor emergency stop. The abrupt deceleration of the rotor results in extraordinary loading situations and deflections which in the worst case increase stresses up to the strength limit. In case of a defect, for example if the grid connection is lost, the aerodynamic torque will no longer meet any resistance from the generator and the wind turbine will immediately start to accelerate until the braking systems are applied. This load case will result in critical rotor loadings if the braking response is not fast enough. The rotor blades must therefore be pitched very rapidly towards feather to prevent rotor overspeed. The fast pitching may itself result in critical loading since the aerodynamic angle of attack will be momentarily negative, leading to thrust acting in the negative direction, [6]. A proper modelling and understanding of the shut-down process is of great importance since dimensioning the turbine too conservatively will increase the costs and the opposite situation will jeopardise safety. The modelling of an emergency brake situation is also a good test of the aeroelastic model capability to predict extraordinary situations such as transients and extreme load ranges.

The model presented is based on the commercial FE package MSC.Marc, [7], which focuses on nonlinear design and analysis. The number of suitable finite element systems is very limited, due to the inherent complexity of a wind turbine. The many rotations together with the extreme number of time steps required in a dynamic analysis, place great demands upon the software. Another requirement is the ability to communicate with other software. MSC.Marc offers communication through user-written Fortran subroutines.

When developing a large system such as an aeroelastic code, it is important to verify the code with experimental data. The developed code has been verified, in normal operational conditions, with experimental data from the Swedish experimental wind farm at Alsvik, on a three-bladed, stall controlled Danwin 180 kW, [8]. The aim of the present work was to verify the code's ability to predict the dynamic behaviour when load cases were of a more extreme nature. Verification results of safety stop situations, based on measurements from the nowadays removed Tjæreborg turbine, are presented and discussed.

2 Structural model

2.1 Structural modelling

The simulations were performed with MSC.Marc, which is a commercial finite element program for modelling of linear and nonlinear problems involving e.g. contacts, nonlinear material effects and structural dynamics, [7]. This allows the software to be used as a tool throughout the complete design process, e.g., in dimensioning specific parts of the structure, like hub, bedplate, etc. Another aspect was the wide range of element types available. The possibility of running computations in parallel makes the code suitable for shell element implementation of e.g. the blades.

The main problem when using a commercial FE program in wind turbine applications, is the application of aerodynamic loads. MSC.Marc offers the possibility to communicate through Fortran user subroutines, which allows arbitrary spatial or temporal distribution of loads. Other examples of user subroutines used are e.g. routines for implementation of local coordinate systems and routines for definition of constraint conditions for applying arbitrary homogeneous constraints between nodal displacements. All subroutines used, including subroutines for aerodynamics, were linked with the MSC.Marc library and a new executable was created using *Compaq Visual Fortran Standard Edition 6.6.B*, [9]. All loads were applied in the deformed state. Further, were all tying constraints and springs updated in each iteration, associated with local coordinate systems, meaning allowance for large deformations.

2.2 Aerodynamic modelling

A subroutine package AERFORCE was used for the calculation of the aerodynamic forces acting on the blades, [10]. The aerodynamic model is based on the blade element momentum (BEM) method, which today is the most common method in aeroelastic codes. In spite of limitations in the method itself, the BEM method is still the best tool available for aeroelastic calculations. Several modifications of the method have been developed. In AERFORCE the BEM method is extended to incorporate:

- Dynamic inflow: unsteady modelling of the inflow for cases with unsteady blade loading or unsteady wind.
- Inclined flow to the rotor disc (yaw model).
- Unsteady blade aerodynamics: the inclusion of 2D attached flow, unsteady aerodynamics and a semi-empirical model for 2D dynamic stall.

All properties related to structural geometry and kinematics, such as blade velocities, blade element lengths, etc., were calculated and inputted in the deformed state. However, the induction is calculated as the average value of the respective blade

elements. The induction contributions due to yaw are calculated for each radial element. Additional models are included for the modelling of tower shadow effects and dynamic stall. The models are described in [11, 12], respectively.

2.3 Wind field simulation

In most cases of design simulations, the turbulent wind field is not available by experiments. Instead, the turbulent wind field is obtained by using a wind data generator software. SOSIS-W, [13], is an artificial wind data generator used as a stand alone program for providing the pseudo-random wind field series to use in the structural simulation. Depending on the input to SOSIS-W, it is possible to simulate different types of wind conditions and situations. The input parameters are, e.g., statistical properties of the wind in all three directions, length scales of turbulence, hub height, etc.

The results presented in the verification examples were calculated using wind measurements and generated wind series as input. The measurements, given at hub height on one elevation, were spatially distributed in space with statistical correct coherent turbulence components in all three directions. The generated wind series were derived based on a random seed. The results are comparable for verification in a representative average way as long as the statistical properties of the simulated wind data series, for a given time duration, coincide with the measured.

2.4 Calculation scheme

The section aims to give a brief insight to the calculation steps performed in a simulation. The wind turbine structural model is determined in the MSC.Marc input file. Input and parameters are further described in the numerical example. A measured or synthetic wind field is created to be read by AERFORCE. As the loads are varying over time and space, the equations of motion are solved numerically in a step-by-step manner using an implicit integration scheme. During the step-by-step response calculation, the aerodynamic loads are evaluated at each iteration and time step.

The following sequence is called by MSC.Marc:

1. Save x,y,z displacement components for nodes of interest, e.g. blade nodes and orientation nodes.

2. Save x,y,z velocity components for each blade node and the rotational speed of the rotor.

3. Derive the transformation matrices, $\mathbf{S}_{\mathrm{gr}}$ (between the global and the rotor system) and $\mathbf{S}_{\mathrm{ge}}$ (between the global and the blade element system), based on the x,y,z components saved at step 1. Calculate the transformation matrix between the rotor and the global system, $\mathbf{S}_{\mathrm{re}}$.

4. From the synthetic wind speeds, calculate aerodynamic forces.

   (a) read data from input file, e.g. blade information such as chord length, thickness, area, twist, pitch, profile number, etc. Step 4(a) is only performed at the first time step since the values are not time dependent.

   (b) process the data read at step 4(a) For instance interpolate data between input airfoil tables and modify $\mathbf{S}_{\text{re}}$ to include the contributions from twist.

   (c) Calculate the wind speed acting on each blade element depending on the rotor position.

   (d) Input necessary parameters to AERFORCE and calculate the forces acting on each blade element.

5. Transform blade element forces to the global load vector.

6. Calculate generator moment and write result to the global load vector.

The data is then transferred back to MSC.Marc, where the equilibrium iterations of the time step are performed. Note that all loads were applied in the deformed state updated in each iteration. The beam element types used were either modelled with circular or rectangular cross sections, where shear centre, mass centre and pitch axis were assumed to coincide. Due to the offset of the aerodynamic centres, the pitching torques were accounted for. All aerodynamic loads were applied as nodal forces acting on the centre of each aerodynamic blade element, i.e., on the end-nodes of each structural beam element. It should be emphasised that user defined cross sections of any shape, allowing non-coincident mass and shear centres, could be introduced in the model. It would also be possible to apply loads as line forces rather than point forces in the model. However, the difference between the two implementations is assumed small when the blade discretisation is relatively dense.

3 Tjæreborg turbine and measurement system

3.1 Site and turbine details

The Tjæreborg wind turbine was a horizontal axis upwind turbine developed in the late eighties as part of the Wind Energie Große Anlagen (WEGA) programme, [14]. The machine was installed near Esbjerg in Denmark, and was removed in August 2001 due to an accident in the generator, [15]. The three-bladed rotor with a diameter of 61.1 m, was connected to a 2 MW enlarged slip induction generator through a three-stage planetary gearbox. The 3 degree tilted rotor was running at a constant speed of 22.3 r.p.m., which gave a blade tip speed of 71 m/s. The concrete tower was of 57 m height and shaped as a parabola near the base, gradually turning conical.

The blade pitch system consisted of two parts. A central double acting hydraulic servo cylinder which was common for the three blades and three hydraulic safety

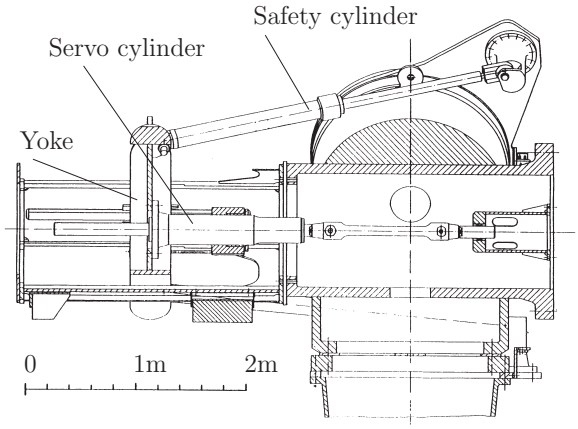

Figure 1: Blade pitch system. Reprinted from [14].

cylinders, one for each blade, with an on/off function. The servo cylinder was used to regulate the power above rated wind in the operating pitch range -2 to $+35$ degrees, Figure (1). The second system worked independently on each blade. Each blade was therefore equipped with a gas accumulator, which in case of emergency could be used to apply the safety cylinders. The cylinders gave a pitch range of 55 degrees. The two systems worked accumulatively, which mean that the blade's total pitch angle is the sum of the two relative angles. The system is tolerant to one fault, since pitch angles of two blades in the range 55 to 90 degrees, are enough to bring the turbine to a safe idling speed. The turbine was also equipped with a mechanical disk brake that could be manually activated in case of emergency. The disk brake could stop the rotor without any aerodynamic braking.

3.2 Data acquisition and anemometry

Since the Tjæreborg site was intended for experimental measurements, it was equipped with two meteorological masts, each being of 90 m height. The two meteorological masts and the turbine were placed on a line in the dominant wind direction. The distance between the turbine and each mast was 120 m, which corresponded to two rotor diameters, [16]. The turbine was equipped with a large number of sensors and strain gauges to allow measurements of various kinds. Some of the signals are listed below. In the experiments utilised in the present project, the following signals were recorded with a sampling frequency of 25 Hz, [17]:

- Wind speed and wind direction at hub height
- Root flapwise and edgewise bending moment in each blade root
- Torque in low and high speed shafts

- Two bending moments in main shaft
- Pitch angle in the range -2 to $+35$ degrees
- Rotation speed of high and low speed shaft
- Rotor azimuthal position
- Nacelle position
- Electrical power

The pitch angle was only measured in the operating range, hence the actual pitch angle with contributions from the three safety cylinders were not available. However, an approximate pitch rate during an emergency stop is given in [18]. The signals mentioned above were not all available in each campaign. It was, for example, common that measurements from only one or two of the blades were available.

3.3 Data collected

The collected data were recorded 1988–1993 and are available on *www.winddata.com*, [19]. The database is compiled and maintained in Denmark by the Technical University of Denmark (DTU). The database is searchable, and by specifying, e.g., min-max criteria it is easy to find unique time series such as extreme wind conditions, or shut-down sequences.

3.4 Description of studied campaigns

Three campaigns were selected for verification from the database. One normal operation case to ensure that the turbine properties were set as expected and two emergency shut down campaigns. The normal operational case was simulated using both measured and random seed generated wind data. The measured wind speeds were spatially distributed in space using SOSIS-W, [13]. The turbulence intensities in v, w directions, were set to 0.8 and 0.5 times the intensity in u direction, respectively. The coherence exponentials were set to 8.8.

- **Campaign 1, normal operation** A 600 s long sequence with a mean wind speed of 10.5 m/s and turbulence intensity of 8.0 %. The campaign was recorded 14-11-92, time 02:59 and saved as 0259_250.dat.
- **Campaign 2, emergency stop below rated wind** The stop sequence part of a 600 s long campaign with a mean wind speed of 11.5 m/s and turbulence level of 6.5 %. The campaign was recorded 24-02-92, time 13:30 and saved as 1330_250.dat.

- **Campaign 3, emergency stop above rated wind** The stop sequence part of a 600 s long campaign with a mean wind speed of 17.4 m/s and turbulence level of 7 %. The sequence was recorded 10-03-92 at 15:41 and saved as 1541_250.dat.

3.5 Instrument problems and measurement quality

In 1991 it was discovered that a 2 Hz filter in the amplifiers for the strain gauges had been applied. The damage to the collected data was, however, small due to the low response contribution of the turbine above 2 Hz. Despite the minor influence on the data, only measurements collected after 1991 were used in the present study.

Other problems during the measurement period were that the mean moments in flap and edge direction were drifting. The maximum drifting was in the order 2–5 % during a typical measurement period of 600 s. There were also problems with the mean level calibration of the strain gauges mounted on the blades. Mean level comparisons between the measured and simulated edge and flap moments were therefore not made.

4 Analysis and modelling of the Tjæreborg turbine

The goal with the study was to verify the code in extreme load case situations. All calculations were based on the same structural properties and aerodynamical data.

4.1 Machine parameters

The basic machine parameters are tabulated in Table (1). The turbine is a three bladed pitch controlled rotor with a rated power of 2 MW, at a rated wind speed of 15 m/s. The cut-in speed is 5 m/s and the cut-out speed is 25 m/s. Five airfoil tables, covering the full 360 degrees range of angle of attack, were used in the calculations, [20].

4.2 Rotor

The rotor was modelled with a six degree-of-freedom elastic beam element. Each blade was modelled by fourteen elements, and to each blade element additional massless elements were attached. The massless elements were used to calculate the transformation matrices needed by AERFORCE in order to keep track of the position and pitch angle of the blades. The mass of the blade was modelled with a consistent mass matrix. Sectional mass properties can be found together with the

Table 1: Basic description of the Tjæreborg turbine.

Rotor		**Blades**		**Masses (t)**	
Number of blades	3	Material	GRP	Blades	27.1
Rotor diameter	61.1 m	Blade length	29 m	Hub	22.1
Hub height	61 m	Root chord	3.3 m	Tower	665.0
Rotor speed	22.4 rpm	Tip chord	0.9 m	Towerhead	224.6
Tilt	3°	Blade profiles	NACA 4412–4443	Total weight	889.6

blade coordinates and the stiffness properties in Table (2). No damping was introduced beside the numerical damping of the integration method described in Section (4.5).

The pitch system was accomplished by using constraint equations in a rotating coordinate system. All degrees of freedom were locked, except the rotational degree of freedom around the blade axis. Figure (3) illustrates the connections, on two of the three blades, between rotor hub and blades, where the constrained node pairs are n11–n12 and n13–n14. Rotational dampers were used in the connection between each node pairs, to give a softer settling to the desired pitch angle. The actual pitching of the blades was carried out by control moments that were set depending on each blade's desired pitch angle. According to [21] the pitch rate, $\dot{\theta}_{\mathrm{P}}$, can be expressed by the following relation between electrical power and pitch angle:

$$\dot{\theta}_{\mathrm{P}} = 0.02(P_{\mathrm{E}} - 2000)/(1 + \theta_{\mathrm{P}}/4.6) \tag{1}$$

with P_{E} in kW and θ_{P} in degrees. The last term of the relation reduces the gain of the controller as the wind and pitch angle increase. The combined mechanical and electrical loss of power has been tabulated in [21], and was translated to the linear relation, $P_{\mathrm{E}} = 0.9433P_{\mathrm{Shaft}} - 50.2$. Time integration of the pitch rate gave the desired pitch angle θ_{sp}, which acted as input to the pitch servo, i.e., the control moment in the present study. The pitch servo was modelled as the inner loop in the control algorithm according to the schematic block diagram in Figure (2), where:

PID1	Controller 1. Power to pitch rate.
Sat1.	Limits the pitch rate.
Disc. Int.	Integration to pitch angle.
Sat2.	Limits the pitch angle.
PID2	Controller 2. Pitch angle to pitching moment.
System	Wind turbine dynamics.
Sat2.	Limits the pitch angle.
P	Electrical power; set point, error and actual.
$\dot{\theta}_{\mathrm{sp}}$	Pitch rate set point.
θ	Pitch angle; set point, error and actual.
M_{sp}	Pitch moment set point.

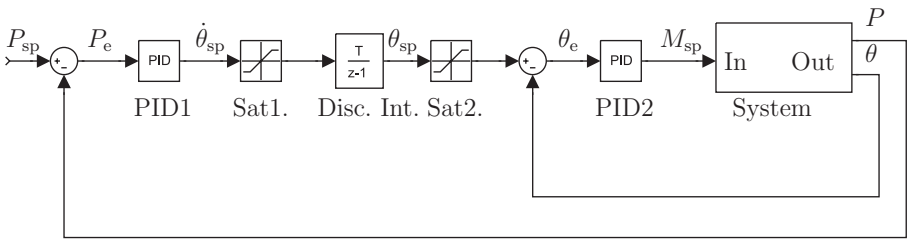

Figure 2: Blade pitch control system.

The power signal, P_{E}, was 3-P filtered to reduce the influence of the tower shadow effects, [22]. The control system was only used in the verification of campaign 3 before the emergency brake was applied. In the emergency brake situation, the desired pitch angle was set according to a predefined pitch sequence. Hence, just the inner loop in the control block scheme was used. Since only pitch angle measurements from the pitch servo, i.e., up to 35 degrees, were obtainable, the pitch rate had to be guessed for the complete pitch sequence. According to [18], the total initial pitch rate could be as high as 16 deg/s, compared to the servo mechanism's maximum pitch rate 6.5 deg/s. The desired pitch angle sequence was implemented in the simulations in two steps. The first step with a pitch rate of 16 deg/s applied in about 2 seconds and a second step with a pitch rate of about 5 deg/s, applied until the desired pitch angle was reached. The pitch rate values were decided by scaling down the high speed shaft speed to the corresponding low speed shaft speed and comparing this with measurements. The pitch rate parameters could be iteratively found to match the deceleration of the rotor.

4.3 Tower

The tower was modelled using circular hollow straight beam elements with a thickness of 0.25 m. The tower was discretised into seventeen elements and was rigidly connected to the ground. The connection between tower-top and bedplate was described by a combination of springs and constraint equations. The connection was modelled rather stiff due to limited knowledge about yaw stiffness and measured eigenfrequencies. The mass properties were calculated based on the geometrical data and the density of concrete, 2600 kg/m^3. The tower data can be found in Table (3). No damping except the numerical damping was introduced. The drag coefficient was set to $C_d = 0.6$ for the calculation of tower shadow effects.

4.4 Bedplate and drivetrain

The bedplate and drivetrain were schematically modelled as described by Figure (3). The bedplate, with corner nodes n2, n4, n6 and n8 in the figure, was modelled relatively rigid with elastic beam elements. The mass of the bedplate was applied as a point mass of 154000 kg at the centre of gravity. No moments of inertia were

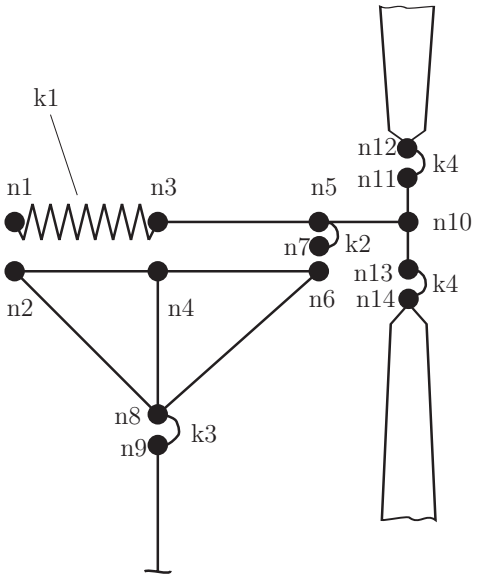

Figure 3: Bedplate and drive train.

specified for the nacelle, to compensate for the lumped mass assumption, due to small rotations of the stiff tower.

The drive train consisted of rotor shaft, between the hub centre, node n10 and node n3, and the spring-damper configuration between nodes n1 and n3, Figure (3). Node n10 was given a concentrated mass of 42500 kg and a concentrated moment of inertia about the rotating shaft of 60000 kgm^2, representing the mass properties of the hub. The hub mass includes all the rotating parts in front of the main shaft flange except the blades. The moment of inertia with contribution from the generator, main shaft, brake disk and gearbox, applied to node n1, was set to $8 \cdot 10^5$ kgm^2.

The connection between rotor and bedplate was achieved by using constraint equations on nodes n1–n2, n3–n4 and n5–n6–n7. These equations ensured that all displacements were equal between node pairs. Figure (3) illustrates the general case, where the n5, n6 and n7 nodes enable both tilt and rolling degrees of freedom at the coupling point. However, the present model only included effects from the rotor axle's own stiffness, due to limited knowledge about the stiffness and the coupled eigenfrequencies. Hence, node n7 and spring k2 are redundant. In the figure, the node sets n1–n2, n3–n4, n5–n6 should in fact be located at the same coordinates, but for illustrative reasons the axle is shown above the bedplate. The nodes were used to specify constraint equations expressing slave (dependent) degrees of freedom as linear combinations of master (independent) degrees of freedom. Nodes n1–n2, n3–n4 and n5–n6 were connected in x, y, z translations and y, z rotations, where the x-axis coincides with the shaft direction. The connection between bedplate and tower, n8–n9, was achieved by springs and constraint equations. The nodes were constrained to represent a pin joint connection between the parts. The spring constants

in the connection decide the rotational stiffness.

The generator was modelled as an asynchronous generator with approximately 2 % slip. The synchronous rotor speed was about 2.29 rad/s:

$$M_{\text{gen}} = 18.6 \cdot 10^6(\omega_{\text{rot}} - 2.29) \tag{2}$$

where ω_{rot} is the generator rotational velocity, measured in each time iteration. The expression introduces a penalty moment, striking towards the reference rotational speed. Equation (2) was modified with a time variable t to be used the first 20 seconds of simulation, to prevent overloading:

$$M_{\text{gen}} = 18.6 \cdot 10^6(\omega_{\text{rot}} - \frac{2.29t}{20}) \tag{3}$$

The generator moment was turned off after the emergency stop sequence was started. According to [18], the delay time was about 1.1 s, and this value was used.

4.5 Integration method and parameters

MSC.Marc allows three time integration methods. The Single Step Houbolt (SSH) was used in this work, [23, 24]. The SSH method is unconditionally stable, second-order accurate and asymptotically annihilating. The method is designed to include numerical dissipation characteristics, particularly for higher frequencies, and uses two parameters. The results in the numerical example are derived with $\gamma_1 = 3/2$ and $\gamma = -1/2$

4.6 Software specific parameters

Many parameters affect the simulation of a wind turbine. In a typical 600 s simulation, the turbine spins approximately 450 revolutions, and about 100,000 time increments are required. When each increment needs 4–5 iterations to converge the stability of the core is important. The calculations were performed using the full Newton-Raphson method for equilibrium iterations in each time increment, together with a sparse direct solver. The updated Lagrangian procedure was used together with an option that allows large incremental rotations for beam elements. The use of the procedure has two consequences. First, the element stiffnesses are assembled in the current configurations of the elements. Second, the stress and strain output is given in the coordinate system which is applicable in the updated configuration of the element. A consistent mass formulation was used.

Displacement checking was used as the criterion for convergence. The maximum allowable value of change in displacement increment divided by the displacement increment, was chosen as $\frac{\|\delta u\|_\infty}{\|\Delta u\|_\infty} < 10^{-4}$. Here, Δu is the displacement increment vector and δu the correction vector. A disadvantage with this approach is that it produces at least one iteration, regardless of the accuracy of the prediction in the time increment.

Concentrated dashpots have been used in this study to model the damping of, e.g., the generator and pitching system.

4.7 Measured and simulated natural frequencies

As a part of the WEGA-I measurement project the structural frequencies were determined, [17]. Most of the stiffness and mass distribution properties of the turbine are listed in [21]. By using slightly updated model characteristics, the model's first tower, flap and edge modes corresponded within 3 % of the measured frequencies. The natural frequencies of the model were: tower 0.78–0.81 Hz, flapwise 1.17 Hz, edgewise 2.30 Hz and transmission 1.9 Hz. The transmission was modelled with a stiff rotor axle and torsional spring of $1.1 \cdot 10^8$ Nm/rad, [21]. The primary shaft torsion spring, k1, was acting between node n1–n3 as illustrated in Figure (3). The yaw system stiffness, k3 in Figure (3), was set to $1.0 \cdot 10^{10}$, $4.0 \cdot 10^{12}$ and $4.0 \cdot 10^{12}$ Nm/rad, for the yaw, rolling and pitching direction, respectively. Unfortunately the report gave no information about the coupled eigenfrequencies, e.g. combined yaw and flap mode, which made the coupling stiffnesses difficult to set.

4.8 Simulation procedure

The properties of the model were verified by calculating the given eigenfrequencies of the turbine. Some slight modifications of the stiffness and mass properties were introduced to match the experimental eigenfrequencies. For additional verification, simulations were performed also under normal conditions, campaign 1. After a successful normal operational verification the two emergency stop situations were simulated. The parameters that could be set to control the blade pitching behaviour were; the shut down delay time of the generator from when pitching started, the pitch rate of the blade and the delay time of the second step of the pitching. The last parameter was the final pitching angle position, which determined the idling speed. These parameters were determined inversely based on identification of the measured time series, with no parameter changes between the two emergency stop sequences. The azimuthal location of the rotor, when the emergency stop started, was decided by studying the measured azimuthal and pitch time series. The final parameters were set as: pitch rate step 1, 16 rad/s, pitch rate step 2, 5 rad/s. The delay time between the two steps was 1.8 s and the delay time to generator switch off, from when the pitch sequence started, was set to 1.1 s. The idling pitch angle was set to 86 degrees. The emergency brake was applied at an azimuthal angle of 306 and 42 degrees for campaign 2 and 3, respectively.

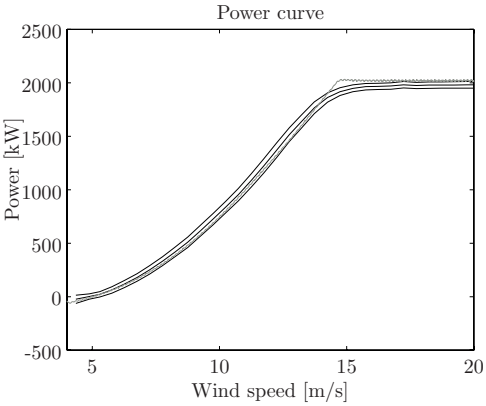

Figure 4: Measured, including ±95 % confidence interval and predicted power performance.

5 Results obtained from the numerical simulations

The results are mainly presented as figures and tables. When different colours are used in the figures, the light grey indicates simulated data and the black indicates measured data.

The first step in the verification was to compare the measured and the simulated power curve. The simulated power curve was obtained by stepping a uniform wind speed from 4 m/s to 25 m/s under a 10 min period. The simulated and measured power curves are presented in Figure (4). The measured net power curve is shown together with a ±95 % confidence interval. The simulated power curve was filtered due to the pronounced tower shadow influence. The simulated gross power was transformed to the corresponding net power using the relation described in Section (4.2). The results of the normal operational case, campaign 1, are presented as plotted time series and power spectral densities in Figure (5). The results were calculated with both measured and generated winds as input. Figures (5a,c,e) shows the net power, the flap moment of blade 1 and the rainflow cycles of the flap moment of blade 1, respectively, when measured wind was used as input. Figures (5b,d) gives the power spectral density of the flap and edge moments when generated wind was used as input. The rainflow cycles count of the root flap moment of blade 1, for the same input are presented in Figure (5f).

Studying the statistics of the time series in the case of measured wind, in the normal operational case, campaign 1, it was seen that the net mean power level as well as the standard deviation was under-predicted by 5 %. The mean flap and edge statistics were not available due to large mean level offset in the measurements. The standard deviations were calculated for both flap and edge moments of the three blades. The

deviations were all within 3 % of the measured. When generated wind was used as input, the mean power level error was under-predicted by 4 % and the standard deviation under-predicted by 12 %. The standard deviation errors of the flap and edge moments in the generated wind case, were all within 3 % of the measured.

A rainflow counting algorithm was used to compare the influence of the simulated versus the measured flap load in a fatigue manner. The results from the rainflow analysis are presented in Figures (5e) and (5f) for the two realisations of campaign 1. Further comparisons between the two cases were made using the more convenient equivalent load range R_{eq} [25, 26]. The equivalent loads were calculated and a comparison was made between measured flap and edge moments and the simulated results. In the case of $6 \leq m \leq 12$, where m describes the slope of the fatigue curve, the equivalent loads of the flap moments were calculated to -12 to -9 % and 0 to 3 %, for measured and generated winds as input, respectively. The edge moment variation was in both cases within 3 % of the measured.

The emergency stop results are presented in Figures (6) and (7), corresponding to campaigns 2 and 3, respectively. The results plotted are a selection of the studied time series available, but focuses on the results where the largest effects of the emergency stop are present, i.e., flap moment, shaft torque, etc. The large mean level offset in the measured data required mean level shifting of the measured flap and edge moments for comparison with simulated data. In some cases the mean level was needed to be shifted by as much as 2000 kN. Figure (6a) gives the blade tip deflection in the rotor system. The blade tip deflection out of plane goes from about +2 m to almost −2 m during a 1.4 s period. The in plane deflection increases when the emergency brake is applied and idles between 0.8 to −0.5 m. Figure (6b) shows the shaft torque. When the brake is applied the shaft torque goes from about 670 kNm to −500 kNm for the simulated and from 670 kNm to −800 kNm for the measured. Figures (6c–e) shows the flap moments of the three blades and Figure (6f) gives their average. Averaging the flap moments cancels out the effect of gravity and 1P load components. The load ranges between max and min response gives 1850 and 1960 kN for simulated and measured responses, respectively. Figure (7) gives some results from campaign 3. Figure (7a) gives the speed of the rotor which starts at a normal operational speed to be decelerated, at the emergency shut down, down to the idling speed. Figure (7b) gives the shaft torque. The shaft torque goes from about 950 kNm, for both simulated and measured responses, to negative moments of −630 and −950 kNm, respectively. Figures (7c–f) give the flap moments of the three blades and their average. The load ranges were 1720 and 1650 kN for the simulated and the measured cases, respectively.

6 Discussion

There are many sources of uncertainties in a verification where many parameters are involved. The most obvious uncertainties are the ones related to the wind input. Despite the modification of the measured wind, with spatial distribution in u, v, w direction and correction for yaw misalignment, errors are present. The ideal case is

to measure all the wind components, within a square, in direct connection to the rotor. The present case is instead wind measurements, extrapolated in space from one elevation, 120 m away from the rotor. The measured wind will therefore be shifted in time compared to the turbine measurements. Even though the wind speed might be close at the turbine compared to the mast, the relatively short time series of 600 seconds is probably not enough to statistically say that the wind properties are the same. Generated wind data based on the statistics of the measured wind are consequently affected by the same type of errors.

The iterative method used to match the pitch rate to the desired rotational deceleration speed of the rotor, may hide errors in the aerodynamic model, as errors in the pitch rate setting might compensate for errors in the aerodynamic calculations, with the net result that the predicted rotor speed is accurate.

Other types of limitations are the model itself, as the structural model is just a model of the real structure, even when a FE software is used. The real structure consists of many parts connected to each other with bolts and bearings. The structure is then discretised with a limited, although rather high, number of degrees of freedom using spring and beam elements. The stiffness properties of some of the coupling degrees of freedom were not easily determined and estimations were used. The aerodynamic method is another source of error. The model is e.g. very dependant on the airfoil data. However, in spite of a number of limitations in the method itself, the BEM method is still the best tool available, within reasonable computation time, for getting good first order predictions of thrust, torque and efficiency for turbine blades under a large range of operating conditions. The model is, however, definitely capable of catching the overall dynamics of the studied turbine in normal as well as in this extreme case.

The power curve of the turbine was calculated and compared to measured data. Calculating the power curve as described in Section (5) and comparing it with a measured power curve is not fully relevant. The comparison is rather done as a control that the blade parameters like chord, airfoils, radius, blade element length, etc., are reasonable. Comparing the curves indicates an underestimation of the predicted power from cut in speed to slightly below rated wind speed. Approaching rated wind speed, the simulated power turns to be over-predicted. Consequently, because the pitch control starts working, the rated power is reached at 14.6 m/s rather than the observed 15 m/s. The linear relation used to transform the power in the shaft to electrical power might also explain the under-predicted rated wind speed.

The comparison of the normal operational case was done using both measured and generated wind as input. The conclusion is that the modified wind measurement gives slightly under-predicted flapwise fatigue loads and power production. In the generated wind case, the seed given as input to the wind generator model will affect the output and consequently the predicted fatigue loads. Conclusions based on one realisation are therefore not really significant but will give an indication on the trend. Figures (5e) and (5f), show the trend towards a slight over-prediction of the fatigue loads in the generated wind case. However, equivalent loads based on the generated wind case were almost in perfect agreement with the experimental results.

The edgewise fatigue loads, determined primarily by the weight of the rotor blades, were as expected in good agreement for both the measured and generated wind cases. Mean level drifting of the measured data was also a source of uncertainty. The power density of both flap and edge loads were calculated. The results show that the model corresponds well to the real structure. Interesting is the enhanced edgewise blade frequency peak at 2.3 Hz with the characteristic ± 1P splitting.

The range between max and min flap moment corresponds very well to measurements for both of the two emergency brake campaigns and the errors were limited to 6 %. The slight under-prediction of the flapwise peak below rated wind speed may be explained by the underestimated power at that wind speed according to Figure (4). The largest flap peak was seen in campaign 2, when the turbine was running below rated speed. The explanation is that the torque and rotor thrust increases up to the rated power and when the blades start pitching, the rotor thrust drops off. The specified pitch rate in the two-step pitch mechanism seems to give a very close behaviour in time. The transient response of the flap moment, as well as the deceleration of the rotor, is captured very well. When the blade is pitched, the flapwise bending moment will include contributions from the gravity load, i.e., the inherent weight bends around the flapwise axis. The shaft torques were under-predicted compared to measurements. One reason might have been that the stiffness or the axle moment of inertia was not modelled correctly. Parameter studies shows that the shaft torque in the emergency case was very sensitive to those parameters. However, the results presented are based on the parameters given in [21].

With the discretisation used in the present work, approximately 1000 DOFs, the required computer time of 600 seconds of simulation was about 8 hours on a standard 2.4 GHz PC with 1 Gb ram.

7 Conclusions

Three campaigns were studied and used for verification of the aeroelastic code. One campaign under normal operational conditions to ensure that the model behaved as expected and two campaigns, one below and one above rated wind speed, to verify the model in the extreme case of an emergency stop.

Despite the possible error sources, e.g. that it is impossible to distinguish between errors in the aerodynamic model and errors in the pitch rate setting, mentioned in Section (6), the simulated results show very good agreement with the experimental data. It is especially interesting and promising that the results coincide so well for the extreme load case of an emergency stop. The model predicts the large negative flap moment very well. That is important, since under certain circumstances, the load case can increase bending stress on the rotor blades up to the strength limit. The shaft torque was more difficult to model. The results are highly dependent on properties like shaft stiffness, shaft damping, generator slip, etc. The overall behaviour is captured but the simulations underestimate the peak in the emergency case. One reason might have been that the stiffness or the axle moment of inertia

was not modelled correctly.

The successful modelling of the emergency stop proves the simulating tool's ability to deal with extreme load conditions and the associated nonlinearities. The code is believed to be very useful in the design of today's and tomorrow's large flexible turbines. However, the computational time is long, compared to modal formulation models, which makes the tool more suitable for extreme or special load case simulations rather than for certification purpose analyses, where hundreds of simulations need to be performed.

8 Further research

Although the developed model has been shown very effective in the scrutinised example, there are many possible areas for further studies. An interesting and important area is to investigate the effect on loads and dynamics in the case of very flexible wind turbines. Another study, directly connected to the mentioned, that would be of great interest for wind turbine producers, is to determine in which cases nonlinear finite element models are needed and in which cases faster methods, like e.g. modal approaches, are sufficient to determine the turbine's dynamical behaviour. Also in several other aspects, the limitations of commonly used calculations with respect to parameter variations can be verified by the general simulations.

9 Acknowledgement

The author would like to thank the people behind *www.winddata.com* that have created an invaluable database for wind energy researchers. Thanks also to Kurt S. Hansen and Stig Øye at the Technical University of Denmark for providing all kinds of information regarding the studied turbine. Thanks to Anders Björck at Swedish Energy Agency for explanations and advise regarding the aerodynamic model and Ingemar Carlén at Teknikgruppen AB for the wind data model.

Support from the Swedish Energy Agency is gratefully acknowledged. Contract/grant number: P12020-1.

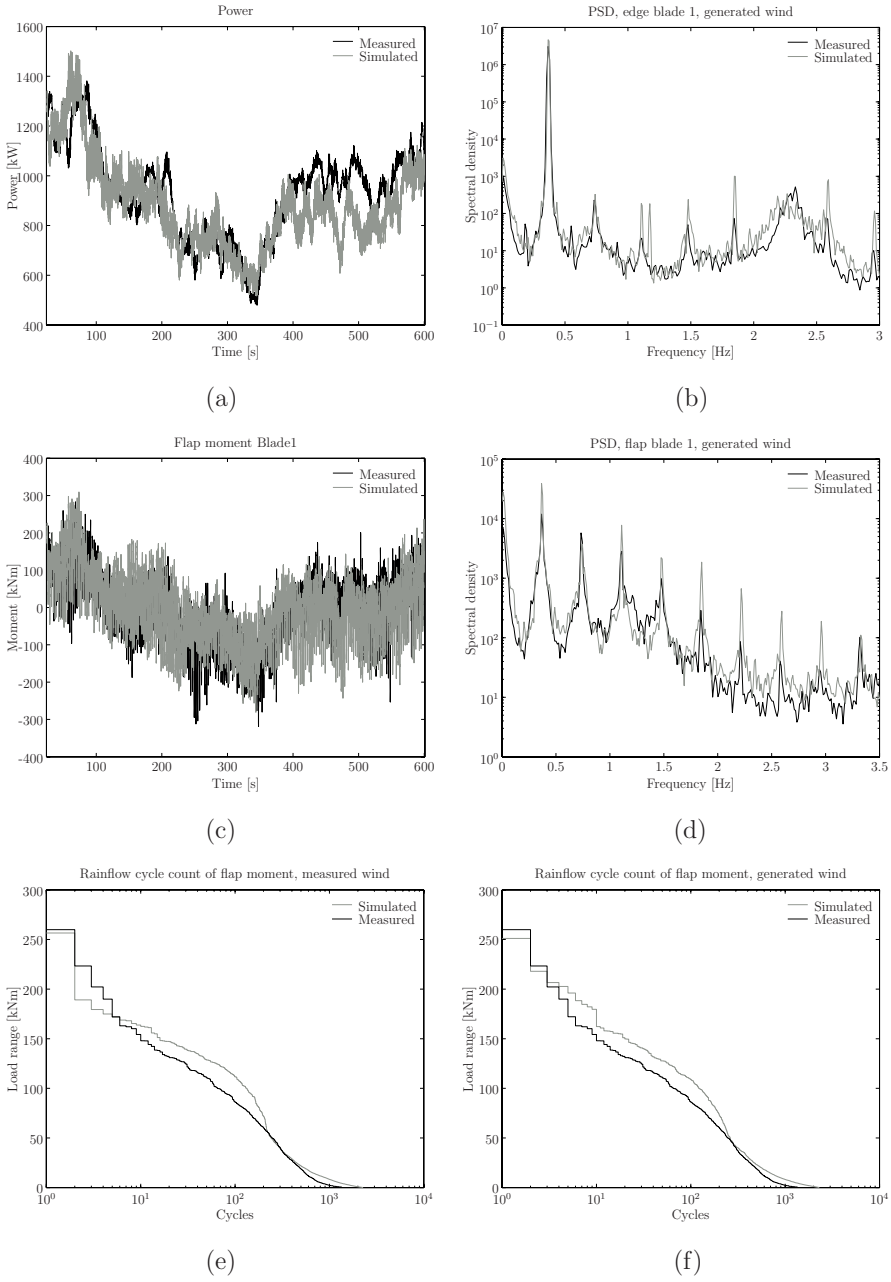

Figure 5: Campaign 1: Electrical power, (a). Power spectrum flap moment blade 1, (b). Flap moment blade 1, (c). Power spectrum edge moment blade 1, (d). Rainflow cycles, (e). Rainflow cycles with generated wind input, (f).

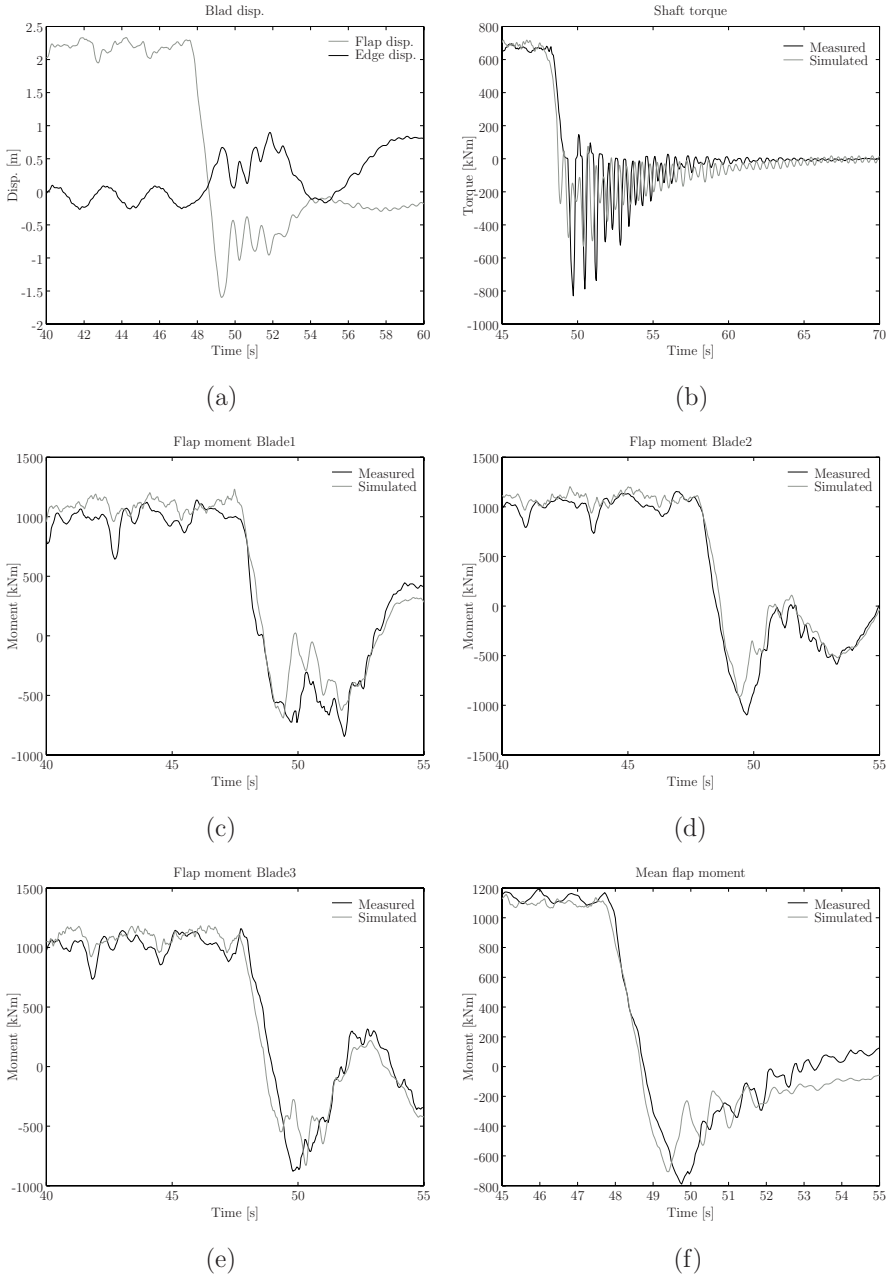

Figure 6: Campaign 2: Blade disp., (a). Shaft torque, (b). Flap moment blade 1, (c). Flap moment blade 2, (d). Flap moment blade 3, (e). Mean flap moment, (f).

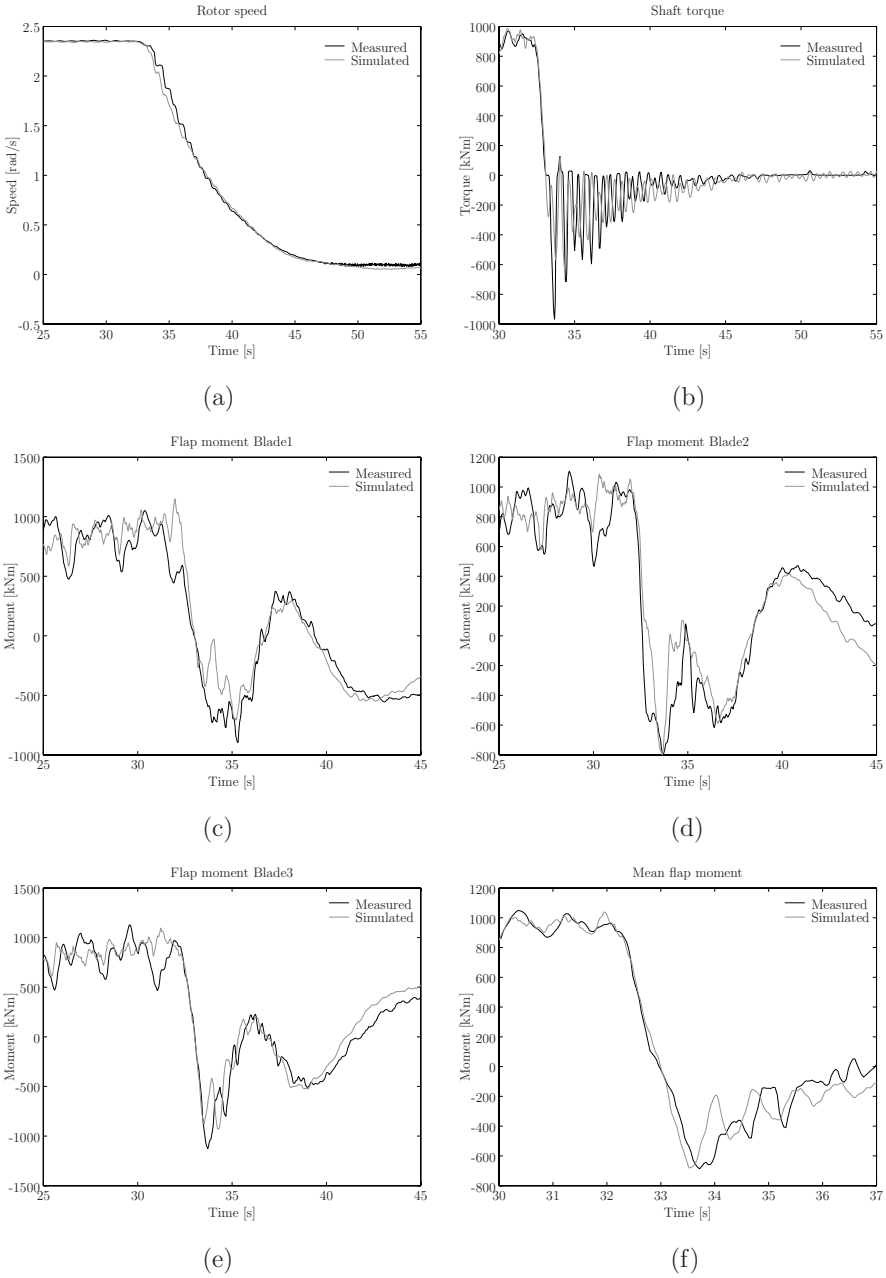

Figure 7: Campaign 3: Rotor speed, (a). Shaft torque, (b). Flap moment blade 1, (c). Flap moment blade 2, (d). Flap moment blade 3, (e). Mean flap moment, (f).

REFERENCES

1. Garrad Hassan and Partners. BLADED for Windows, A design Tool for Wind Turbine Performance and Loading.
   Internet online, 2001. http://www.garradhassan.com/bladed/index.htm.

2. Øye S. FLEX4, Simulation of Wind Turbine Dynamics. In BM Pedersen, ed., State of the Art of Aerolastic Codes for Wind Turbine Calculations. Lyngby, Denmark, 1996; 71–76.

3. Lindenburg C, Hegberg T. PHATAS-IV user's manual. Program for Horizontal Axis wind Turbine Analysis and Simulation. Version IV. Technical Report ECN-C−99-093, Netherlands Energy Research Foundation ECN, Petten, 2000.

4. Larsen TJ, Hansen AM. Aeroelastic effects of large blade deflections for wind turbines. In Delft University of Technology, ed., The Science of making Torque from Wind. Roskilde, Denmark, 2004; 238–246.

5. Ganander H. The Use of a Code-generating System for the Derivation of the Equations for Wind Turbine Dynamics. Wind Energy 2003;6:333–345.

6. Hau E. Windturbines: Fundamentals, Technologies, Application and Economics. München: Springer, 2000.

7. MSC Software Corporation. Features of MSC.Marc.
   Internet online, 20 Januari, 2003.
   http://www.marc.com/Support/Library/Features_of_Marc_2001.pdf.

8. Ahlström A. Development and verification of an aeroelastic simulation tool for wind turbine calculations, 2004. Submitted.

9. Compaq Fortran. Language Reference Manual. Technical Report AA-Q66SD-TK, Compaq Computer Corporation, Houston, Texas, 1999.

10. Björck A. AERFORCE: Subroutine Package for unsteady Blade-Element/Momentum Calculations. Technical Report TN 2000-07, FFA, Bromma, Sweden, 2000.

11. Björck A. DYNSTALL: Subroutine Package with a Dynamic stall model. Technical Report FFAP-V-110, FFA, Bromma, Sweden, 2000.

12. Björck A. Blade-Tower Interaction: Calculations Compared to Wind Tunnel Test Results. Technical Report FFAP-V-107, FFA, Bromma, Sweden, 1999.

13. Carlén I. SOSIS-W Version 1.3. Technical report, Teknikgruppen AB, Sollentuna, Sweden, 2000.

14. Hau E, Langenbrinck J, Palz W. WEGA Large Wind Turbines. Berlin: Springer, 1993.

15. ELSAMPROJECT A/S. The Tjæreborg Wind Turbine.
Internet online, 31 August, 2004. http://www.afm.dtu.dk/wind/tjar.html.

16. ELSAMPROJECT A/S. The Tjæreborg Wind Turbine - Final Report.
Technical Report EP92/334, CEG, DG XII contract EN3W.0048.DK,
Fredericia, Denmark, 1992.

17. ELSAMPROJECT A/S. The Tjæreborg Wind Turbine - Loads During
Normal Operation Mode. Technical Report EP94/456, CEG, DG XII contract
EN3W.0048.DK, Fredericia, Denmark, 1994.

18. Øye S. Simulation of loads on a pitch controlled wind turbine during an
emergency stop. Technical Report VK-246, Department of Fluid Mechanics,
DTH, Lyngby, Denmark, 1993.

19. WindData.com. Database of Wind Characteristics.
Internet online, 31 August, 2004. http://www.winddata.com.

20. Øye S. Tjæreborg wind turbine (Esbjerg) Geometric and operational data.
Technical Report VK-184, Department of Fluid Mechanics, DTH, Lyngby,
Denmark, 1990.

21. Øye S. Tjæreborg wind turbine (Esbjerg) Structural dynamics data. Technical
Report VK-186, Department of Fluid Mechanics, DTH, Lyngby, Denmark,
1991.

22. Mathworks. Signal Processing Toolbox.
Internet online, 25 October, 2004. http://www.mathworks.com/.

23. MSC Software Corporation. MSC.Marc Volume A, Theory and User
Information. Technical Report MA*V2003*Z*Z*Z*DC-VOL-A, 2003.

24. Chung J, Hulbert GM. A family of single-step Houbolt time integration
algorithms for structural dynamics. Computer Methods in Applied Mechanics
and Engineering 1994;118:1–11.

25. Sutherland HJ. Fatigue Analysis of Wind Turbines. Technical Report
SAND99-0089, Sandia National Laboratories, Albuquerque, New Mexico, 1999.

26. Thomsen K. The Statistical Variation of Wind Turbine Fatigue Loads.
Technical Report Risø-R-1063, Risø National Laboratory, Roskilde, Denmark,
1998.

A Detailed description of the Tjæreborg wind turbine

A.1 Blade properties

Table 2: Geometrical and structural data of the Tjæreborg turbine blades.

Radial pos. (m)	**Chord (m)**	**Rel. Thick. (%)**	**Twist (deg.)**	**EI flap (MNm^2)**	**EI edge (MNm^2)**	**Mass (kg/l)**
1.46	0.01	40.0	0.0	1.5e10	1.5e10	3000
2.75	0.01	40.0	0.0	8.00e9	8.00e9	1500
2.96	0.01	40.0	0.0	2.00e9	2.00e9	510
6.46	3.30	30.6	8.0	5.86e8	1.40e9	390
9.46	3.00	24.1	7.0	2.40e8	8.51e8	315
12.46	2.70	21.1	6.0	1.21e8	5.24e8	250
15.46	2.40	18.7	5.0	6.09e7	3.28e8	206
18.46	2.10	16.8	4.0	3.05e7	2.08e8	173
21.46	1.80	15.5	3.0	1.43e7	1.23e8	138
24.46	1.50	14.4	2.0	5.68e6	6.18e7	94
27.46	1.20	13.3	1.0	1.71e6	2.64e7	55
28.96	1.05	12.8	0.5	7.7e5	1.60e7	40
29.86	0.96	12.5	0.2	4.5e5	1.16e7	31
30.56	0.89	12.2	0.0	2.7e5	8.60e6	25

A.2 Tower properties

Table 3: Geometrical and structural data of the Tjæreborg tower.

Height (m)	**Outer diameter (m)**	**Height (m)**	**Outer diameter (m)**	**Height (m)**	**Outer diameter (m)**
0.0	7.41	22.0	5.00	43.0	4.50
4.5	6.72	25.5	4.84	46.5	4.44
8.0	6.25	29.0	4.75	50.0	4.38
11.5	5.84	32.5	4.69	53.5	4.31
15.0	5.50	36.0	4.63	57.0	4.25
18.5	5.22	39.5	4.56		

Paper 3

Influence of wind turbine flexibility on loads and power production

By Anders Ahlström
Department of Mechanics, KTH, SE-100 44 Stockholm, Sweden

Submitted to Wind Energy

Summary Most aeroelastic codes used today assume small blade deflections and application of loads on the un-deflected structure. However, with the design of lighter and more flexible wind turbines, this assumption is not obvious. By scaling the system mass and stiffness properties equally, it is possible to compare wind turbines of different degrees of slenderness and at the same time keep system frequencies the same in an un-deformed state. The developed model uses the commercial finite element system MSC.Marc, focused on nonlinear design and analysis, to predict the structural response. The aerodynamic model named AERFORCE, used to transform the wind to loads on the blades, is a Blade-Element/Momentum model. A comparison is made between different slenderness ratios in three wind conditions below rated wind speed. The results show that large blade deflections have a major influence on power production and the resulting structural loads and must be considered in the design of very slender turbines.

Key words: wind turbine; structural dynamics; aeroelasticity; finite element; simulation

1 Introduction

Wind turbines are designed larger and more flexible than before. The consequence is large blade deflections that require special design and computational considerations regarding loads, displacements, blade/tower collisions, etc. The aeroelastic tools available in the design process are generally based on modal analysis or a finite element (FE) representation. The general approach is to assume small displacement and applying the aerodynamic loads in the un-deflected state. However, as the blades in some situations deflect considerably, the validity of the small displacement assumption needs to be investigated. Previous work regarding large blade deflection has been carried out at Risø, using an updated version of their aeroelastic code HAWC, [1]. The reference concludes that frequencies change with the applied load when a rotor at standstill is excited with white noise. The aim with the present work is to investigate the effects of large blade deflections, on some generally studied load components, at operational speed. The work also concludes in which tip deflection/rotor radius ratio nonlinearities will be evident. The study is carried out by scaling the mass and stiffness equally in the wind turbine model. In that way, it is possible to change the flexibility and mass of the wind turbine but maintain the system frequencies, i.e. give deflected situations for which simple models would give identical results. Simulating the wind turbine with different scaling factors, using the same wind data input, gives the large deflection influence on the loads in a comparable way. The aeroelastic model used is based on a commercial FE software, to which is added a stochastic wind generator and a blade aerodynamic evaluation function. The aeroelastic code has been verified in normal as well as extreme load cases, [2, 3].

2 Structural model

2.1 Structural modelling

The simulations were performed with MSC.Marc, which is a commercial finite element program for modelling of linear and nonlinear problems involving e.g. contacts, nonlinear material effects and structural dynamics, [4]. The beam elements used in the present work were either described as circular pipe or rectangular cross sections, where for simplicity shear centre, mass centre and pitch axis were assumed to coincide. All aerodynamic loads were applied as nodal forces acting on the centre of each aerodynamic blade element, i.e., on the end-nodes of each structural beam element. All loads were applied in the deformed state. Figure (1) illustrates the pitching moments and blade forces in the deformed state.

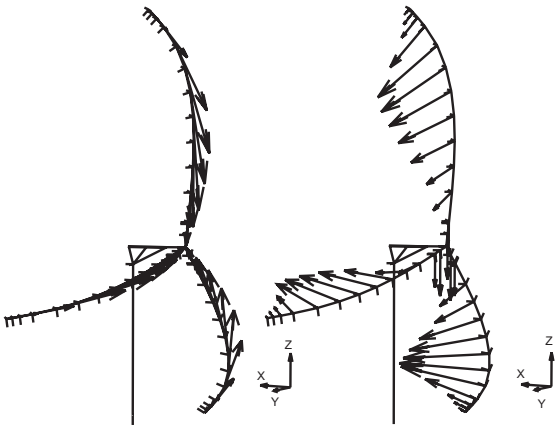

Figure 1: Pitching moments and blade forces in the deformed state.

2.2 Aerodynamic modelling

A subroutine package AERFORCE was used for the calculation of the aerodynamic forces acting on the blades, [5]. The aerodynamic model is based on the blade element momentum (BEM) theory. In AERFORCE the BEM method is extended to incorporate, [5]:

- Dynamic inflow: unsteady modelling of the inflow for cases with unsteady blade loading or unsteady wind.
- Inclined flow to the rotor disc (yaw model).
- Unsteady blade aerodynamics: the inclusion of 2D attached flow, unsteady aerodynamics and a semi-empirical model for 2D dynamic stall.

All properties related to structural geometry and kinematics, such as blade velocities, blade element lengths, etc. were calculated and inputted in the deformed state. However, the induction is calculated as the average value of the respective blade elements. The induction contributions due to yaw are calculated for each radial element. Additional models are included for the modelling of tower shadow effects and dynamic stall. The models are described in [6, 7], respectively. The simulations were performed without the tower shadow model, to eliminate the effects of the blade flexibility on results, as the distance changes to the tower. Slender designs will in real implementations be less influenced by tower shadow effects as the tower radius is decreased.

2.3 Wind field simulation

The turbulent wind field was obtained by using the wind data generator software, SOSIS-W, [8]. SOSIS-W is an artificial wind data generator used as a stand alone

program for providing the pseudo-random wind field series to use in the structural simulation. The wind velocities were calculated in all three directions.

3 Wind turbine model

The wind turbine data is based on the Tjæreborg turbine, [9]. The turbine had a three-bladed rotor with a diameter of 61.1 m and was connected to 2 MW enlarged slip induction generator. The 3 degree tilted rotor was running at a constant speed of 22.3 r.p.m., which gave a blade tip speed of 71 m/s. The concrete tower was 57 m high and shaped as a parabola near the base, gradually turning conical towards the top. Five airfoil tables, covering the full 360 degrees range of angle of attack, were used in the calculations, [10]. Stiffness and mass parameters are described in [3, 10, 11].

3.1 Rotor

The rotor was modelled with a six degree-of-freedom elastic beam element. Each blade was modelled by fourteen elements, and to each blade element additional massless elements were attached. The massless elements were used to calculate transformation matrices needed in the simulations.

3.2 Tower

The tower was modelled using circular hollow beam elements with a thickness of 0.25 m. The tower was discretised into seventeen elements and was rigidly connected to the ground. The connection between tower-top and bedplate was described by a combination of springs and constraint equations, [3]. The connection was modelled as rather stiff due to limited knowledge about yaw stiffness and measured eigenfrequencies.

3.3 Bedplate and drivetrain

The bedplate and drivetrain were modelled with hollow circular elements. The mass of the bedplate was applied as a point mass at the centre of gravity. The connection between bedplate and drivetrain was achieved by using constraint equations, [3]. The connection between bedplate and tower was accomplished by springs and constraint equations. The nodes were constrained to represent a pin joint connection between the parts. Springs were used to model the rotational stiffness. The generator was modelled as an asynchronous generator with approximately 2 % slip. The synchronous rotor speed was 2.29 rad/s. All point masses, concentrated moments of inertia and springs were scaled equally according to the scale factor used in the simulations.

3.4 Simulation methods

The calculations were performed using an implicit dynamic evaluation algorithm, based on the full Newton-Raphson method for equilibrium iterations in each time increment, together with a sparse direct solver. The Updated Lagrangian (UL) procedure was utilised, which means that the FEM equations are formulated with reference to the last accepted solution, [12]. The Single Step Houbolt (SSH) algorithm was used for time integration, [13]. A consistent mass matrix was employed.

3.5 Simulated natural frequencies

Using a model which was representing the real design of the turbine, the natural frequencies of the un-deformed unstressed turbine model were calculated as:

- 0.80 Hz, 1st tower transverse and longitudinal
- 1.13 Hz, 1st asymmetric rotor flap
- 1.14 Hz, 1st symmetric rotor flap
- 1.16 Hz, 1st symmetric rotor flap/tilt
- 1.89 Hz, 1st rotor torsion (free shaft)
- 2.23 Hz, 1st symmetric/asymmetric rotor edge
- 2.97 Hz, 2nd asymmetric rotor flap/yaw
- 3.00 Hz, 2nd symmetric rotor flap/tilt
- 3.07 Hz, 2nd symmetric rotor flap
- 4.49 Hz, 2nd symmetric rotor edge

The modal analyses were obtained using MSC.Marc utilising the Lanczos method, [12].

4 Numerical example

The project aimed to give a deeper insight into phenomena associated with large geometrical deformations. By scaling the mass and stiffness properties equally it is possible to change the flexibility of the structure and at the same time keep the eigenfrequencies unchanged in the un-deformed state. The concept can be described by the generalised eigenproblem:

$$(\psi \mathbf{K} - \omega^2 \psi \mathbf{M})\mathbf{y} = 0 \tag{1}$$

where the nontrivial solution of the eigenproblem gives the circular frequencies ω_i and the corresponding mode shapes $\mathbf{y}_i$. If the mass $\mathbf{M}$ and stiffness $\mathbf{K}$ matrices are scaled equally, by a scaling factor ψ, the eigenvalues remain the same. Practically, the scaling of the mass and stiffness matrices were achieved by scaling densities, elastic moduli, concentrated springs and point masses equally.

In real wind turbines the scalability is limited, especially regarding the mass of the generator and gearbox. Simulating the wind turbine with different scaling factors, using the same wind data input, gives the large deflection influence on the loads. All other parameters were kept the same, meaning that the same amount of power should be produced in the case of zero deflection. The pitching flexibility is determined by the torsional stiffness of the blades, since no pitch bearing was implemented in the present study. All structural parameters are described in [3].

The responses of three wind campaigns below rated wind speed were studied. The mean wind speeds were 7, 10, 13 m/s, referred to as campaigns 1–3, respectively, with the same turbulence intensities 1.5, 1.2, 0.75 m/s in u,v,w directions, respectively. Each campaign was 600 s long and created with the same randomisation seed. The wind was described in 144 gridpoints across the rotor.

5 Results

Results are given as mean and standard deviation (std) values with respect to the scaling factor, ψ, of some load, power and deflection components. The results were calculated at $\psi = 0.2, 0.4, ..., 1.0$. Interpolation between points was achieved in Matlab, [14], using 4th degree polynomials.

The power, Figure (2a), equivalent load, Figures (2c–d) and load, Figures (3a–f), quantities are normalised with respect to the results obtained with $\psi = 1.0$. The relative power, Figure (2b), is plotted versus the flap displacement normalised with rotor radius and so is the blade tip deflection in the flapwise direction, Figure (2c). Figure (2d) gives the rotation in the flapwise direction of the blade tip element around its centre. The equivalent loads were calculated with $m = 12$, following the standard equation, [15]:

$$R_{\text{eq}} = \left(\frac{\sum n_i R_i^m}{n_{\text{eq}}} \right)^{1/m} \tag{2}$$

Figures (2e–f) give the flap and torque equivalent loads, respectively. Power spectral density (PSD) plots are given in Figures (4a–f).

6 Discussion

As the blades deflect, the effective rotor area changes. A reduction of the effective rotor area by 15 % was reached in the case of $\psi = 0.2$, using campaign 3 as wind input. Hence, the power will be reduced in approximately the same ratio. According

to Figure (2a), the power drops off suddenly when $\psi < 0.5$. The maximum loss was 20 %, which besides the reduced rotor area is explained by a 8 % tip speed decrease, together with highly inclined peripheral blade elements. Plotting the power loss with respect to the flap tip deflection/blade length ratio, Figure (2b), shows that the power is reduced by a maximum 3 % if the ratio is below 0.1. The figure further shows that large blade deflections have a stronger influence on the relative power loss at low wind speeds.

Mean and standard deviations of each 600 s campaign were calculated from the simulations for blade root edge, flap and torsional moments. The mean edge moment was, as expected, proportional to the mean power and the standard deviation was proportional to the weight of the turbine blade. The reduced rotor area decreases the thrust and consequently the mean flap moments. The standard deviation of the flap moments reduces considerably with slender blades. The main reason was the centrifugal stiffening effects that will decrease the flapping motion. The blade torque increases with the deflection as all loads on the blades will have a moment arm to the pitch axis. According to Figure (3e) the pitching moment was increased by 50 % in the worst case. The standard deviations were almost unaffected.

The equivalent fatigue loads were reduced with decreasing scaling factors for both flap and edge moments. The largest fatigue reducing effects were obtained in the edge direction because of the dominating gravity component. The pitching moment fatigue load was almost unaffected in campaign 1. The high wind case, campaign 3, increased the equivalent fatigue load by up to 20 % depending on ψ.

Frequency response spectra were derived for all scaling factors during the three wind campaigns. As the blades are deflected, their inertia and stiffness will change referred to the hub centre. When the rotating blades deflect, the centrifugal forces act radially outwards the perpendicular axis of rotation, thereby stiffening the blades. The power spectrum of the flap root moment was dominated by peaks at all multiples of the rotational frequency, 0.37 Hz, hence only small peaks were visible due to flap vibrations. The stiffening effect due to centrifugal forces could be estimated by using the Southwell formula, [16]

$$\omega_1 = \sqrt{\omega_{1,0}^2 + \phi_1 \Omega^2} \tag{3}$$

in which $\omega_{1,0}$ is the corresponding frequency for the non-rotating blade and Ω the rotating speed of the rotor. The ϕ_1 value is dependant on the mass and stiffness distribution and is typically set to 1.73, [16]. Equation (3), gives with $\omega_{1,0} = 1.14$ Hz and $\Omega = 22.3$ r.p.m. an increase of the first symmetric flapwise frequency to 1.24 Hz, compared to the obtained frequencies 1.295 and 1.325 Hz, visible in Figure (4e), for campaign 1 and 3, respectively. The additional increase, approximately 4 %, depending on wind campaign and ψ, is explained by the effect of blade deflection stiffening. The double peak visible in Figure (4e), at about 1.5 Hz, contributes the 4P component as well as a forward flapwise whirling component at approximately 1.14+Ω Hz. The first edgewise frequencies, ω_e, were more or less unchanged in the edgewise spectrum. However, with lower scaling factors, meaning larger blade deflections, the edgewise frequency peaks decrease and the $\omega_e + \Omega$ peaks increase, see Figures (4a,d), respectively. Small $\omega_e + \Omega$ peaks are visible in the low wind speed

of campaign 1. The $\Omega_e \pm \phi$ frequencies are related to gyroscopic effects and coupling to the flexible shaft and tower, causing whirling of the rotor, [17]. Hence, increased whirling at large blade deflections was the reason for the increased $\omega_e + \Omega$ peak. As the blades deflect, the edgewise deflection interacts with the torsional twist as is seen in Figures (4c,f), respectively. Especially the second edgewise frequency is dominant in the torque spectra.

7 Conclusions

The key to reliable and cost optimised wind turbines in the multi-megawatt class is slender design. A consequence is that blade deflections may increase to a point where small deflection theory is no longer relevant in the context of aeroelastic design.

An aeroelastic tool based on the finite element software MSC.Marc has been used to determine the nonlinear effects of large blade deflections. The model is formulated for large deformations and the aerodynamic loads are applied on the deformed geometry.

The study has been carried out by comparing different wind turbine configurations during normal operation in turbulent wind fields. The mean wind speed levels were 7, 10 and 13 m/s, respectively. The different configurations were obtained by scaling the system mass and stiffness properties equally. In that way, it was possible to change the flexibility and mass of the wind turbine without affecting the system frequencies in an un-deformed state.

Results show that nonlinearities due to large blade deflections are present and must be considered in the design of very light and flexible wind turbines. The results are based on a specific wind turbine, but the trends and relative quantities are applicable to other configurations. The study shows that when tip deflection in the flapwise direction exceeds 10 percent of the blade radius, the power drops off considerably. The fine line between moderate and/or considerable power decrease makes detailed modelling necessary for both structural and economical reasons. Halving the mass and stiffness of the original structure, meaning tip deflection/blade radius ratios of 0.08, 0.11 and 0.15, will give power losses of 2.5, 3 and 4 % for the wind cases 7, 10 and 13 m/s, respectively. The halved mass and stiffness case, reduce the equivalent flap and edge loads by about 15 % and 50 %, respectively. The equivalent pitching moment is, however, slightly increased. The wind turbine will produce less power with a softer design, but the material costs will decrease. However, slightly longer blades may be used to compensate for the reduced power production.

The flap and edge root bending moments decrease with slender blade designs and so do the corresponding equivalent loads. The pitching moment increases because the large blade deflection will create a moment arm with respect to the pitch axis. In worst case, the mean pitching moment of a 600 s simulation is increased by 50 %.

The aeroelastic codes used today with the small blade deflection assumption are believed to be accurate enough in most normal situations and certainly for certification purposes where computational speed is critical. Care must, however, be taken

in simulating extreme situations and in the design of even lighter and more flexible machines. In these situations, aeroelastic tools must be used, which are able to properly deal with large blade deflections.

8 Acknowledgement

Thanks to Torben J. Larsen at Risø for initiating ideas to the project. Thanks to Kurt S. Hansen and Stig Øye at the Technical University of Denmark for providing documentation and structural data of the studied turbine. Thanks to Anders Björck at the Swedish Energy Agency for the aerodynamic model and Ingemar Carlén at Teknikgruppen AB for the wind data model.

Support from the Swedish Energy Agency is gratefully acknowledged. Contract/grant number: P12020-1.

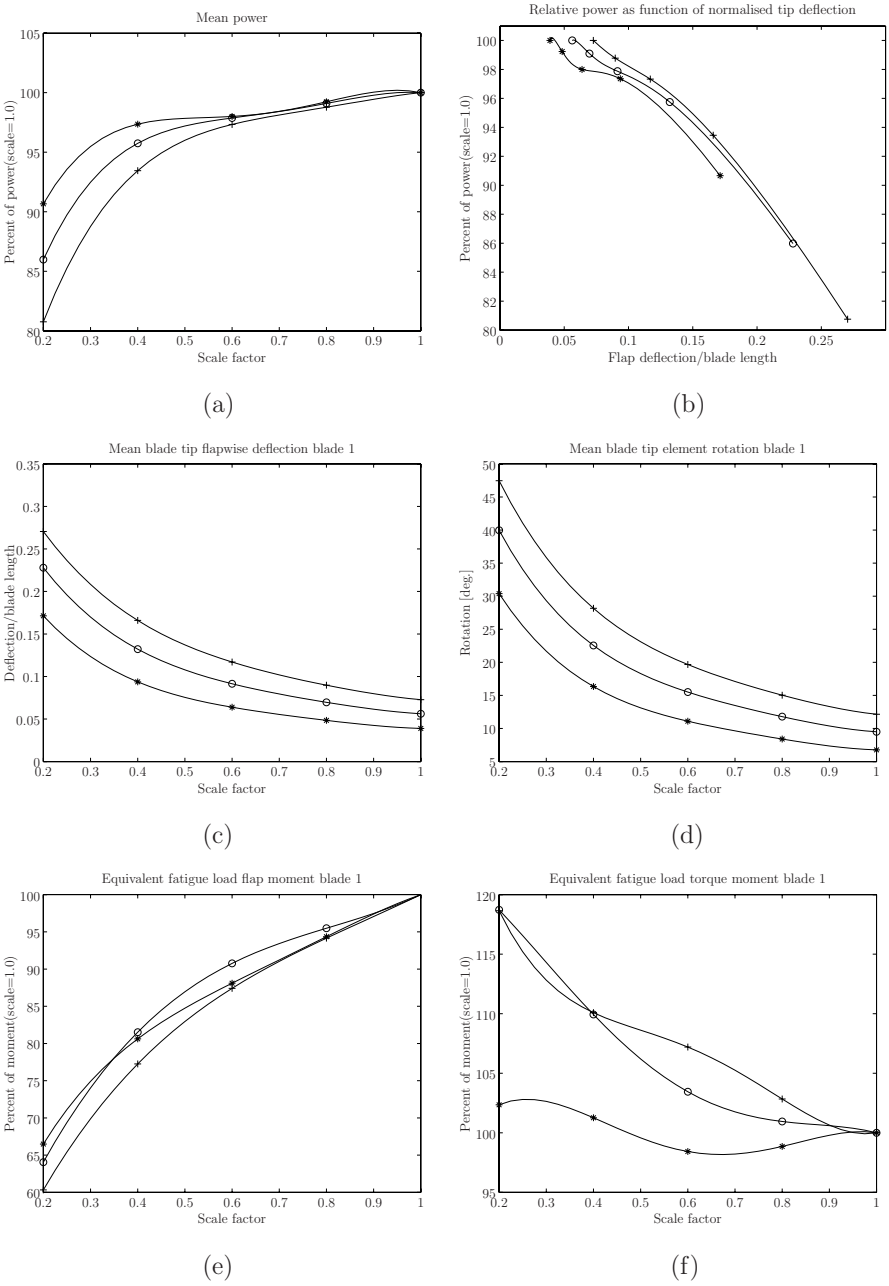

Figure 2: Results from simulations, Dots '*'=7 m/s, 'o'=10 m/s, '+'=13 m/s; Mean power, (a). Mean power as function of deflection, (b). Blade 1 tip displacement, (c). Blade 1 tip element rotation, (d). Equivalent fatigue flap blade 1, (e). Equivalent fatigue torque blade 1, (f).

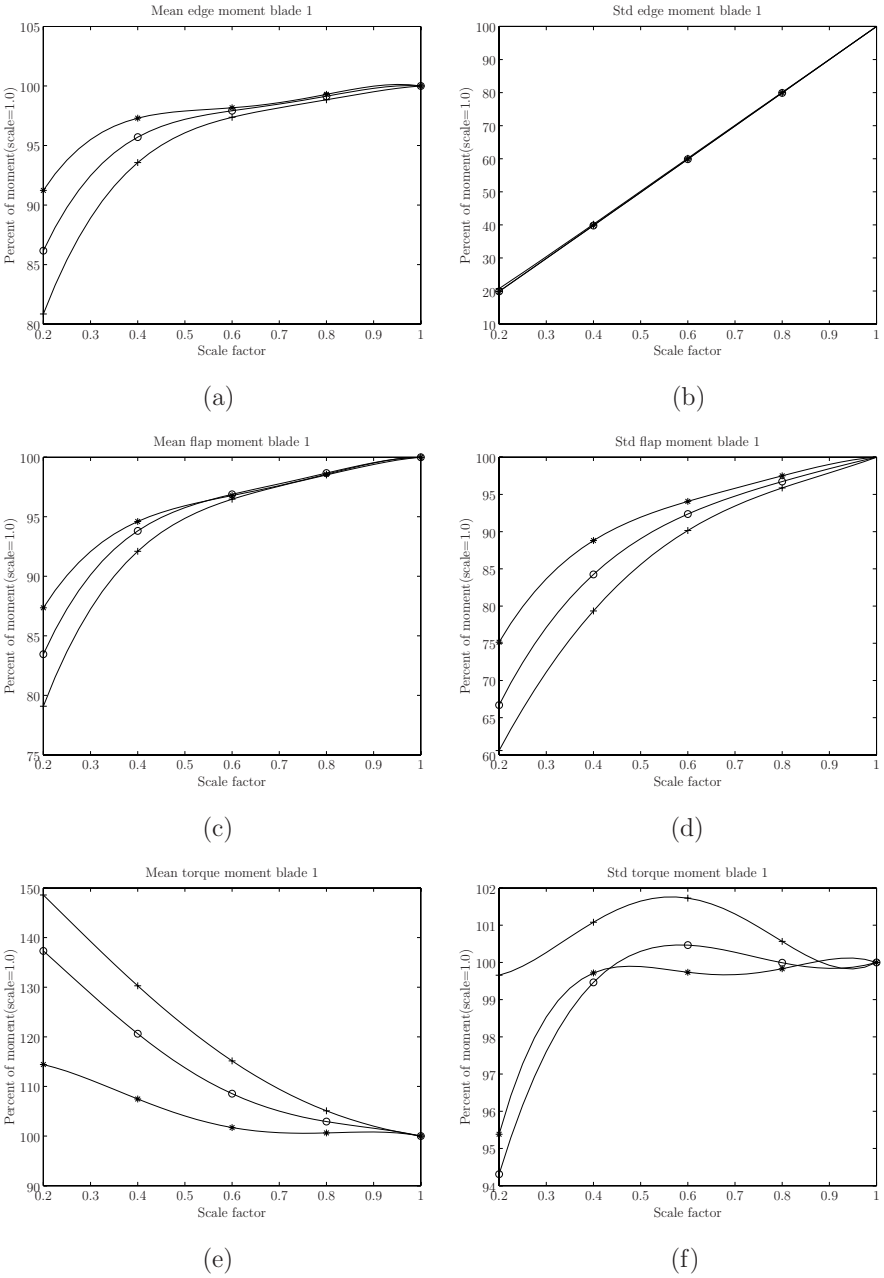

Figure 3: Results from simulations, Dots '*'=7 m/s, 'o'=10 m/s, '+'=13 m/s; Results blade 1: Mean edge moment, (a). Std edge moment, (b). Mean flap moment, (c). Std flap moment, (d). Mean torque moment, (e). Std torque moment, (f).

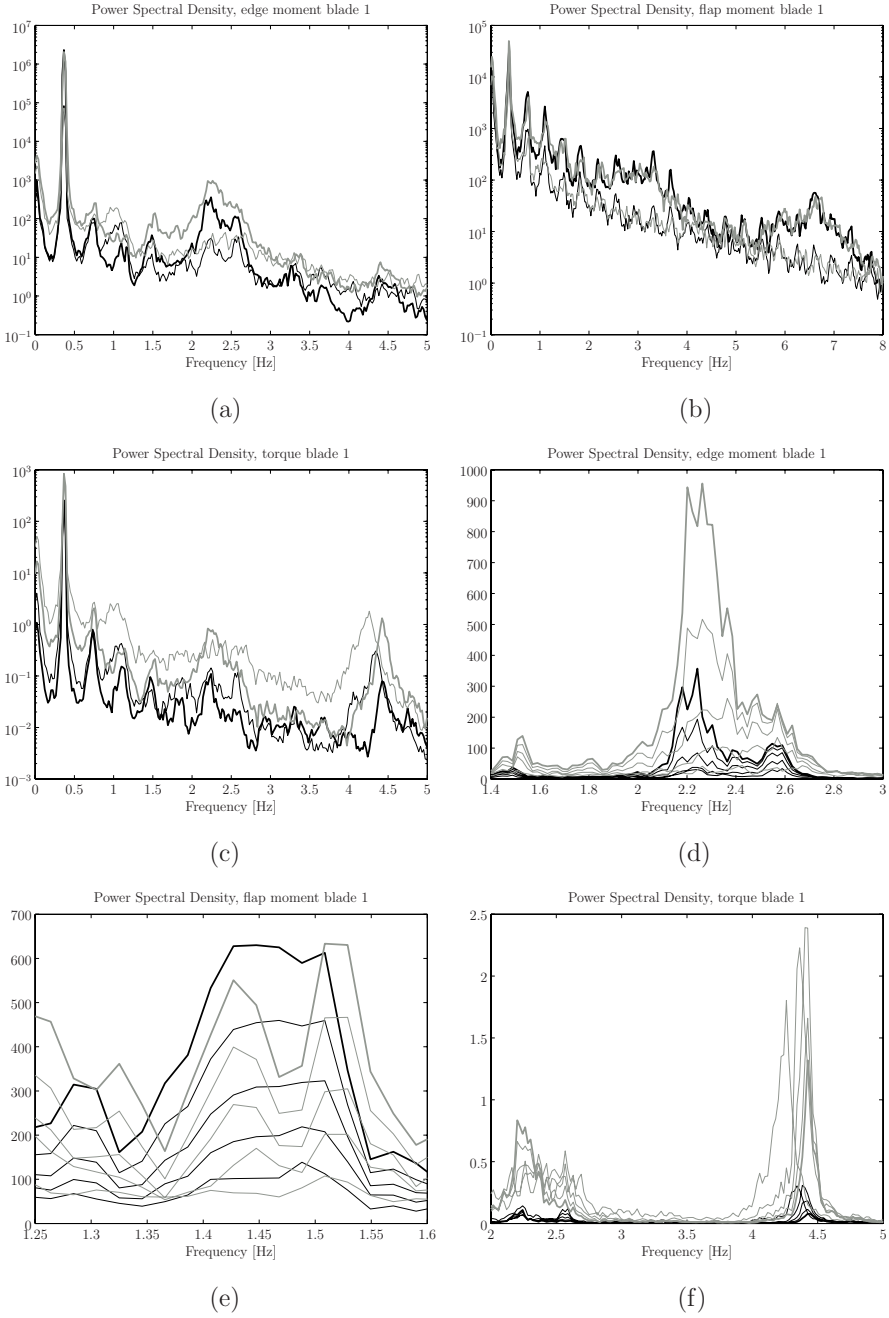

Figure 4: Results from simulations, Black line=7 m/s, grey line=13 m/s, thick lines $\psi = 1.0$, thin lines $\psi = 0.2$ in (a–c) and $\psi = 0.2, 0.4, ..., 0.8$ in (d–f); Results blade 1: PSD edge moment, (a). PSD flap moment, (b). PSD torque moment, (c). PSD edge moment, (d). PSD flap moment, (e). PSD torque moment, (f).

REFERENCES

1. Larsen TJ, Hansen AM. Aeroelastic effects of large blade deflections for wind turbines. In Delft University of Technology, ed., The Science of making Torque from Wind. Roskilde, Denmark, 2004; 238–246.

2. Ahlström A. Development and verification of an aeroelastic simulation tool for wind turbine calculations, 2004. Submitted.

3. Ahlström A. General FEM simulation of extreme load cases on wind power structures, 2004. Submitted.

4. MSC Software Corporation. Features of MSC.Marc.
Internet online, 20 Januari, 2003.
http://www.marc.com/Support/Library/Features_of_Marc_2001.pdf.

5. Björck A. AERFORCE: Subroutine Package for unsteady
Blade-Element/Momentum Calculations. Technical Report TN 2000-07, FFA, Bromma, Sweden, 2000.

6. Björck A. DYNSTALL: Subroutine Package with a Dynamic stall model. Technical Report FFAP-V-110, FFA, Bromma, Sweden, 2000.

7. Björck A. Blade-Tower Interaction: Calculations Compared to Wind Tunnel Test Results. Technical Report FFAP-V-107, FFA, Bromma, Sweden, 1999.

8. Carlén I. SOSIS-W Version 1.3. Technical report, Teknikgruppen AB, Sollentuna, Sweden, 2000.

9. ELSAMPROJECT A/S. The Tjæreborg Wind Turbine - Loads During Normal Operation Mode. Technical Report EP94/456, CEG, DG XII contract EN3W.0048.DK, Fredericia, Denmark, 1994.

10. Øye S. Tjæreborg wind turbine (Esbjerg) Geometric and operational data. Technical Report VK-184, Department of Fluid Mechanics, DTH, Lyngby, Denmark, 1990.

11. Øye S. Tjæreborg wind turbine (Esbjerg) Structural dynamics data. Technical Report VK-186, Department of Fluid Mechanics, DTH, Lyngby, Denmark, 1991.

12. MSC Software Corporation. MSC.Marc Volume A, Theory and User Information. Technical Report MA*V2003*Z*Z*Z*DC-VOL-A, 2003.

13. Chung J, Hulbert GM. A family of single-step Houbolt time integration algorithms for structural dynamics. Computer Methods in Applied Mechanics and Engineering 1994;118:1–11.

14. Mathworks. Matlab manual.
Internet online, 2002. http://www.mathworks.com/.

15. Sutherland HJ. Fatigue Analysis of Wind Turbines. Technical Report SAND99-0089, Sandia National Laboratories, Albuquerque, New Mexico, 1999.

16. Burton T, Sharpe D, Jenkins N, Bossanyi E. Wind Energy Handbook. Chichester: John Wiley & Sons, 2001.

17. Thomsen K, Petersen JT, Nim E, Øye S, Petersen B. A Method for Determination of Damping for Edgewise Blade Vibrations. Wind Energy 2000; 3:233–246.